

University of Nevada, Reno

**Demographic and phenotypic reactions to climate
by western North American woodrats (*Neotoma* spp.)**

A dissertation submitted in partial fulfillment of the
requirements for the degree of the Doctor of Philosophy in
Ecology, Evolution, and Conservation Biology

by

Angela D. Hornsby
Dr. Marjorie Matocq / Dissertation Advisor

December, 2016

© by Angela D. Hornsby 2016
All Rights Reserved



THE GRADUATE SCHOOL

We recommend that the dissertation
prepared under our supervision by

ANGELA D. HORNSBY

Entitled

**Demographic And Phenotypic Reactions To Climate
By Western North American Woodrats (Neotoma Spp.)**

be accepted in partial fulfillment of the
requirements for the degree of

DOCTOR OF PHILOSOPHY

Dr. Marjorie Matocq, Advisor

Dr. Guy Hoelzer, Committee Member

Dr. Matt Forister, Committee Member

Dr. Peter Weisberg, Committee Member

Dr. Scott Mensing, Graduate School Representative

David W. Zeh, Ph. D., Dean, Graduate School

December, 2016

ABSTRACT

Species can react or adapt to climate in many ways, which can be studied through both space and time and using a number of perspectives and tools. North American woodrats (*Neotoma* spp.) are widespread across a variety of climates and also represented extensively in late Quaternary deposits, making them an excellent system for studying the effects of climate in a variety of ways. My dissertation includes three chapters that employ several methods and perspectives to explore how *Neotoma* spp. have reacted and adapted to climate. In my first chapter, I use a statistical phylogeographic approach to determine the accuracy of quantitative demographic signals derived from common proxies of Pleistocene-Holocene population history, finding that these proxies accurately reflect the most recent population expansion but may fail to capture other demographic events for a variety of reasons. In my second chapter, I use ancient DNA to determine the pattern and pace of *Neotoma* spp. turnover along a 33,000-year elevational transect, finding that the turnover was abrupt, final, and reflects the role of species interactions in reaction to climate. In my third chapter, I use geometric morphometrics to assess the developmental causes and morphometric consequences of adherence to ecogeographic rules, finding that *N. cinerea* are smaller in warmer and less productive climates, that the size differences among climates are established prior to weaning, and that smaller-bodied groups avoid pedomorphism through a break in the size-shape (allometric) relationship. Though these chapters do not build explicitly as a single narrative, they address complementary pieces of this very large question and provide a step towards a more complete and integrated view of the myriad effects of climate through space and time.

ACKNOWLEDGEMENTS

Thank you to...

... the many people who provided crucial help or formative advice in the course of this work, including but not limited to Felisa Smith, Hendrik Poinar, Mel Kuch, Ana Duggan, and Miriam Zelditch. Thanks as well to the entire crew in the McMaster Ancient DNA Centre for welcoming an itinerant ecologist to their group so warmly.

... my funders, including the NSF Nevada EPSCoR program, the American Society of Mammalogists, the UNR Graduate Student Association, the UNR EECB program, and the Gordon and Betty Moore Foundation.

... the many museums that provided the specimens so fundamental to each of my chapters, and the staff at those museums who ensured I had everything I needed to do the best research I could. Special thanks to Jim Patton and Chris Conroy for welcoming me time and again (and again, and again) on my research vacations to the MVZ.

... the EECB program, including the faculty and students who have been so great to work with in a variety of settings. Special thanks to Chris Feldman and Beth Leger, who let me loose in the Museum of Natural History and trusted me to make my own way in curation and displays. Thanks as well to the staff in EECB, NRES, CABNR, and the Graduate School, who keep all the wheels on our science machines turning.

... my committee, including Guy Hoelzer, Matt Forister, Peter Weisberg, Scott Mensing, and Cheryll Glotfelty, who have been nothing but thoughtful, supportive, and challenging in the best ways possible. Thanks, too, to Pat Chatham, who told me to assemble my team, and was herself a key player if not long in the game.

... the Matocq lab and Evol Doers, especially Feldman, Peter Murphy, Brandi Coyner, Jason Malaney, Jen Rippert, and Alan de Queiroz, for their support and help over the years on the very rough drafts of my early work and ideas.

... my friends in Reno, who have been my teammates, labmates, roommates, board-mates, museum-display-mates, confidants, and inspirations. Melvin, Sarah, Cynthia, Lara, Kevin, Mark, Josh, and Joanne—you have all helped me be a better version of myself and taught me to view the world in fairer light. What a lucky person to have such friends.

... Dan, who has supported me in everything I've tried to do, and in all the ways (useful or otherwise) that I've tried to do them. Your humor, empathy, sincerity, and bravery strike me every day. I'm a better person because of you.

... my mom, dad, and sisters, for every step of everything. Sometimes trite points are just plain true: I would not have finished this without your love and support.

... my adviser, Marjorie Matocq, who has provided me with an extraordinarily positive model of scientific rigor, enthusiasm, optimism, responsibility, tact, honesty, and warmth, which I can only hope to continue absorbing and carrying into my future career. I ended up in a variety of holes during my time as a grad student—sometimes I dug them myself out of curiosity, sometimes I wandered into them accidentally, and sometimes the ground opened beneath me and I was deep inside before I even realized it. Every single time, she lowered a rope (sometimes many ropes) and waited until I could figure out how to pull myself out. Of all the important gifts she gave me, her patience had the greatest impact on my growth as a young scientist, and my growth as a person learning to navigate the steep edges of their own life. It made all the difference.

TABLE OF CONTENTS

OVERVIEW	Error! Bookmark not defined.
CHAPTER ONE	9
<i>Testing late Quaternary demographic hypotheses derived from ecological niche models and paleoecological assemblages</i>	
Introduction	9
Methods	12
Results	20
Discussion	23
References	29
Figures	34
Appendix 1-1	38
Appendix 1-2	40
Appendix 1-3	51
CHAPTER TWO	54
<i>Ancient DNA from paleofeces shows the pattern and pace of small mammal species turnover across 30,000 years in Death Valley, CA/NV</i>	
Introduction	54
Methods	58
Results	64
Discussion	66
References	69
Tables	73
Figures	78
Appendix 2-1	83
CHAPTER THREE	86
<i>Growth mechanisms and morphometric consequences of adherence to ecogeographic rules in a widespread rodent (Neotoma cinerea)</i>	

Introduction	86
Methods	90
Results	98
Discussion	102
References	106
Tables	110
Figures	117
Appendix 3-1	125
Supplemental tables	127
Supplemental figures	139

LIST OF TABLES

Table 1-S1. Genetic samples (specimens or isolates) of <i>Neotoma cinerea</i> ($n = 33$) and <i>N. lepida</i> ($n = 39$) in the area of interest.	38
Table 1-S2. Parameter prior values and distributions for <i>N. cinerea</i> . For normal priors, min and max were set to +/- 2 standard deviations.	43
Table 1-S3. Parameter prior values and distributions for <i>N. lepida</i> . For normal priors, min and max were set to +/- 2 standard deviations.	48
Table 1-S4. Comparison of univariate summary statistics from observed the simulated datasets under each scenario. Numbers indicate the proportion of simulated data sets with a value below the observed value. Summary statistics are abbreviated as: NHA, number of haplotypes; MPD, mean pairwise difference; VPD, variance of pairwise difference; MNS, mean number of the rarest nucleotide at segregating sites; VNS, variance in number of the rarest nucleotide at segregating sites.	51
Table 2-1. Characteristics of strata, aDNA extracts, and sequence data, including duplicated samples for a subset of strata. For strata reaching the minimum read threshold, the read proportion for predominant species in each stratum is shaded, and proportions reaching the mixing threshold indicating presence of multiple species are boxed.	73
Table 2-2. Loci and 24-bp windows used as mini barcodes for species identification.	77
Table 2-S1. GUIDs/IDs, species, and locations for modern samples used in reference library construction.	83
Table 3-1. Top model relating adult body size to climate, including estimates, standard errors, t -values (df), and P -values. All parameters have been standardized.	110
Table 3-2. Models testing the effects of climate on growth initiation, rate, and termination in respective growth phases, including estimates, standard errors (SE), t -values, and P -values. All parameters have been standardized.	111
Table 3-3. Comparison of nested models with static and ontogenetic allometries pooled (common allometry) or separated (separate allometries) [<i>advanced.prodD.lm(shape ~ log(size), log(size) + stage, group = stage, slope = log(size)</i>)].	112
Table 3-4. Comparison of nested models with and without the effect of climate	113

group on ontogenetic trajectories in age-shape space [*advanced.prodD.lm(shape ~ log(age), log(age) + climgroup, group = climgroup, slope = log(age))*].

Table 3-5. Pairwise comparisons of ontogenetic trajectories in age-shape space, including direction and length of shape change. Absolute difference in length or angle direction (with *Z* scores in parentheses) are above the diagonal, and *P* values are below the diagonal. 114

Table 3-6. Comparison of nested models with and without the effect of climate group on allometric trajectories in size-shape space [*advanced.prodD.lm(shape ~ log(size), log(size) + climgroup, group = climgroup, slope = log(size))*]. 115

Table 3-7. Pairwise comparisons of allometric trajectories in size-shape space, including direction and length of shape change. Absolute difference in length or angle direction (with *Z* scores in parentheses) are above the diagonal, and *P* values are below the diagonal. 116

Table 3-S1. GUID, latitude, longitude, sex, and age scores (exoccipital-supraoccipital [occsut], basioccipital-basisphenoid suture [bassut], and M3 molar eruption and wear [molerup]) of specimens analyzed. 127

Table 3-S2. Measurement view, type, abbreviation, and description of landmarks used in geometric morphometric analyses. Marker code refers to landmark placement on Figure 3-1. 135

Table 3-S3. Age scores (1–6) for cranium developmental characters, with known ages (literature) and estimated ages (this study). 136

Table 3-S4. Ranked candidate models and AICs from model selection relating adult body size to climate. 137

Table 3-S5. Top models ($\Delta\text{AIC} < 2$) from model selection relating adult body size to climate, including estimates, standard errors (SE), *t*-values, and *P*-values. All parameters have been standardized. Scale for all parameters is 95 km. 139

Table 3-S6. Reduced models relating age and sex to body size in each growth phase. 140

LIST OF FIGURES

- Figure 1-1.** Ranges, occurrence records, and ecological niche models for *Neotoma cinerea* and *N. lepida*, with the area of interest outlined in red. (A-B) Location of genetic samples (white circles), paleoecological assemblages (black squares; C, Camels Back Cave; H, Hidden Cave; G, Gatecliff Shelter), species ranges (grey shade), and buffered range extent used for niche modeling (dotted line). (C-D) Current occurrence records (white circles) used for niche modeling, and current niche models with darker shade indicating higher habitat suitability. (E-F) mHOL occurrence records, and niche models projected to mHOL climate. (G-H) LGM occurrence records, and niche models projected to LGM climate. (I-J) Niche models projected to LIG climate. 35
- Figure 1-2.** Scenarios of change in effective population size (N_e) for (A) *N. cinerea* and (B) *N. lepida*, derived from subfossil abundances (RACs) and ecological niche models (ENMs). Solid lines show N_e for each scenario, and dotted lines show the minimum and maximum (± 2 standard deviations) of the distributions used for modeling. 36
- Figure 1-3.** Posterior probabilities of demographic scenarios for (A-B) *N. cinerea* and (C-D) *N. lepida* across values of n (number of closest simulations to the observed data). For both direct and logistic regression plots, posterior probabilities are reported for ten levels of n , with 95% highest posterior densities shaded. 37
- Figure 1-S1.** Plots of principal component analyses of summary statistics from simulated (small circles) and observed (large yellow circle) data, including separate plots for *Neotoma cinerea* all models (A) and top model alone (B), and *N. lepida* all models (C) and top model alone (D). Each simulated dataset is represented by one circle. Open circles are prior combinations, and closed circles are posteriors. 53
- Figure 2-1.** Location of paleomidden strata (A) in Death Valley National Park (black outline) and (B) along the Titus Canyon elevational transect. Strata are colored by age in calibrated years before present (cal YBP). 79
- Figure 2-2.** Positions of 24-bp windows across four mitochondrial loci with (red) and without (grey) discriminatory power between *Neotoma* spp. Discriminatory power was determined as no (zero proportion) heterospecific genetic distances equaling zero, based on known sequences in the reference database. 80
- Figure 2-3.** Proportion of aDNA reads from each species in strata with ≥ 50 total reads. Asterisks mark strata that reached the mixing threshold indicating presence of multiple species. 81
- Figure 2-4.** (A) Paleoclimate proxies from regional (Leviathan chronology) and 82

hemispheric (GISP2 Greenland ice core) sources. Higher values in both proxies indicate warmer temperatures. (B) Strata with ≥ 50 aDNA reads plotted by age and elevation in Titus Canyon, and colored by species present. Strata that reached the mixing threshold are represented by pie charts showing proportion of reads from each species. The cold Younger Dryas (YD, light blue) and warm Bølling-Allerød (BA, light red) are shaded.

- Figure 3-1.** Locations of *Neotoma cinerea* skulls against species range map (dark grey), colored according to climate cluster (see text). 118
- Figure 3-2.** Cranial landmarks for geometric morphometric analysis. Landmarks with filled circles were taken from either the ventral or dorsal view of the skull, and landmarks with open circles were taken from both views and used to unify the data for each specimen into a single 3D shape. Landmarks off the midline were taken from both sides of the skull. See Table 3-S2 for anatomical descriptions of landmark placement. Engraving from Baird 1857. 119
- Figure 3-3.** Predicted ages and centroid sizes of *N. cinerea* skulls, split by sex: (A) black = female, (B) grey = male. Dotted lines show divisions between growth phases at 60, 140, and 240 days after birth. 120
- Figure 3-4.** Relationship between adult *Neotoma cinerea* size and (A) mean annual temperature (bio1) and (B) net primary productivity (NPP), both at 95 km scale. The linear model for each sex (black = female, grey = male) is shown with 95% confidence interval shaded. 121
- Figure 3-5.** (A) Climate (temperature and NPP at 95 km resolution) at specimen collection localities, colored according to climate groups at $k = 3$: ‘high temperature, high NPP’ (green); ‘low temperature, low NPP’ (blue); ‘high temperature, low NPP’ (red). (B) Boxplots of adult size split by sex and climate group and coded by significance in each sex separately. 122
- Figure 3-6.** Plots of common age or allometric component (CAC), first residual shape component (RSC1) against CAC, and predicted shape from trajectory analyses. (A-C) Ontogenetic trajectories in age-shape space, split by climate group. (D-F) Allometric trajectories in size-shape space, split by climate group. 123
- Figure 3-7.** Mean cranial shapes of juveniles and adults in each climate group, from the dorsal-ventral (left) and side views (right). 124
- Figure 3-S1.** Pairwise Procrustes shape distances for multiple measurements within the same specimen and among specimens. 142
- Figure 3-S2.** Difference in age index (on a scale of 3–18) between specimens aged multiple times. 143

- Figure 3-S3.** Adult (age > 240 days) male centroid sizes across ages and at different levels of (A) temperature and (B) NPP. 144
- Figure 3-S4.** Guide to age scores for cranial developmental characters, including specimen GUID for reference. 145
- Figure S5.** Relationship between age indices (scored from cranial characters) and predicted log age, with 95% confidence interval shaded. 146

OVERVIEW

Species often survive in a variety of climates across both space and time. This is facilitated by two major classes of reaction or adaptation to climate: (1) demographic changes and extension or contraction of the species range elevationally, latitudinally, or along other geographic environmental clines; or (2) changes in morphology, phenology, physiology, or behavior. Relatively few study systems allow us to empirically observe these changes through geological time, so these systems provide important insight on the effects of major, millennial-scale climate changes. Likewise, geographic variation across climates in modern time gives us insight into the phenotypic patterns associated with different climates, and allows us to dig deeper to determine the mechanisms underlying these patterns. Together, these perspectives offer complementary ways to explore the potential processes, rates, constraints, and consequences involved in a species' reaction and adaptation to climate.

My dissertation work seeks to add to our understanding of these processes across geographic space and through climate changes over time. I address these questions using woodrats (genus *Neotoma*), for which we have an excellent paleorecord and substantial foundational research that provide context for the ecological and evolutionary dynamics of these species. Studies of the paleomidden record and modern specimens throughout western North America suggest that *Neotoma* spp., and particularly the well-studied *N. cinerea* and *N. lepida*, have reacted to climate in several ways: they have moved elevationally and latitudinally (Guralnick 2007; Moritz et al. 2008) over time, by colonizing on the leading range edge and experiencing local extirpation on the trailing

edge (Grayson 1987, 2006); and they differ phenologically (Smith and Charnov 2001) and morphologically (Smith et al. 1995; Smith and Betancourt 1998; Lyman and O'Brien 2005; Smith and Betancourt 2006; Patton et al. 2008; Smith et al. 2009; Cordero and Epps 2012; Hornsby and Matocq 2012; Hornsby and Matocq 2014) in both space and time. Further, with their complementary ecological tolerances, these species offer a good contrast of potential reactions to major climate changes. The bushy-tailed woodrat (*N. cinerea*) is a one of Brown's (1971) classic montane mammals, and its large body size and heavy pelage help it tolerate cold (Smith 1997). In contrast, the desert woodrat (*N. lepida* complex) is associated with relatively hotter and drier habitats, facilitated by its small body size and thin pelage. Because we have evidence of their dynamics through time, and because they are widespread across the climatically diverse western North America, these species are ideal targets for asking questions about reactions and adaptations to climate both temporally and spatially.

My dissertation includes three chapters that employ a variety of methods and perspectives to explore how *Neotoma* spp. have reacted and adapted to climate. Though these chapters do not build explicitly as a single narrative, they address complementary pieces of this very large question and provide a step towards a more complete and integrated view of the myriad effects of climate through space and time. Following is a brief summary of the goals, methods, and findings of each chapter.

CHAPTER ONE SUMMARY

Testing late Quaternary demographic hypotheses derived from ecological niche models and paleoecological assemblages

Species in regions with dynamic climatic and geological histories often undergo major shifts in geographic range and demography as a function of their environment. These shifts can have profound consequences on patterns of genetic and phenotypic variation; thus, a major current focus of molecular ecology and biogeography is to understand how taxa have responded to past changes and how they may respond to future change. To understand these changes, biogeographers use many tools and types of data, including several that are assumed to reflect signatures of population demographic history. The purpose of this chapter is confirm or refute these assumptions by testing whether two common qualitative sources of historical biogeographic information (ecological niche models, ENMs; and rarified abundance counts, RACs) indicate the same demographic histories for *Neotoma* spp. as those reflected in modern patterns of genetic variation.

To test this, I developed ecological niche models and gathered paleoecological subfossil abundances from the literature for two ecologically disparate rodents (desert-adapted *Neotoma lepida* and montane-adapted *N. cinerea*) in western North America. I converted these two common indicators of historical demography into testable quantitative hypotheses (scenarios) of population size change in these species. I estimated past population sizes by scaling habitat suitability and subfossil abundance against modern effective population size calculated from genetic data, and used the resulting values to parameterize, simulate, and compare demographic scenarios in an approximate Bayesian computation framework. Scenarios were assigned posterior probabilities based on their ability to produce genetic patterns (as measured by summary statistics) similar to the observed patterns.

The top scenario for the desert-adapted *N. lepida* was derived from subfossil abundance data but was a poor overall fit to the observed data, while neither subfossils nor habitat suitability closely matched patterns in the montane-adapted *N. cinerea*. These results caution against interpreting these proxies as quantitative indicators of past population size. While this approach carries the same challenges in comparing census and effective population sizes as other statistical phylogeographic work, it offers a way to begin testing the relationship between population history and the proxies meant to represent it.

CHAPTER TWO SUMMARY

Ancient DNA from paleofeces shows the pattern and pace of small mammal species turnover across 30,000 years in Death Valley, CA/NV

The ways in which species and communities react to climate change provide insight into how biodiversity is shaped and structured over time. Paleoecological deposits offer direct observation into the past, often spanning several major climatic events across the Pleistocene-Holocene transition around 11,700 years before present. While many types of deposits are subject to broad spatial and temporal mixing, fecal pellets such as those in *Neotoma* spp. paleomiddens offer precise locations to understand species occupancy patterns in response to climate. The purpose of this chapter is to use ancient DNA (aDNA) to determine the patterns and rates of *Neotoma* species turnover across a 30-km long, 1,300-m elevational, and 33,000-year transect in Titus Canyon, Death Valley National Park, CA/NV, which encompasses the major climatic warming through the Pleistocene-Holocene transition.

To execute this project, I built genomic libraries using aDNA extracted from pools of *Neotoma* spp. fecal pellets from Titus Canyon paleomiddens. I enriched these libraries for mitochondrial DNA using RNA baits designed from modern *Neotoma* sequences, and sequenced these enriched libraries on a high-throughput platform. To preserve library complexity in these pooled samples, I chose to identify each read to species rather than combine reads in consensus haplotypes. To create a reference database for this read identification, I developed mini-barcodes from modern mitochondrial sequences using a sliding window analysis, and retained only those windows with discriminatory power between species. I queried the aDNA reads against this custom database, determined the proportion of each species present based on the read identifications, and compared these patterns to hemispheric and local paleoclimate proxies to investigate the timing and rate of species turnover.

I found that both the montane-adapted *Neotoma cinerea* and desert-adapted *N. lepida* were present in Titus Canyon over time, and that the turnover from the former to the latter occurred abruptly during the Pleistocene-Holocene transition around 13,000 years ago. As *N. lepida* was present sparsely and intermittently in Titus Canyon well before the end of the Pleistocene, I conclude that the turnover between these species occurred only once climatic temperature exceeded the tolerance of the larger, behaviorally dominant *N. cinerea*. This result contrasts with patterns of turnover between these species inferred from other deposits and methods, and highlights the importance of ecological interactions in species reactions to climate.

CHAPTER THREE SUMMARY

Growth mechanisms and morphometric consequences of adherence to ecogeographic rules in a widespread rodent (*Neotoma cinerea*)

Ecogeographic rules lie at the intersection of two deep-rooted topics in evolutionary biology: intraspecific diversification and convergent evolution. These rules are used to describe broad-scale patterns in phenotype across taxa, which presumably arise due to convergent or parallel evolution in response to the same climatic forces. Some of the most broadly studied rules describe intraspecific body size patterns, including Bergmann's rule (inverse relationship with temperature) and resource rule (positive relationship with ecosystem productivity). However, we have a poor understanding of either the proximal mechanisms or secondary consequences of body size differences across climates. The purpose of this chapter is to determine whether the widespread bushy-tailed woodrat (*Neotoma cinerea*) adheres to these ecogeographic rules, how differences in the timing and rate of growth across climates lead to adherence, and whether groups in warmer or less productive climates retain juvenile shape (pedomorphism) as a consequence of their smaller size.

To address these questions, I sampled *N. cinerea* skulls from natural history collections representing a variety of climates across the species' broad geographic range and post-weaning through adult ages. I used cranial features to estimate the age of each skull and digitized 3D landmark data to represent specimen size and shape. I used model selection to determine which climatic variables affected adult size, and local linear models across developmental stages to determine whether differences in adult size were caused by changes in the initiation, termination, or rate of growth at earlier ages. To distinguish between three alternative hypotheses of adult *N. cinerea* shape

(pedomorphism, isometry, and allometric repatterning), I used geometric morphometric analyses to construct phenotypic trajectories in multivariate shape and size-shape spaces, and compared the lengths and directions of these vectors.

I found that temperature and ecosystem productivity influenced *N. cinerea* body size even from the earliest observed ages, and this size difference carried into adulthood with no other changes in growth rate or duration. However, these differences in size did not affect final adult shape. Although adults from the high temperature, low productivity climates were smaller than adults from other climates, their higher rate of shape change per unit size compensated for this difference to cause relative isometry rather than pedomorphism. Studies such as this extend the ways in which we explore ecogeographic rules, allowing us to understand not only whether species adhere to a rule, but also the processes and consequences of adherence.

REFERENCES

- Brown, J. H. 1971. Mammals on mountaintops: nonequilibrium insular biogeography. *American Naturalist* 105:467-478.
- Cordero, G. A. and C. W. Epps. 2012. From desert to rainforest: phenotypic variation in functionally important traits of bushy-tailed woodrats (*Neotoma cinerea*) across two climatic extremes. *Journal of Mammalian Evolution* 19:135–153.
- Grayson, D. K. 1987. The biogeographic history of small mammals in the Great Basin - observations on the last 20,000 years. *Journal of Mammalogy* 68:359-375.
- Grayson, D. K. 2006. The Late Quaternary biogeographic histories of some Great Basin mammals (western USA). *Quaternary Science Reviews* 25:2964-2991.
- Guralnick, R. 2007. Differential effects of past climate warming on mountain and flatland species distributions: a multispecies North American mammal assessment. *Global Ecology and Biogeography* 16:14-23.
- Hornsby, A. D. and M. D. Matocq. 2012. Differential regional response of the bushy-tailed woodrat (*Neotoma cinerea*) to late Quaternary climate change. *Journal of Biogeography* 39:289-305.
- Hornsby, A. D. and M. D. Matocq. 2014. Patterns of evolutionary divergence and convergence in the bushy-tailed woodrat (*Neotoma cinerea*). *Journal of Mammalian Evolution* 21:243-256.
- Lyman, R. L. and M. J. O'Brien. 2005. Within-taxon morphological diversity in late-quaternary *Neotoma* as a paleoenvironmental indicator, Bonneville Basin, Northwestern Utah, USA. *Quaternary Research* 63:274-282.
- Moritz, C., J. L. Patton, C. J. Conroy, J. L. Parra, G. C. White, and S. R. Beissinger. 2008. Impact of a century of climate change on small-mammal communities in Yosemite National Park, USA. *Science* 322:261-264.
- Patton, J. L., D. G. Huckaby, Álvarez-Castañeda, and S. Ticul. 2008. The evolutionary history and a systematic revision of woodrats of the *Neotoma lepida* group. *UC Publications in Zoology* 135:1-411.
- Smith, F. A. 1997. *Neotoma cinerea*. *Mammalian Species* 564:1-8.
- Smith, F. A. and J. L. Betancourt. 1998. Response of bushy-tailed woodrats (*Neotoma cinerea*) to late Quaternary climatic change in the Colorado Plateau. *Quaternary Research* 50:1-11.
- Smith, F. A. and J. L. Betancourt. 2006. Predicting woodrat (*Neotoma*) responses to anthropogenic warming from studies of the palaeomidden record. *Journal of Biogeography* 33:2061-2076.
- Smith, F. A., J. L. Betancourt, and J. H. Brown. 1995. Evolution of body-size in the woodrat over the past 25,000 years of climate-change. *Science* 270:2012-2014.
- Smith, F. A. and E. L. Charnov. 2001. Fitness trade-offs select for semelparous reproduction in an extreme environment. *Evolutionary Ecology Research* 3:595-602.
- Smith, F. A., D. L. Crawford, L. E. Harding, H. M. Lease, I. W. Murray, A. Raniszewski, and K. M. Youberg. 2009. A tale of two species: Extirpation and range expansion during the late Quaternary in an extreme environment. *Global and Planetary Change* 65:122-133.

CHAPTER ONE

Testing late Quaternary demographic hypotheses derived from ecological niche models and paleoecological assemblages

INTRODUCTION

Species in regions with dynamic climatic and geological histories often undergo major demographic changes as a function of their environment (Van Tuinen et al. 2008, Spaeth et al. 2009, Galbreath et al. 2010, Hornsby and Matocq 2012). These events can have profound consequences on patterns of genetic and phenotypic variation; thus, a major focus of molecular ecology and biogeography is to understand how taxa have responded to past environmental changes (Knowles 2009, Carstens et al. 2013, Forester et al. 2013). Advances in these fields provide an array of methods to test hypotheses of population history (Knowles 2009, Beaumont 2010, Carstens et al. 2013, Pelletier and Carstens 2014), with renewed focus on testing informed alternative scenarios—that is, converting independent indicators of population history into biologically relevant and testable hypotheses of population history.

Most of our understanding of population change through the late Quaternary comes from inferences using indirect evidence from genetic patterns or habitat modeling. Some of the most popular tools in this realm are ecological niche models (ENMs; e.g., Phillips et al. 2006, Phillips and Dudik 2008), which can be projected through time to offer detailed estimates of past habitat suitability. In most studies, a correlation between

population size and the amount or degree of suitable habitat from ENMs is assumed but not explicitly tested or used to parameterize downstream analyses. The major exceptions to this involve spatially explicit models which explore demography by equating habitat suitability with carrying capacity (K) and thus census size (N) and effective population size (N_e ; Currat et al. 2004, Knowles and Alvarado-Serrano 2010, Ray et al. 2010, Brown and Knowles 2012); however, these methods also assume rather than evaluate a correlation between habitat suitability and demography. In order to utilize ENMs in these and other advanced ways, it is important to first establish that there is a relationship between population size and habitat suitability inasmuch as we are able to model and project it through time.

While many study systems necessarily rely on indirect reconstructions of population history, others provide extensive direct physical evidence. Some of the best sources of direct evidence are late Quaternary subfossil assemblages in western North America, including paleomiddens, caves, natural pitfall traps, and other deposits representing thousands of years of ecosystem change. Subfossil specimens can be identified through morphological or molecular methods to illustrate distributional changes through time, and they can also show phenotypic changes that may be part of a suite of reactions to climate change within a taxon (Smith et al. 1995, Barnosky and Bell 2003, Lyman and O'Brien 2005, Smith and Betancourt 2006). Western North America, and the Great Basin and Mojave deserts in particular, have a nearly unparalleled late Quaternary record of changes in small mammal communities in particular (Grayson 2006), making this an ideal region for examining how to maximize use of direct evidence in understanding demographic change through time.

Subfossils are used commonly to illustrate distributional changes or to validate models of past occupancy using presence/absence (Martinez-Meyer et al. 2004, Waltari and Guralnick 2009, de Lima et al. 2014), though the data for many assemblages also include per-species abundance as number of identified specimens (NISP). These NISPs have long been the basis of our qualitative understanding of small mammal community changes through time (Grayson 2000, 2006). The relationship between the abundance of a taxon in an assemblage and its abundance at the time of deposition is critical in the analysis of these datasets, and this relationship is likely dictated in part by the mode of deposition. For instance, many plant subfossils in the Great Basin and Mojave deserts come from paleomiddens constructed by the bushy-tailed woodrat (*Neotoma cinerea*) and desert woodrat (*N. lepida*), but because modern woodrats are biased samplers of vegetation around their houses (Dial and Czaplewski 1990), some paleoecologists avoid drawing inferences from abundance data (e.g., Nowak et al. 1994). In contrast, most of the analyzed small mammal assemblages in these regions were deposited by raptors as regurgitated pellets, which, at least in modern time, provide an accurate representation of relative small mammal numbers both within and between species (Hadly 1999, Terry 2010, Heisler et al. 2016). If we assume that all small mammal remains are affected similarly by taphonomic processes, then relative subfossil abundance from strata of any age should accurately reflect relative abundance at the time of deposition. If there is a relationship between relative abundance and absolute abundance, subfossil assemblages may be useful as quantitative indicators of population size and demographic history (e.g., Hadly et al. 2004).

Rapidly developing methods in population genetics and statistical phylogeography offer ways to test complex demographic hypotheses, but the value of these tests will always be limited by the quality of the hypotheses initially defined. The purpose of this study is to present methods for converting ENMs and subfossil assemblages into testable quantitative hypotheses, and to ultimately consider whether these sources of information are fair indicators of demographic history. I illustrate these concepts by exploring whether ENMs and subfossil abundances accurately reflect late Quaternary population size changes in two rodents, *N. cinerea* and *N. lepida*, by converting ENMs and subfossil abundances into hypotheses of effective population size, then simulating data under these demographic hypotheses (scenarios), and finally using approximate Bayesian computation (ABC) to compare the simulated genetic patterns to the current observed genetic patterns in each species.

METHODS

Study system

I focus this study on *N. cinerea* and *N. lepida*, as they are common across western North America currently and in the paleorecord, and because they have complementary climatic tolerances and thus expected reactions to climate change. The bushy-tailed woodrat (*N. cinerea*) is one of Brown's (1971) classic small montane mammals, and its large body size and heavy pelage contribute to its excellent cold tolerance (Smith 1997). The desert woodrat (*N. lepida*) is associated with relatively hotter and drier habitats, facilitated by its small body size and thin pelage. The generic expectation is that *N.*

cinerea would predominate in cooler time periods (e.g., Wisconsinan last glacial maximum [LGM] and previous Illinoian glaciation [ILL]) while *N. lepida* would predominate in warmer time periods (e.g., mid-Holocene [mHOL] and Sangamonian last interglacial [LIG]), both of which are supported qualitatively by the paleorecord (Smith et al. 1998, Grayson 2006, Smith et al. 2009). Although both species carry genetic signatures of population expansion across the Great Basin (Patton et al. 2008, Hornsby and Matocq 2012), the current data and analyses do not specify when these population expansions may have occurred (e.g., post-glacial vs. post-mHOL climatic optimum).

I defined the area of interest for analyses to include Omernik's (1995) level III ecoregions Central Basin and Range, Northern Basin and Range, and Mojave Basin and Range west of the Colorado River (Figure 1-1). Together, these areas encompass the southern extent of *N. cinerea* and northern extent of *N. lepida*, both currently and historically (Neotoma Paleoecology Database, neotomadb.org; December 2015), and includes members of only one mitochondrial clade per species: INT of *N. cinerea* (Hornsby and Matocq 2012) and 2A of *N. lepida* (Patton et al. 2008). This area of interest covers 416,659 km².

***N_e* estimation: current**

In order to convert subfossil abundances and habitat quantities into testable quantitative demographic hypotheses, I first estimated the current effective population size (N_e) for each species in the area of interest using genetic data from full contemporary mitochondrial cytochrome *b* (cytb) sequences (1143 bp). To minimize the influence of closely related animals on the genetic patterns, I excluded specimens collected from the

same location (geographic coordinates). The final datasets included sequences from previous studies as well as new sequences from museum vouchers (Appendix 1-1, Table 1-S1) totaling *N. cinerea* $n = 33$ and *N. lepida* $n = 39$. I calculated current N_e for each species from per-sequence theta (θ ; population mutation rate) and per-sequence mutation rate (μ) in the equation $N_e = \theta/\mu$, appropriate for the maternally inherited mtDNA. I used the per-sequence, strict-clock μ mean and standard deviation for *Neotoma* *cytb* from previously published work (Hornsby and Matocq 2012), and calculated Watterson's per-sequence estimate, θ_w , which outperforms most other estimators at many levels of n and θ (Wang 2005), using DnaSP v5.10 (Rozas and Rozas 1995, Librado and Rozas 2009).

N_e estimation: subfossil abundances

I identified assemblages containing *N. cinerea* and *N. lepida* through the Neotoma Paleoecology Database (neotomadb.org; January 2015) and primary literature. I narrowed this set of assemblages to those within the area of interest, and containing subfossils of both focal species dating to the recent past (< 1,000 BP): Camels Back Cave (Schmitt and Lupo 2005, Schmitt and Shaver 2005), Gatecliff Shelter (Davis et al. 1983, Grayson 1983), and Hidden Cave (Davis 1985, Grayson 1985). All of these assemblages are from mixed depositional vectors, which may include woodrats (*Neotoma* spp.), predators (particularly raptors), and humans. All dates are presented in calibrated years before present (years BP) with a reference of year 1950. I calibrated ^{14}C dates as needed using the IntCal13 curve for the northern hemisphere (Reimer et al. 2013) in Calib7.1 (calib.qub.ac.uk/calib/); when posterior date distributions were multimodal, I chose the peak with the largest relative area under the probability distribution (Reimer et al. 2013).

For strata with multiple dates, we averaged the means and combined the standard deviations as $\sqrt{(\sum i^2)/n}$.

To make the strata comparable and estimate error in number of identified specimens (NISP, including *cfs.*), I calculated rarified abundance counts (RACs) of each species in each stratum using function `rrarefy` in package *vegan* (Oksanen et al. 2016) in R (R Core Team 2016). Rarefaction consisted of 100 replicates of 100 random samples without replacement, from which I calculated mean and standard deviation of each focal species in each stratum. Because these relative subfossil abundances are dependent on the total NISP in each stratum, I discarded strata with $NISP < 100$ to exclude spurious values arising from very low sampling. To determine the effect of taxonomic level on NISPs and RACs, I also calculated RACs of the focal species relative to all mammal species and relative to only rodents (order Rodentia).

To convert the subfossil RACs into estimates of N_e for each focal species, I divided the RAC of each stratum by the RAC of the most recent stratum, yielding relative differences in RAC compared to the most recent stratum. Assuming that the RAC of the most recent stratum reflects the current population size, I then multiplied the relative RAC differences by current N_e to estimate N_e for each stratum. I carried through combined error from N_e estimation and RACs as

$$\sqrt{(var(x) + (var(y)) + (\bar{x} * var(y)) + (\bar{y} * var(x))).}$$

N_e estimation: niche models

I developed habitat suitability models using program Maxent v3.3.3k (Phillips et al. 2006, Phillips and Dudik 2008). For each taxon, I built models of current habitat suitability with the model training extent encompassing the full ranges of both species extended by a 150 km buffer (Figure 1-1A-B). Occurrence records consisted of museum collection localities downloaded from VertNet (vertnet.org, 2 Dec 2015). To match the temporal extent of the environmental layers, I removed records dating earlier than 1950. To match the precision of the environmental layers, I removed records with latitude and longitude decimal degree coordinate precision < 0.01 . Finally, I removed duplicate localities and thinned to records > 25 km apart using package *spThin* (Aiello-Lammens et al. 2015) in R.

I built a fully factorial set of 15 candidate models for each species using three different sets of the 19 Bioclim variables (Hijmans et al. 2005) at 2.5 arc-min resolution (about 3.5 km^2 at 40 degrees latitude) and five levels of the overall regularization multiplier (β , Phillips et al. 2006, Phillips and Dudik 2008; λ , Elith et al. 2011) for each species. The variable sets were (A) all 19 Bioclim variables: BIO1-19; (B) all variables that were within the training range when projected to paleoclimates in preliminary models: BIO1-4, BIO6-7; and BIO9-19; and (C) maximum number of variables from set B with $|r| < 0.7$ at occurrence points: BIO2, BIO3, BIO6, BIO7, BIO12, BIO18. To determine the optimal model tuning, I set the regularization multiplier to one of five values: 1 (default), 2, 4, or 7, or 10, similar to other studies (Warren and Seifert 2011, Radosavljevic and Anderson 2014). I maintained all other defaults in Maxent, including the auto features option allowing full flexibility to fit models with various response curves and interaction terms. I replicated each model five times, and calculated the mean

and standard deviation from the Maxent logistic outputs projected to current, mHOL (CCSM4; worldclim.org), LGM (CCSM4; worldclim.org), and LIG (Otto-Bliesner et al. 2006; worldclim.org) climate reconstructions.

Because I was equally interested in model performance for current and paleoclimatic projections, I used two metrics to guide model selection. For the current time, I calculated the corrected Akaike information criterion (AICc) from the raw Maxent output of each niche model using ENMTools v1.3 (Warren et al. 2010). For mHOL and LGM, I used a novel hindcast performance score to validate the models projected to these times. This score was designed to balance the ability of a model to predict paleorecord occurrence points against the potential for over-prediction, and relies on occurrence points determined from identified specimens in subfossil assemblages. I chose these occurrence points for each species and time from primary literature and the Neotoma Paleoecology Database, and thinned them to > 25 km, as above. I restricted mHOL points to those with a median age between 5,000 to 7,000 BP and maximum age < 11,700 BP (Pleistocene-Holocene transition), and LGM points to those with an age interval overlapping 21,000 to 25,000 BP and minimum age > 11,700; no occurrence records were available for LIG validation, therefore this score could not be calculated for that time. As needed, I calibrated ^{14}C dates as above. To calculate the hindcast performance score for each species and time, I averaged the logistic Maxent output values at the paleorecord occurrence points, and divided by the average of the logistic output values across a larger extent (-98 to -145 longitude, 22 to 66 latitude). The higher this hindcast performance score, the more precisely the model was able to predict paleorecord occurrence points relative to the larger extent. To determine the best model for each

species, I ranked all models according to the three metrics (AICc, mHOL hindcast score, LGM hindcast score), summed these ranks, and selected the single highest ranked model.

To convert the highest ranked model to demographic scenarios for each species, I first divided the calculated N_e by the average Maxent logistic output across cells in the area of interest. This yielded an estimate of current population density in relation to probability of occurrence. To determine past N_e , I multiplied this density estimate by the averaged logistic output in the area of interest during past time intervals (mHOL, LGM, and LIG). I carried through combined error from N_e estimation and Maxent logistic output standard deviation in the same manner as for RACs (see above).

Model selection: Approximate Bayesian computation

I used the program DIYABC v2.0.4 (Cornuet et al. 2014) to construct and compare the demographic hypotheses derived from the subfossil abundances and niche models. For each species, I constructed nine scenarios according to the estimates of N_e derived from various sources (Appendix 1-2). These scenarios included one null scenario (no population size change), one scenario derived from the niche model projections, five scenarios derived from the subfossil abundances, and two generic scenarios designed to represent generalized hypotheses of population size change through the late Quaternary (Fig. 2). For montane species such as *N. cinerea*, these generic scenarios involved larger populations sizes during colder glacial periods (LGM and ILL) and smaller population sizes during warmer interglacial periods (mHOL and LIG); for desert species such as *N. lepida*, the assumptions were the converse.

I simulated 1,000,000 data sets for each scenario, and used multivariate analyses of normalized summary statistics (number of haplotypes, mean pairwise difference, variance in pairwise difference, mean numbers of rarest nucleotide at segregating sites, and variance in mean number of rarest nucleotide at segregating sites) to compare the distances of the simulated data from the observed data. After restricting simulations to the closest 2% of datasets, I selected the top scenario for each species using two outputs: the direct output, showing the proportion of datasets from each demographic scenario that were in nearest n datasets (n_δ) to the observed; and the logistic regression output, which is an extension of the direct output using distances between the simulated and observed datasets as the predictor variable and scenario as the response variable. In both outputs, relatively flat lines indicate that the scenario(s) fit the data consistently across values of n_δ (Cornuet et al. 2014). For each species, I selected the scenario (hereafter, “top scenario”) with the highest posterior probability across values of n_δ .

As posterior probabilities can determine relative model fit but not quality, we compared the observed and simulated data to determine quality of fit of initial and top scenarios (Cornuet et al. 2014). In all cases, I made these comparisons by assessing the aforementioned summary statistics, either alone (univariate) or in tandem (multivariate, via principle components analysis), calculated from each dataset. To evaluate whether the initial scenarios were parameterized well enough to fit the observed data (scenario pre-evaluation; Cornuet et al. 2014), I ensured that there was univariate and multivariate overlap in observed data versus data simulated from the prior parameter distributions. To assess performance of the top scenario for each species (model checking; Cornuet et al. 2014), I ensured overlap of the prior and posterior multivariate distributions of summary

statistics from simulated data against the observed data. I also checked the top scenario by calculating different summary statistics (Tajima's D and number of private segregating sites) than those used for model selection, and determined whether the values from the observed data fell within the values of the simulated data. Finally, I evaluated type I error (confidence in model selection; Cornuet et al. 2014) by determining the proportion of instances in which a scenario other than the true model had the highest direct or logistic posterior probability. I evaluated both global (using simulations from all scenarios) and scenario-specific (using simulations from only the top scenario) confidence.

RESULTS

N_e estimation: current

The per-sequence estimates of θ_w were *N. cinerea* $\theta_w = 16.02$ and *N. lepida* $\theta_w = 26.10$. Carrying through uncertainty (standard deviation) in μ , we calculated current effective population sizes \pm standard deviation in the area of interest as *N. cinerea* $N_e = 794,335 \pm 970$ and *N. lepida* $N_e = 1,294,277 \pm 1580$. As both species show strong signals of demographic expansion (Tajima's D ; *N. cinerea* $D = -1.89$, $P < 0.05$; *N. lepida* $D = -1.91$, $P < 0.05$; Tajima 1989), these estimates of N_e are likely lower than census population size, N .

As an independent comparison for one of the two species, *Neotoma cinerea* density has been roughly estimated as one individual per 20 acres of habitat (Banfield 1974). This calculates to a census size of *N. cinerea* $N = 5,147,934$ in area of interest,

and a ratio of effective to census population size $N_e/N = 0.15$. However, suitable habitat for *N. cinerea* and other montane species constitutes a minority of this area (sensu Brown 1971, Waltari and Guralnick 2009, Hornsby and Matocq 2012), so this value of N may constitute an extreme maximum estimate of census size. Though it is still likely that $N_e/N < 1$, it is plausibly closer to 1 than 0.15.

N_e estimation: subfossil abundances

Camels Back Cave and Gatecliff Shelter had sufficient data to assess RACs relative to both total mammals and rodents only, while Hidden Cave had sufficient data only for the former. Demographic scenarios derived RACs were the most restricted temporally, with only one assemblage (Camels Back Cave) extending near the Pleistocene-Holocene transition ca. 10,000 years BP, and the others extending to the early Holocene ca. 7,000-8,000 years BP (Figure 2).

N_e estimation: niche models

The final occurrence datasets for niche modeling consisted of $n = 190$ *N. cinerea* and $n = 115$ *N. lepida* records across the full species ranges (Figure 1-1C-D), and the hindcast occurrence points in the area of interest included *N. cinerea* mHOL $n = 23$ and LGM $n = 10$ and *N. lepida* mHOL $n = 8$ and LGM $n = 3$ (Figure 1E-H) For *N. cinerea*, the best model featured variable set C and regularization multiplier of 7 (Figure 1-1C), and for *N. lepida*, the best model featured variable set C and regularization multiplier of 10 (Figure 1-1D).

Model selection: Approximate Bayesian computation

In both the direct and logistic analyses, the top scenario for *N. cinerea* was a generic scenario of demographic history (generic.1; Figure 1-3A-B) involving population expansion at the beginning of the ILL glaciation, contraction at the end of the ILL glaciation, moderate expansion at the beginning of the LGM, and contraction at the end of the LGM (Figure 2A). As the 95% highest posterior densities did not overlap, this model was significantly different from all other models across values of n_s . In pre-evaluation of *N. cinerea* scenarios, the observed data fell at the margin of scenarios in the multivariate plot of summary statistics (Appendix 1-3 Fig. 1-S1A). Considering these summary statistics individually, there were no statistics for which all scenarios exceeded the observed value in the same manner (too high or too low), and no scenarios for which > 20% of simulations exceeded the observed values of all summary statistics (Appendix 1-3 Table 1-S4). Combined, these suggest that data simulated under the defined scenarios were able to fit the observed data within reason. In model checking of the scenario generic.1, the observed data fell at the margin of the multivariate plot of prior and posterior summary statistics (not shown), and the simulated data encompassed the observed data in all univariate summary statistics (Appendix 1-3 Fig. 1-S1B). Global confidence in model selection for *N. cinerea* was high, with a type I error rate of 3.6% (direct approach) and 2.2% (logistic approach); confidence in selection of generic.1 specifically was likewise high, with error rates of 1.9% and 1.5%, respectively.

The top scenario for *N. lepida* was derived from the Camels Back Cave assemblage relative to rodent specimens (Camels.RODE; Figure 1-3C-D), and featured a brief demographic expansion in the mid-Holocene (Figure 2B). The 95% highest

posterior densities of several models overlapped in the direct analysis, while in the more powerful logistic analysis (Cornuet et al. 2014), the top scenario did not broadly overlap with any others. As with *N. cinerea*, the observed data fell at the margin of scenarios in the multivariate plot of summary statistics in scenario pre-evaluation (Appendix 1-3 Fig. 1-S1C). Considered individually, none of the scenarios resulted in > 20% of simulations exceeding the observed values of all summary statistics (Appendix 1-3 Table 1-S4). However, all scenarios showed insufficient numbers of haplotypes, with the majority of simulated datasets falling short of the observed value. This suggests that the scenarios fit the observed data only marginally well, and may not represent quality options for model selection. As with *N. cinerea*, the observed data fell at the margin of the multivariate plot of simulated prior and posterior summary statistics from the top scenario (Appendix 1-3 Fig. 1-S1D), but the simulated data from the top scenario encompassed the observed data in only three of five univariate summary statistics (Appendix 1-3 Table 1-S4). Accordingly, confidence in model selection for *N. lepida* was low, with global type I error rates of 39.5% (direct) and 42.4% (logistic). Type I error in selection of the top scenario, Camels.RODE, was 20.7% (direct) and 21.4% (logistic), with the scenario derived from Camels Back Cave relative to all mammal specimens (Camels.ALL) accounting for the majority of misspecifications.

DISCUSSION

The goal of this study was to convert ENMs and subfossil abundances to testable hypotheses of demographic history, and to determine whether they accurately reflect

demographic changes relative to genetic patterns observed in current populations. The top scenario for desert-adapted *N. lepida* was derived from subfossil abundance data but was a poor overall fit to the observed data, while neither subfossils nor ENMs closely matched patterns in montane-adapted *N. cinerea*.

The failure of these hypothesized demographic scenarios to match observed genetic patterns was surprising based on general *a priori* expectations. For *N. cinerea*, several of the demographic scenarios from both subfossil abundances and ENMs are consistent with our broad understanding of the environmental requirements of this species and the geological history of the area of interest. As a montane-associated species, *N. cinerea* is expected to have larger population sizes during relatively cool interglacial periods, and smaller population sizes during the relatively warm interglacials (Galbreath et al. 2009, Waltari and Guralnick 2009). These expectations are borne out qualitatively in most scenarios derived from ENMs and subfossil abundances (Figure 1-2A), though each scenario included only some of the *a priori* expectations, e.g., Holocene contraction (Camels.ALL, Hidden.ALL), LGM expansion (ENM), and post-LIG expansion (ENM). The fact that the top scenario (generic.1, Figure 1-2A) included several major demographic events, and covered the broadest stretch of time considered, may indicate that subfossil abundances and ENMs were simply not able to capture the demographic events or timescales that most influenced the observed genetic patterns. For *N. lepida*, the subfossil and ENM scenarios did not as uniformly reflect *a priori* expectations, with the exception of an early Holocene expansion evident in several scenarios (Camels.ALL, ENM) including the top scenario (Camels.RODE).

The common theme between the top scenarios for both species is that they each incorporate one major population expansion with timing that is biologically realistic and consistent with *a priori* expectations—post-LIG expansion in *N. cinerea*, and Holocene expansion in *N. lepida*. Population expansion leaves well-characterized patterns in genetic variation (Tajima 1989, Rogers and Harpending 1992, Fu 1997, Schneider and Excoffier 1999), making it relatively easy to identify expansions compared to population contractions. Further, genetic patterns, and in particular those derived from limited sequence data, may simply not carry strong signatures of demographic events beyond the most recent population expansion (Grant et al. 2012). In this light, the top scenarios for both species are biologically and theoretically justifiable, but the genetic data (cytb) may not have sufficient variation to capture other events in the demographic history; the rate of molecular evolution may simply be too low for the degree of temporal resolution in the demographic scenarios derived from subfossil abundances and ENMs.

Of course, the failure of a scenario to match observed data may lie in its parameters rather than the data used for assessment. An ENM may be a poor indicator of demographic history for many reasons, including technical problems like failure to develop an accurate habitat model or presence of no-analog paleoclimates (e.g., Veloz 2009), and biological phenomena such as intraspecific interactions (e.g., Gutierrez et al. 2014) or niche instability through time. Localized niche instability in particular may be a challenge in this system, as *Neotoma* species are known to change body size and thus thermal niche in response to climate change (Smith et al. 1995, Smith and Betancourt 1998, Smith et al. 1998, Smith and Betancourt 2003, 2006); however, by modeling

habitat across the full range of each species, we attempted to capture the full realized niche space and thus avoid the influence of any local climatic adaptation.

Likewise, the paleorecord may be a poor indicator of demographic history if any of several assumptions are faulty. These methods assume that each stratum was deposited over a sufficiently long time period (i.e., time averaged) to capture broad relative abundance rather than peaks and lows of multi-year population cycles (Hadly 1999, Terry 2008). They also assume that percent NISP in the assemblage is a fair indicator not only of relative abundance at the time of deposition, which is well-supported (Terry 2010, Heisler et al. 2016), but also absolute abundance which is much harder to confirm. We assume that the depositional biases, if present, are consistent across strata; for example, Homestead Cave subfossils are dominated by nocturnal species of small mammals across strata, indicating that the depositional agents (raptor species) have been consistently nocturnal and thus should not bias assemblage composition (Terry 2007). In this study, RACs calculated relative to all mammal specimens or rodents only differed slightly, indicating that choice of taxonomic level for total NISP may be unimportant in this context, and thus that there were no obvious depositional biases. Finally, in this study we treat individuals across the entire Great Basin as single populations of each species, thus the demographic hypotheses are being developed from localized information (assemblages) and tested against regional information (genetic patterns in the Great Basin). The demographic scenarios derived from the paleorecord may simply better reflect localized population dynamics, and this could be tested by comparing each assemblage to population-level genetic patterns in the immediate area rather than the entire region.

The most challenging issue in approaches like this may be difficulties in equating N and N_e . These values can differ tremendously based on a variety of factors including population history (Kalinowski and Waples 2002, Storz et al. 2002, Shrimpton and Heath 2003, Palstra and Fraser 2012), and when $N_e/N \neq 1$, analyses using either as an estimate of the other will be skewed. The best estimate, $N_e/N = 0.15$ (in *N. cinerea*), may actually be much closer to 1 depending on how much of the area of interest is considered suitable habitat, so the use of N_e and N interchangeably could be supported in this case. However, it will be important for future work either to verify that $N_e/N \approx 1$, or to adjust population size estimates based on this calculated or expected ratio (e.g., Hadly et al. 2004).

Despite the issues raised, this study provides useful points of departure for converting independent sources of information into quantitative hypotheses of demographic history. Methods for converting ENMs to hypotheses of demographic history will be applicable across study systems. If applied broadly, tests of the relationship between habitat suitability and demography on a biogeographic scale may help us understand whether ENMs are accurate indicators of population history, and if not, what factors prevent them from being so. Methods for converting subfossil abundances will be applicable in regions such as western North American, for which such data are available. Fortunately, accessibility of these data are improving through efforts such as Neotoma Paleoecology Database (neotomadb.org), making the practice of deriving demographic hypotheses from these records easier and potentially more rigorous. As we attempt to formulate biologically plausible hypotheses for statistical phylogeography and biogeography, it will become more important to understand the benefits and limitations of both indirect (e.g., ENM) and direct (e.g., subfossil

assemblage) indicators of population histories, and to explore ways of combining these to create more robust reconstructions of demographic history.

REFERENCES

- Aiello-Lammens, M. E., et al. 2015. *spThin*: an R package for spatial thinning of species occurrence records for use in ecological niche models. - *Ecography* 38: 541-545.
- Banfield, A. W. F. 1974. *The Mammals of Canada*. - University of Toronto Press.
- Barnosky, A. D. and Bell, C. J. 2003. Evolution, climatic change and species boundaries: perspectives from tracing *Lemmys curtatus* populations through time and space. - *Proceedings of the Royal Society of London Series B-Biological Sciences* 270: 2585-2590.
- Beaumont, M. A. 2010. Approximate Bayesian computation in evolution and ecology. - *Annual Review of Ecology, Evolution, and Systematics*, Vol 41 41: 379-406.
- Brown, J. H. 1971. Mammals on mountaintops - nonequilibrium insular biogeography. - *American Naturalist* 105: 467-&.
- Brown, J. L. and Knowles, L. L. 2012. Spatially explicit models of dynamic histories: examination of the genetic consequences of Pleistocene glaciation and recent climate change on the American Pika. - *Molecular Ecology* 21: 3757-3775.
- Carstens, B. C., et al. 2013. Model selection as a tool for phylogeographic inference: an example from the willow *Salix melanopsis*. - *Molecular Ecology* 22: 4014-4028.
- Cornuet, J. M., et al. 2014. DIYABC v2.0: a software to make Approximate Bayesian Computation inferences about population history using single nucleotide polymorphism, DNA sequence and microsatellite data. - *Bioinformatics* 30: 1187-1189.
- Curat, M., et al. 2004. SPLATCHE: a program to simulate genetic diversity taking into account environmental heterogeneity. - *Molecular Ecology Notes* 4: 139-142.
- Davis, J. O., et al. 1983. Geology of Gatecliff Shelter: physical stratigraphy. - In: D. H. Thomas (ed) *The archaeology of Monitor Valley: 2. Gatecliff Shelter*. pp. 39-63.
- Davis, J. O. 1985. Sediments and geological setting of Hidden Cave. - In: D. H. Thomas (ed) *The archaeology of Hidden Cave, Nevada*. pp. 80-103.
- de Lima, N. E., et al. 2014. Phylogeography and ecological niche modelling, coupled with the fossil pollen record, unravel the demographic history of a Neotropical swamp palm through the Quaternary. - *Journal of Biogeography* 41: 673-686.
- Dial, K. P. and Czaplewski, N. J. 1990. Do woodrat middens accurately represent the animals' environments and diets? The Woodhouse Mesa study. - In: J. L. Betancourt, et al. (eds), *Packrat middens: the last 40,000 years of biotic change*. University of Arizona Press, pp. 43-58.
- Elith, J., et al. 2011. A statistical explanation of MaxEnt for ecologists. - *Diversity and Distributions* 17: 43-57.
- Forester, B. R., et al. 2013. Integrating ensemble species distribution modelling and statistical phylogeography to inform projections of climate change impacts on species distributions. - *Diversity and Distributions* 19: 1480-1495.
- Fu, Y. X. 1997. Statistical tests of neutrality of mutations against population growth, hitchhiking and background selection. - *Genetics* 147: 915-925.
- Galbreath, K. E., et al. 2009. When cold is better: climate-driven elevation shifts yield complex patterns of diversification and demography in an alpine specialist (American pika, *Ochotona princeps*). - *Evolution* 63: 2848-2863.

- Galbreath, K. E., et al. 2010. Isolation and introgression in the Intermountain West: contrasting gene genealogies reveal the complex biogeographic history of the American pika (*Ochotona princeps*). - *Journal of Biogeography* 37: 344-362.
- Grant, W. S., et al. 2012. Limits of Bayesian skyline plot analysis of mtDNA sequences to infer historical demographies in Pacific herring (and other species). - *Molecular Phylogenetics and Evolution* 65: 203-212.
- Grayson, D. K. 1983. The archaeology of Monitor Valley, 2. Gatecliff Shelter, Paleontology of Gatecliff Shelter: Small mammals. - *Anthropological Papers of the American Museum of Natural History* 59: 1-552.
- Grayson, D. K. 1985. The paleontology of Hidden Cave: Birds and mammals. - In: D. H. Thomas (ed) *The Archaeology of Hidden Cave, Nevada*. *Anthropological Papers of the American Museum of Natural History*, pp. 125-161.
- Grayson, D. K. 2000. Mammalian responses to Middle Holocene climatic change in the Great Basin of the western United States. - *Journal of Biogeography* 27: 181-192.
- Grayson, D. K. 2006. The Late Quaternary biogeographic histories of some Great Basin mammals (western USA). - *Quaternary Science Reviews* 25: 2964-2991.
- Gutierrez, E. E., et al. 2014. Can biotic interactions cause allopatry? Niche models, competition, and distributions of South American mouse opossums. - *Ecography* 37: 741-753.
- Hadly, E. A. 1999. Fidelity of terrestrial vertebrate fossils to a modern ecosystem. - *Palaeogeography Palaeoclimatology Palaeoecology* 149: 389-409.
- Hadly, E. A., et al. 2004. Genetic response to climatic change: Insights from ancient DNA and phylogenetics. - *Plos Biology* 2: 1600-1609.
- Heisler, L. M., et al. 2016. Owl pellets: a more effective alternative to conventional trapping for broad-scale studies of small mammal communities. - *Methods in Ecology and Evolution* 7: 96-103.
- Hijmans, R. J., et al. 2005. Very high resolution interpolated climate surfaces for global land areas. - *International Journal of Climatology* 25: 1965-1978.
- Hornsby, A. D. and Matocq, M. D. 2012. Differential regional response of the bushy-tailed woodrat (*Neotoma cinerea*) to late Quaternary climate change. - *Journal of Biogeography* 39: 289-305.
- Kalinowski, S. T. and Waples, R. S. 2002. Relationship of effective to census size in fluctuating populations. - *Conservation Biology* 16: 129-136.
- Knowles, L. L. 2009. Statistical Phylogeography. - *Annual Review of Ecology and Systematics* 40: 593-612.
- Knowles, L. L. and Alvarado-Serrano, D. F. 2010. Exploring the population genetic consequences of the colonization process with spatio-temporally explicit models: insights from coupled ecological, demographic and genetic models in montane grasshoppers. - *Molecular Ecology* 19: 3727-3745.
- Librado, P. and Rozas, J. 2009. DnaSP v5: a software for comprehensive analysis of DNA polymorphism data. - *Bioinformatics* 25: 1451-1452.
- Lyman, R. L. and O'Brien, M. J. 2005. Within-taxon morphological diversity in late-quaternary *Neotoma* as a paleoenvironmental indicator, Bonneville Basin, Northwestern Utah, USA. - *Quaternary Research* 63: 274-282.

- Martinez-Meyer, E., et al. 2004. Ecological niches as stable distributional constraints on mammal species, with implications for Pleistocene extinctions and climate change projections for biodiversity. - *Global Ecology and Biogeography* 13: 305-314.
- Nowak, C. L., et al. 1994. A 30000 year record of vegetation dynamics at a semiarid locale in the Great Basin. - *Journal of Vegetation Science* 5: 579-590.
- Oksanen, J., et al. 2016. *vegan: Community Ecology Package*.
- Omernik, J. M. 1995. Ecoregions: a spatial framework for environmental management. - In: W. S. Davis and T. P. Simon (eds), *Biological assessment and criteria: tools for water resource planning and decision making*. Lewis Publishers, pp. 49-62.
- Otto-Bliesner, B. L., et al. 2006. Simulating arctic climate warmth and icefield retreat in the last interglaciation. - *Science* 311: 1751-1753.
- Palstra, F. P. and Fraser, D. J. 2012. Effective/census population size ratio estimation: a compendium and appraisal. - *Ecology and Evolution* 2: 2357-2365.
- Patton, J. L., et al. 2008. The evolutionary history and a systematic revision of woodrats of the *Neotoma lepida* group. - *UC Publications in Zoology* 135: 1-411.
- Pelletier, T. A. and Carstens, B. C. 2014. Model choice for phylogeographic inference using a large set of models. - *Molecular Ecology* 23: 3028-3043.
- Phillips, S. J., et al. 2006. Maximum entropy modeling of species geographic distributions. - *Ecological Modelling* 190: 231-259.
- Phillips, S. J. and Dudik, M. 2008. Modeling of species distributions with Maxent: new extensions and a comprehensive evaluation. - *Ecography* 31: 161-175.
- R Core Team 2016. *R: A Language and Environment for Statistical Computing*. - In: R Foundation for Statistical Computing.
- Radosavljevic, A. and Anderson, R. P. 2014. Making better MAXENT models of species distributions: complexity, overfitting and evaluation. - *Journal of Biogeography* 41: 629-643.
- Ray, N., et al. 2010. SPLATCHE2: a spatially explicit simulation framework for complex demography, genetic admixture and recombination. - *Bioinformatics* 26: 2993-2994.
- Reimer, P. J., et al. 2013. IntCal13 and Marine13 radiocarbon age calibration curves 0-50,000 years cal bp. - *Radiocarbon* 55: 1869-1887.
- Rogers, A. R. and Harpending, H. 1992. Population-growth makes waves in the distribution of pairwise genetic-differences. - *Molecular Biology and Evolution* 9: 552-569.
- Rozas, J. and Rozas, R. 1995. DnaSP, DNA sequence polymorphism: An interactive program for estimating population genetics parameters from DNA sequence data. - *Computer Applications in the Biosciences* 11: 621-625.
- Schmitt, D. N. and Lupo, K. D. 2005. The Camels Back Cave Mammalian Fauna. - In: D. N. Schmitt and D. B. Madsen (eds), *Camels Back Cave*. University of Utah Anthropological Papers, pp. 136-176.
- Schmitt, D. N. and Shaver, M. W. 2005. Site Stratigraphy and Chronology. - In: D. N. Schmitt and D. B. Madsen (eds), *Camels Back Cave*. University of Utah Anthropological Papers, pp. 46-58.

- Schneider, S. and Excoffier, L. 1999. Estimation of past demographic parameters from the distribution of pairwise differences when the mutation rates vary among sites: Application to human mitochondrial DNA. - *Genetics* 152: 1079-1089.
- Shrimpton, J. M. and Heath, D. D. 2003. Census vs. effective population size in Chinook salmon: large- and small-scale environmental perturbation effects. - *Molecular Ecology* 12: 2571-2583.
- Smith, F. A., et al. 1995. Evolution of body-size in the woodrat over the past 25,000 years of climate-change. - *Science* 270: 2012-2014.
- Smith, F. A. 1997. *Neotoma cinerea*. - *Mammalian Species* 564: 1-8.
- Smith, F. A. and Betancourt, J. L. 1998. Response of bushy-tailed woodrats (*Neotoma cinerea*) to late Quaternary climatic change in the Colorado Plateau. - *Quaternary Research* 50: 1-11.
- Smith, F. A., et al. 1998. The influence of climate change on the body mass of woodrats (*Neotoma*) in an arid region of New Mexico, USA. - *Ecography* 21: 140-148.
- Smith, F. A. and Betancourt, J. L. 2003. The effect of Holocene temperature fluctuations on the evolution and ecology of *Neotoma* (woodrats) in Idaho and northwestern Utah. - *Quaternary Research* 59: 160-171.
- Smith, F. A. and Betancourt, J. L. 2006. Predicting woodrat (*Neotoma*) responses to anthropogenic warming from studies of the palaeomidden record. - In, pp. 2061-2076.
- Smith, F. A., et al. 2009. A tale of two species: Extirpation and range expansion during the late Quaternary in an extreme environment. - *Global and Planetary Change* 65: 122-133.
- Spaeth, P. A., et al. 2009. Phylogeography of *Microtus longicaudus* in the tectonically and glacially dynamic central Rocky Mountains. - *Journal of Mammalogy* 90: 571-584.
- Storz, J. F., et al. 2002. Genetic effective size of a wild primate population: influence of current and historical demography. - *Evolution* 56: 817-829.
- Tajima, F. 1989. The effect of change in population-size on DNA polymorphism. - *Genetics* 123: 597-601.
- Terry, R. C. 2007. Inferring predator identity from skeletal damage of small-mammal prey remains. - *Evolutionary Ecology Research* 9: 199-219.
- Terry, R. C. 2008. Modeling the effects of predation, prey cycling, and time averaging on relative abundance in raptor-generated small mammal death assemblages. - *Palaios* 23: 402-410.
- Terry, R. C. 2010. The dead do not lie: using skeletal remains for rapid assessment of historical small-mammal community baselines. - *Proceedings of the Royal Society B-Biological Sciences* 277: 1193-1201.
- Van Tuinen, M., et al. 2008. Fire and ice: genetic structure of the Uinta ground squirrel (*Spermophilus armatus*) across the Yellowstone hotspot. - *Molecular Ecology* 17: 1776-1788.
- Veloz, S. D. 2009. Spatially autocorrelated sampling falsely inflates measures of accuracy for presence-only niche models. - *Journal of Biogeography* 36: 2290-2299.

- Waltari, E. and Guralnick, R. P. 2009. Ecological niche modelling of montane mammals in the Great Basin, North America: examining past and present connectivity of species across basins and ranges. - *Journal of Biogeography* 36: 148-161.
- Wang, J. L. 2005. Estimation of effective population sizes from data on genetic markers. - *Philosophical Transactions of the Royal Society B-Biological Sciences* 360: 1395-1409.
- Warren, D. L., et al. 2010. ENMTools: a toolbox for comparative studies of environmental niche models. - *Ecography* 33: 607-611.
- Warren, D. L. and Seifert, S. N. 2011. Ecological niche modeling in Maxent: the importance of model complexity and the performance of model selection criteria. - *Ecological Applications* 21: 335-342.

FIGURES

Figure 1-1. Ranges, occurrence records, and ecological niche models for *Neotoma cinerea* and *N. lepida*, with the area of interest outlined in red. (A-B) Location of genetic samples (white circles), paleoecological assemblages (black squares; C, Camels Back Cave; H, Hidden Cave; G, Gatecliff Shelter), species ranges (grey shade), and buffered range extent used for niche modeling (dotted line). (C-D) Current occurrence records (white circles) used for niche modeling, and current niche models with darker shade indicating higher habitat suitability. (E-F) mHOL occurrence records, and niche models projected to mHOL climate. (G-H) LGM occurrence records, and niche models projected to LGM climate. (I-J) Niche models projected to LIG climate.

Figure 1-2. Scenarios of change in effective population size (N_e) for (A) *N. cinerea* and (B) *N. lepida*, derived from subfossil abundances (RACs) and ecological niche models (ENMs). Solid lines show N_e for each scenario, and dotted lines show the minimum and maximum (± 2 standard deviations) of the distributions used for modeling.

Figure 1-3. Posterior probabilities of demographic scenarios for (A-B) *N. cinerea* and (C-D) *N. lepida* across values of n (number of closest simulations to the observed data). For both direct and logistic regression plots, posterior probabilities are reported for ten levels of n , with 95% highest posterior densities shaded.

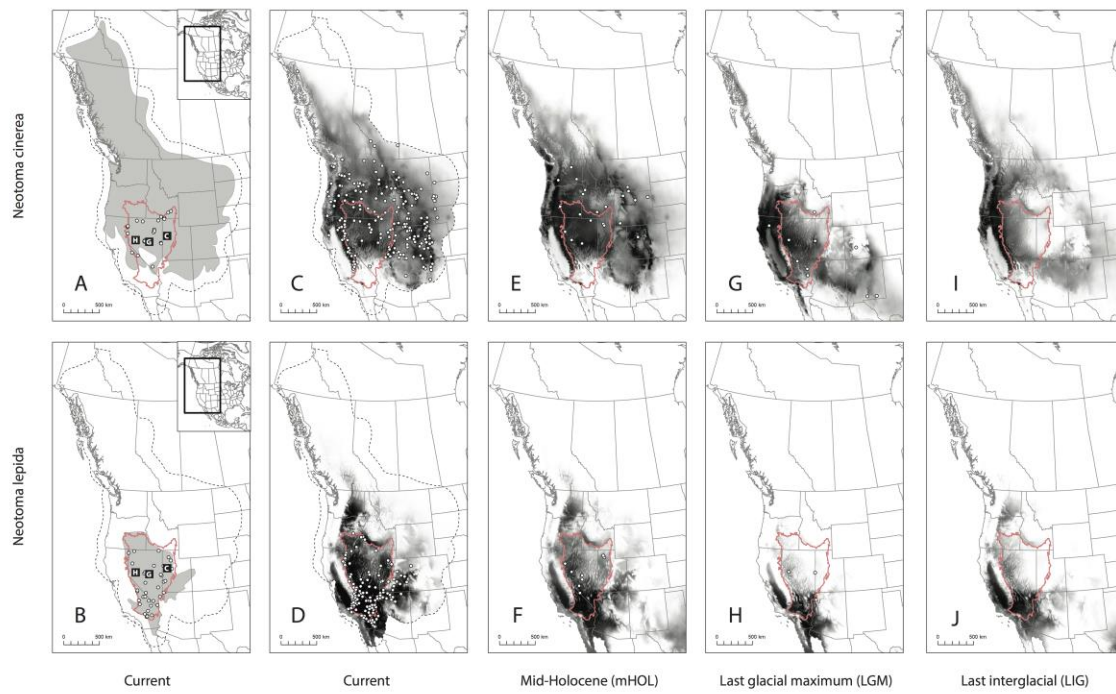


Figure 1-1.

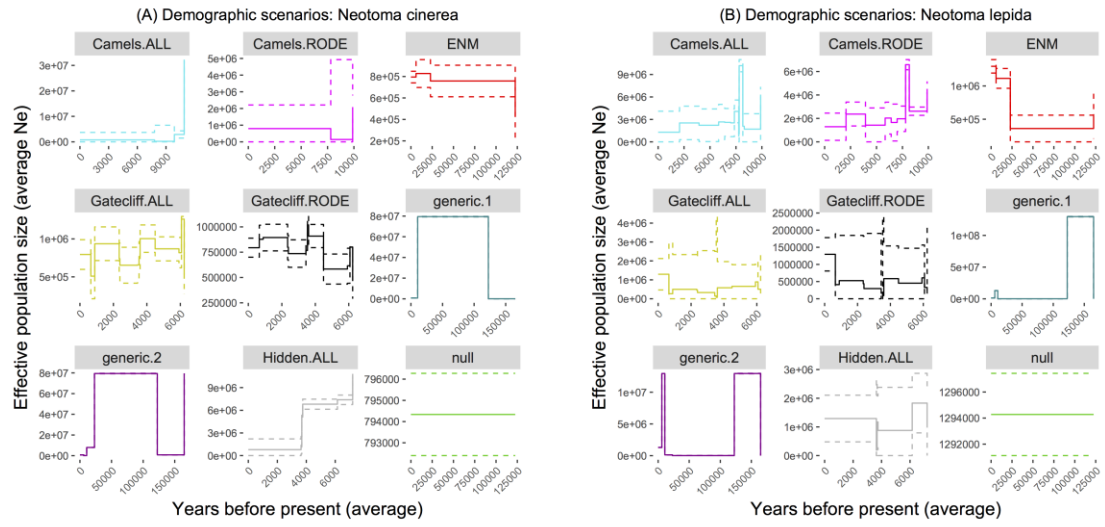


Figure 1-2.

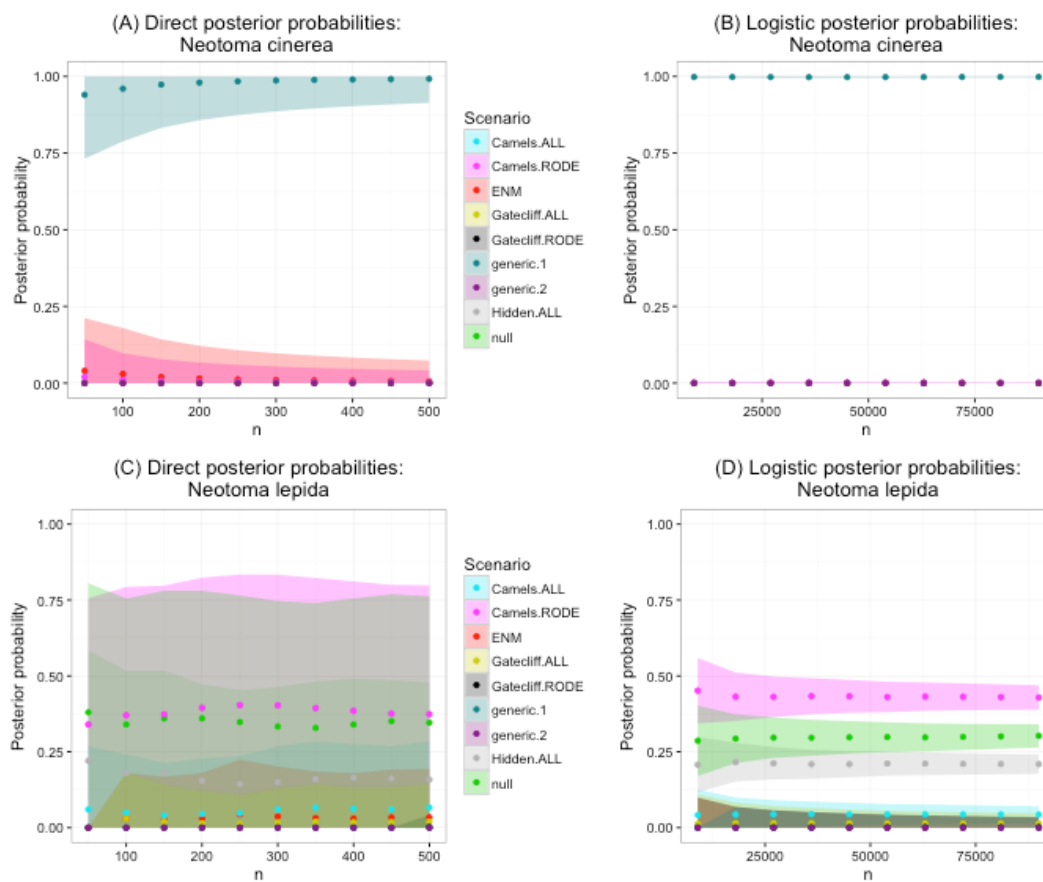


Figure 1-3.

APPENDIX 1-1

Table 1-S1. Genetic samples (specimens or isolates) of *Neotoma cinerea* ($n = 33$) and *N. lepida* ($n = 39$) in the area of interest.

Species	GUID or ID	Latitude	Longitude	GenBank	Reference
<i>N. cinerea</i>	FMNH:Mamm:198278	40.6828	-115.4915	[pending]	this study
<i>N. cinerea</i>	MSB:Mamm:155343	41.9529	-113.6765	[pending]	this study
<i>N. cinerea</i>	MSB:Mamm:224521	42.2033	-114.2725	[pending]	this study
<i>N. cinerea</i>	MVZ:Mamm:197090	40.1035	-120.0801	[pending]	this study
<i>N. cinerea</i>	MVZ:Mamm:197092	41.7600	-114.7807	JN593150	Hornsby & Matocq 2012
<i>N. cinerea</i>	MVZ:Mamm:216409	37.8708	-119.1613	JN593155	Hornsby & Matocq 2012
<i>N. cinerea</i>	MVZ:Mamm:218378	40.8884	-120.1811	JN593156	Hornsby & Matocq 2012
<i>N. cinerea</i>	MVZ:Mamm:218379	40.9664	-120.1375	JQ241193	Hornsby & Matocq 2012
<i>N. cinerea</i>	MVZ:Mamm:219950	37.5310	-118.1651	JN593157	Hornsby & Matocq 2012
<i>N. cinerea</i>	MVZ:Mamm:223394	39.2191	-117.1304	JN593165	Hornsby & Matocq 2012
<i>N. cinerea</i>	MVZ:Mamm:223395	39.2262	-117.1409	JN593166	Hornsby & Matocq 2012
<i>N. cinerea</i>	MVZ:Mamm:223396	39.1144	-114.3005	JQ241195	Hornsby & Matocq 2012
<i>N. cinerea</i>	MVZ:Mamm:223397	39.1144	-114.2995	JN593167	Hornsby & Matocq 2012
<i>N. cinerea</i>	MVZ:Mamm:223398	39.1170	-114.3042	JN593168	Hornsby & Matocq 2012
<i>N. cinerea</i>	MVZ:Mamm:223399	39.1174	-114.3038	JQ241196	Hornsby & Matocq 2012
<i>N. cinerea</i>	MVZ:Mamm:223401	42.6840	-112.9785	JN593169	Hornsby & Matocq 2012
<i>N. cinerea</i>	MVZ:Mamm:223402	41.6210	-117.5461	JQ241198	Hornsby & Matocq 2012
<i>N. cinerea</i>	MVZ:Mamm:223403	41.6197	-117.5452	JN593170	Hornsby & Matocq 2012
<i>N. cinerea</i>	MVZ:Mamm:223404	41.6212	-117.5460	JN593171	Hornsby & Matocq 2012
<i>N. cinerea</i>	MVZ:Mamm:223434	36.2538	-115.6482	JN593186	Hornsby & Matocq 2012
<i>N. cinerea</i>	MVZ:Mamm:228371	40.0919	-120.0882	[pending]	this study
<i>N. cinerea</i>	UMNH:Mamm:29794	39.0227	-114.2656	JN593219	Hornsby & Matocq 2012
<i>N. cinerea</i>	UMNH:Mamm:31873	40.3454	-115.5954	JQ241234	Hornsby & Matocq 2012
<i>N. cinerea</i>	UMNH:Mamm:32202	40.6881	-115.4707	JN593222	Hornsby & Matocq 2012
<i>N. cinerea</i>	UMNH:Mamm:32653	40.5129	-115.4349	JQ241237	Hornsby & Matocq 2012
<i>N. cinerea</i>	UMNH:Mamm:32867	39.2540	-117.1636	[pending]	this study
<i>N. cinerea</i>	UMNH:Mamm:33300	39.2942	-117.1159	[pending]	this study
<i>N. cinerea</i>	UMNH:Mamm:33496	39.3188	-117.1222	[pending]	this study
<i>N. cinerea</i>	UMNH:Mamm:33592	39.3055	-117.1186	[pending]	this study
<i>N. cinerea</i>	UMNH:Mamm:33738	39.3416	-117.1292	[pending]	this study
<i>N. cinerea</i>	UMNH:Mamm:35391	41.6747	-118.5986	[pending]	this study
<i>N. cinerea</i>	UWBM:Mamm:79658	42.0812	-113.6817	JN593237	Hornsby & Matocq 2012
<i>N. cinerea</i>	182cytb	42.8713	-112.4455	JN593122	Hornsby & Matocq 2012
<i>N. lepida</i>	BYUunk10	40.7922	-112.5251	[pending]	this study
<i>N. lepida</i>	BYUunk9	38.2750	-113.8203	[pending]	this study
<i>N. lepida</i>	FMNH:Mamm:168474	38.9939	-114.1720	[pending]	this study
<i>N. lepida</i>	FMNH:Mamm:179415	41.1614	-112.9352	[pending]	this study
<i>N. lepida</i>	MSB:Mamm:157045	36.4254	-117.1947	[pending]	this study

<i>N. lepida</i>	MSB:Mamm:76962	38.3603	-113.5247	[pending]	this study
<i>N. lepida</i>	MSB:Mamm:86623	40.1656	-113.8397	[pending]	this study
<i>N. lepida</i>	MVZ:Mamm:192239	35.9731	-116.2703	[pending]	this study
<i>N. lepida</i>	MVZ:Mamm:195245	35.4748	-114.8558	[pending]	this study
<i>N. lepida</i>	MVZ:Mamm:195266	35.5554	-117.7257	[pending]	this study
<i>N. lepida</i>	MVZ:Mamm:195277	37.0716	-118.2558	[pending]	this study
<i>N. lepida</i>	MVZ:Mamm:195289	37.1713	-118.2118	[pending]	this study
<i>N. lepida</i>	MVZ:Mamm:195291	36.9092	-116.7861	[pending]	this study
<i>N. lepida</i>	MVZ:Mamm:195307	36.9089	-116.7861	[pending]	this study
<i>N. lepida</i>	MVZ:Mamm:195311	35.3842	-115.8948	[pending]	this study
<i>N. lepida</i>	MVZ:Mamm:195313	34.7647	-116.3773	[pending]	this study
<i>N. lepida</i>	MVZ:Mamm:195324	34.0981	-116.4914	[pending]	this study
<i>N. lepida</i>	MVZ:Mamm:197126	41.9469	-114.6916	DQ179838	Matocq et al. 2007
<i>N. lepida</i>	MVZ:Mamm:197130	37.5927	-114.7598	DQ781219	Patton et al. 2008
<i>N. lepida</i>	MVZ:Mamm:197160	41.5827	-120.0325	[pending]	this study
<i>N. lepida</i>	MVZ:Mamm:197165	40.3579	-119.2844	DQ781218	Patton et al. 2008
<i>N. lepida</i>	MVZ:Mamm:197167	41.8157	-119.0950	DQ781220	Patton et al. 2008
<i>N. lepida</i>	MVZ:Mamm:197178	34.0419	-116.5853	[pending]	this study
<i>N. lepida</i>	MVZ:Mamm:198670	34.3627	-116.8563	[pending]	this study
<i>N. lepida</i>	MVZ:Mamm:199362	36.9831	-113.8202	DQ781214	Patton et al. 2008
<i>N. lepida</i>	MVZ:Mamm:199364	38.1020	-116.9102	DQ781215	Patton et al. 2008
<i>N. lepida</i>	MVZ:Mamm:199803	34.2441	-115.7206	DQ781191	Patton et al. 2008
<i>N. lepida</i>	MVZ:Mamm:199811	34.1514	-116.4791	[pending]	this study
<i>N. lepida</i>	MVZ:Mamm:202458	35.9766	-117.9200	[pending]	this study
<i>N. lepida</i>	MVZ:Mamm:202485	36.4738	-114.4533	DQ781221	Patton et al. 2008
<i>N. lepida</i>	MVZ:Mamm:202545	34.1054	-116.4934	[pending]	this study
<i>N. lepida</i>	MVZ:Mamm:223464	35.9674	-115.5428	[pending]	this study
<i>N. lepida</i>	MVZ:Mamm:223466	39.1167	-114.3040	[pending]	this study
<i>N. lepida</i>	UMNH:Mamm:31818	40.1640	-115.5040	[pending]	this study
<i>N. lepida</i>	UMNH:Mamm:31937	39.7901	-112.3639	[pending]	this study
<i>N. lepida</i>	JRG966	36.4580	-116.8700	[pending]	this study
<i>N. lepida</i>	UMNH:Mamm:32868	39.2357	-117.1569	[pending]	this study
<i>N. lepida</i>	UMNH:Mamm:34352	39.3768	-117.0065	[pending]	this study
<i>N. lepida</i>	PL-NELE	39.8825	-119.6128	[pending]	this study

APPENDIX 1-2

Parameters for nine scenarios of population history in *Neotoma cinera* and *N. lepida*.

SCENARIOS AND PARAMETERS: *Neotoma cinerea***scenario 1: null**

Ne

0 sample 1

tHi varNe 1 Ne

tWg varNe 1 Ne

tSi varNe 1 Ne

scenario 2: ENM

Neb

0 sample 1

tHi varNe 1 Nb1

tWg varNe 1 Nb2

tSi varNe 1 Neb3

scenario 3: Camels-ALL

Nec

0 sample 1

tC31 varNe 1 Nc1

tC32 varNe 1 Nc2

tC33 varNe 1 Nc3

scenario 4: Camels-RODE

Ned

0 sample 1

tC31 varNe 1 Nd1

tC32 varNe 1 Nd2

scenario 5: Gatecliff-ALL

Nee

0 sample 1

tG02 varNe 1 Ne1

tG03 varNe 1 Ne2

tG05 varNe 1 Ne3

tG06 varNe 1 Ne4
 tG08 varNe 1 Ne5
 tG10 varNe 1 Ne6
 tG12 varNe 1 Ne7
 tG13 varNe 1 Ne8
 tG17 varNe 1 Ne9
 tG22 varNe 1 Ne10
 tG23 varNe 1 Ne11

scenario 6: Gatecliff-RODE

Nef

0 sample 1

tG02 varNe 1 Nf1
 tG03 varNe 1 Nf2
 tG05 varNe 1 Nf3
 tG06 varNe 1 Nf4
 tG08 varNe 1 Nf5
 tG10 varNe 1 Nf6
 tG12 varNe 1 Nf7
 tG13 varNe 1 Nf8
 tG17 varNe 1 Nf9
 tG22 varNe 1 Nf10
 tG23 varNe 1 Nf11

scenario 7: Hidden-ALL

Neg

0 sample 1

tH02 varNe 1 Ng1
 tH03 varNe 1 Ng2
 tH04 varNe 1 Ng3
 tH05 varNe 1 Ng4
 tH07 varNe 1 Ng5

scenario 8: generic.1

Ne

0 sample 1

tHi varNe 1 Ne
 tWH varNe 1 Nemagmag
 tWg varNe 1 Nemagmag
 tSi varNe 1 Neumag
 tIg varNe 1 Neumag

scenario 9: generic.2

Ne

0 sample 1

tHi varNe 1 Neumag
tWH varNe 1 Nemag
tWg varNe 1 Nemagmag
tSi varNe 1 Ne
tIg varNe 1 Nemagmag

Table 1-S2. Parameter prior values and distributions for *N. cinerea*. For normal priors, min and max were set to +/- 2 standard deviations.

Parameter	Prior shape	Min Ne	Max Ne	Mean Ne	Stdev Ne
Ne	normal	792395	796275	794335	970
tHi	uniform	4500	7500		
tWg	uniform	21000	25000		
tSi	uniform	115000	130000		
Neb	normal	740345	848325	794335	26995
Nb1	normal	697385	957049	827217	64916
Nb2	normal	610861	904353	757607	73373
Nb3	normal	190208	669242	429725	119759
tC31	uniform	7679	7930		
tC32	uniform	9603	10155		
tC33	uniform	10710	11110		
Nec	normal	0	3715782	794335	1460723
Nc1	normal	0	6527038	207218	3159910
Nc2	normal	1485731	4316368	2901050	707659
Nc3	normal	31339320	32276552	31807936	234308
Ned	normal	0	2209637	794335	707651
Nd1	normal	0	4931869	141846	2395012
Nd2	normal	1390384	2779874	2085129	347373
tG02	normal	609	699	654	23
tG03	normal	698	1076	887	95
tG05	normal	2325	2367	2346	11
tG06	normal	2306	2476	2391	43
tG08	normal	3356	3526	3441	43
tG10	normal	3428	3634	3531	52
tG12	normal	3514	3680	3597	42
tG13	normal	4380	4606	4493	57
tG17	normal	5853	5983	5918	33
tG22	normal	6117	6347	6232	58
tG23	normal	5767	6375	6071	152
Nee	normal	598961	989709	794335	97687
Ne1	normal	212156	806349	509252	148548
Ne2	normal	714672	1157708	936190	110759
Ne3	normal	530594	948324	739459	104433
Ne4	normal	417644	890059	653852	118104
Ne5	normal	423609	892874	658242	117316
Ne6	normal	573067	964568	768818	97875
Ne7	normal	823716	1184758	1004237	90260
Ne8	normal	710795	1027139	868967	79086

Ne9	normal	618539	1019520	819029	100245
Ne10	normal	270318	805258	537788	133735
Ne11	normal	1224904	1295566	1260235	17666
Nef	normal	700306	888364	794335	47015
Nf1	normal	739400	1016445	877923	69261
Nf2	normal	762779	1025767	894273	65747
Nf3	normal	675877	920134	798006	61064
Nf4	normal	600694	872188	736441	67873
Nf5	normal	765599	769348	767473	937
Nf6	normal	935410	1102732	1019071	41831
Nf7	normal	794561	1023350	908955	57197
Nf8	normal	435420	731807	583613	74097
Nf9	normal	443130	788832	615981	86426
Nf10	normal	290393	649261	469827	89717
Nf11	normal	798886	802798	800842	978
tH02	uniform	3600	3680		
tH03	uniform	3680	3700		
tH04	uniform	3700	3800		
tH05	uniform	5400	6900		
tH07	uniform	6900	7500		
Neg	normal	0	2209637	794335	707651
Ng1	normal	201415	2550388	1375902	587243
Ng2	normal	4880156	5814997	5347577	233710
Ng3	normal	6144762	7472410	6808586	331912
Ng4	normal	6761389	8018916	7390152	314382
Ng5	normal	10042611	10893790	10468201	212795
Nemagmag	normal	79239500	79627500	79433500	97000
tIg	uniform	130000	200000		
tWH	uniform	10000	11500		
Neumag	normal	79240	79628	79434	97
Nemag	normal	7923950	7962750	7943350	9700

SCENARIOS AND PARAMETERS: *Neotoma lepida***scenario 1: null**

Ne

0 sample 1

tHi varNe 1 Ne

tWg varNe 1 Ne

tSi varNe 1 Ne

scenario 2: ENM

Neb

0 sample 1

tHi varNe 1 Nb1

tWg varNe 1 Nb2

tSi varNe 1 Nb3

scenario 3: Camels-ALL

Nec

0 sample 1

tC09 varNe 1 Nc1

tC11 varNe 1 Nc2

tC20 varNe 1 Nc3

tC23 varNe 1 Nc4

tC24 varNe 1 Nc5

tC26 varNe 1 Nc6

tC28 varNe 1 Nc7

tC29 varNe 1 Nc8

tC30 varNe 1 Nc9

tC31 varNe 1 Nc10

tC32 varNe 1 Nc11

scenario 4: Camels-RODE

Ned

0 sample 1

tC09 varNe 1 Nd1

tC11 varNe 1 Nd2

tC20 varNe 1 Nd3

tC23 varNe 1 Nd4

tC24 varNe 1 Nd5

tC29 varNe 1 Nd6

tC31 varNe 1 Nd7

tC32 varNe 1 Nd8

scenario 5: Gatecliff-ALL

Nee

0 sample 1

tG02 varNe 1 Ne1

tG03 varNe 1 Ne2

tG05 varNe 1 Ne3

tG06 varNe 1 Ne4

tG08 varNe 1 Ne5

tG10 varNe 1 Ne6

tG12 varNe 1 Ne7

tG13 varNe 1 Ne8

tG17 varNe 1 Ne9

tG22 varNe 1 Ne10

tG23 varNe 1 Ne11

scenario 6: Gatecliff-RODE

Nef

0 sample 1

tG02 varNe 1 Nf1

tG03 varNe 1 Nf2

tG05 varNe 1 Nf3

tG06 varNe 1 Nf4

tG08 varNe 1 Nf5

tG10 varNe 1 Nf6

tG12 varNe 1 Nf7

tG13 varNe 1 Nf8

tG17 varNe 1 Nf9

tG22 varNe 1 Nf10

tG23 varNe 1 Nf11

scenario 7: Hidden-ALL

Neg

0 sample 1

tH02 varNe 1 Ng1

tH03 varNe 1 Ng2

tH04 varNe 1 Ng3

tH05 varNe 1 Ng4

tH07 varNe 1 Ng5

scenario 8: generic.1

Ne

0 sample 1

tHi varNe 1 Nemag

tWH varNe 1 Neumag

tWg varNe 1 Neumag

tSi varNe 1 Nemagmag
tIg varNe 1 Neumag

scenario 9: generic.2

Ne

0 sample 1

tHi varNe 1 Nemag

tWH varNe 1 Neumag

tWg varNe 1 Neumagumag

tSi varNe 1 Nemag

tIg varNe 1 Neumagumag

Table 1-S3. Parameter prior values and distributions for *N. lepida*. For normal priors, min and max were set to +/- 2 standard deviations.

Parameter	Prior shape	Min Ne	Max Ne	Mean Ne	Stdev Ne
Ne	normal	1291117	1297437	1294277	1580
tHi	uniform	4500	7500		
tWg	uniform	21000	25000		
tSi	uniform	125000	130000		
Neb	normal	1193048	1395506	1294277	50615
Nb1	normal	963778	1262054	1112916	74569
Nb2	normal	159572	560502	360037	100232
Nb3	normal	212924	891601	552263	169669
tC09	uniform	1355	2764		
tC11	uniform	3784	4090		
tC20	uniform	5491	6181		
tC23	uniform	6295	6542		
tC24	uniform	6753	7232		
tC26	uniform	7259	7429		
tC28	uniform	7164	8385		
tC29	uniform	7735	8587		
tC30	uniform	8197	8404		
tC31	uniform	7679	7930		
tC32	uniform	9603	10155		
Nec	normal	0	4097296	1294277	1401509
Nc1	normal	289105	4772097	2530601	1120748
Nc2	normal	42805	4400235	2221520	1089357
Nc3	normal	314506	5017143	2665824	1175659
Nc4	normal	751924	4463819	2607872	927974
Nc5	normal	703557	4396281	2549919	923181
Nc6	normal	2556900	5595114	4076007	759554
Nc7	normal	0	4296676	1062466	1617105
Nc8	normal	0	4311884	2086297	1112793
Nc9	normal	0	3760090	1699946	1030072
Nc10	normal	9366245	10994471	10180358	407056
Nc11	normal	4728665	7364133	6046399	658867
Ned	normal	131976	2456578	1294277	581151
Nd1	normal	1353031	3395035	2374033	510501
Nd2	normal	0	2896227	1422990	736619
Nd3	normal	673791	3387807	2030799	678504
Nd4	normal	77537	3226087	1651812	787137
Nd5	normal	889625	3057562	1973594	541984

Nd6	normal	2265692	2968621	2617157	175732
Nd7	normal	6152849	7018743	6585796	216474
Nd8	normal	3321605	5159127	4240366	459381
tG02	normal	609	699	654	23
tG03	normal	698	1076	887	95
tG05	normal	2325	2367	2346	11
tG06	normal	2306	2476	2391	43
tG08	normal	3356	3526	3441	43
tG10	normal	3428	3634	3531	52
tG12	normal	3514	3680	3597	42
tG13	normal	4380	4606	4493	57
tG17	normal	5853	5983	5918	33
tG22	normal	6117	6347	6232	58
tG23	normal	5767	6375	6071	152
Nee	normal	465171	2123383	1294277	414553
Ne1	normal	0	2970991	264248	1353372
Ne2	normal	0	2336426	498836	918795
Ne3	normal	0	2175742	452997	861372
Ne4	normal	0	2546061	326266	1109897
Ne5	normal	0	2501535	148303	1176616
Ne6	normal	0	4350594	72803	2138895
Ne7	normal	0	1963367	579728	691819
Ne8	normal	0	1800888	655228	572830
Ne9	normal	0	1974173	892512	540831
Ne10	normal	0	2343816	277730	1033043
Ne11	normal	36352	972105	504229	233938
Nef	normal	808087	1780467	1294277	243095
Nf1	normal	0	1892839	411590	740624
Nf2	normal	0	1845840	527298	659271
Nf3	normal	0	1822075	438038	692019
Nf4	normal	0	1905099	295882	804608
Nf5	normal	164894	165701	165297	202
Nf6	normal	0	2398635	92566	1153034
Nf7	normal	0	1540089	585152	477469
Nf8	normal	0	1472189	452914	509637
Nf9	normal	0	1566630	608294	479168
Nf10	normal	0	2134422	233069	950676
Nf11	normal	329787	331402	330594	404
tH02	uniform	3600	3680		
tH03	uniform	3680	3700		
tH04	uniform	3700	3800		
tH05	uniform	5400	6900		

tH07	uniform	6900	7500		
Neg	normal	480208	2108346	1294277	407035
Ng1	normal	0	2640992	191077	1224957
Ng2	normal	268063	2082546	1175304	453621
Ng3	normal	0	2382416	879676	751370
Ng4	normal	792753	2870159	1831456	519351
Ng5	normal	0	2316174	977017	669579
tWH	uniform	10000	11500		
Nemag	normal	12911170	12974370	12942770	15800
Neumag	normal	0	409730	129428	140151
Nemagmag	normal	129111700	129743700	129427700	158000
tIg	uniform	130000	200000		
Neumagumag	normal	12911	12974	12943	16

APPENDIX 1-3

Results from model comparison through approximate Bayesian computation.

Table 1-S4. Comparison of univariate summary statistics from observed the simulated datasets under each scenario. Numbers indicate the proportion of simulated data sets with a value below the observed value. Summary statistics are abbreviated as: NHA, number of haplotypes; MPD, mean pairwise difference; VPD, variance of pairwise difference; MNS, mean number of the rarest nucleotide at segregating sites; VNS, variance in number of the rarest nucleotide at segregating sites.

Species	Statistic	Observed	Proportion below observed value, per scenario								
			1	2	3	4	5	6	7	8	9
<i>Neotoma cinerea</i>											
	NHA	29	1.00	1.00	0.78	0.99	1.00	1.00	0.73	0.99	1.00
	MPD	7.8636	0.14	0.39	0.00	0.01	0.35	0.45	0.00	0.88	0.00
	VPD	11.8561	0.04	0.18	0.00	0.01	0.14	0.19	0.00	0.89	0.00
	MNS	2.1538	0.01	0.01	0.00	0.01	0.01	0.01	0.00	0.69	0.00
	VNS	2.5609	0.01	0.01	0.01	0.01	0.01	0.01	0.00	0.39	0.00
<i>Neotoma lepida</i>											
	NHA	37	1.00	1.00	0.99	1.00	1.00	1.00	1.00	1.00	1.00
	MPD	12.5154	0.14	0.82	0.00	0.00	0.58	0.64	0.40	0.98	1.00
	VPD	41.8624	0.09	0.59	0.00	0.00	0.44	0.50	0.30	0.91	1.00
	MNS	2.4259	0.00	0.04	0.00	0.00	0.04	0.04	0.02	0.19	0.76
	VNS	6.7075	0.01	0.07	0.00	0.00	0.07	0.08	0.04	0.22	0.72

Figure 1-S1. Plots of principal component analyses of summary statistics from simulated (small circles) and observed (large yellow circle) data, including separate plots for *Neotoma cinerea* all models (A) and top model alone (B), and *N. lepida* all models (C) and top model alone (D). Each simulated dataset is represented by one circle. Open circles are prior combinations, and closed circles are posteriors.

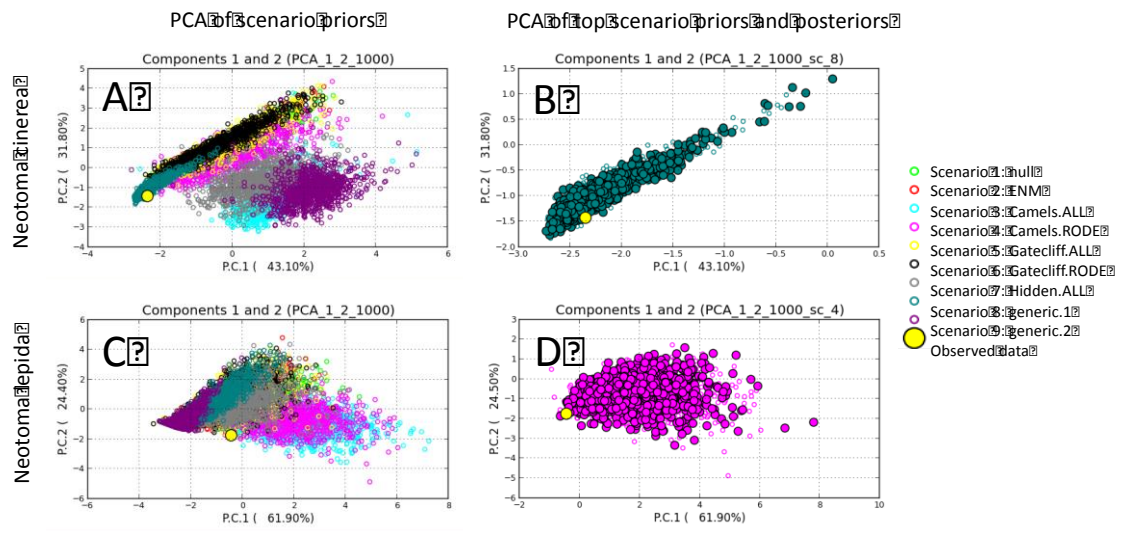


Figure S1.

CHAPTER TWO

Ancient DNA from paleofeces shows the pattern and pace of small mammal species turnover across 30,000 years in Death Valley, CA/NV

INTRODUCTION

The ways in which species and communities react to climate change provide insight into how biodiversity is shaped and structured over time. One of the major challenges in identifying and understanding these reactions is the need for long temporal sampling of ecosystems through major environmental events (Kidwell & Tomasovych 2013). To this end, paleoecological deposits from the late Quaternary are useful because they are relatively abundant and span several major climatic events across the Pleistocene-Holocene transition around 11,7000 years before present (YBP). One of the common findings in studies across this period is that communities do not react as units; rather, species have individualistic demographic and distributional reactions to climate change, often resulting in transient communities with no modern analog (Blois *et al.* 2014; Graham *et al.* 1996; Stewart 2008; Williams & Jackson 2007). These idiosyncracies in species reactions could arise from differences in ecology or adaptive potential to the new abiotic regime, and they highlight the fact that to understand how communities are affected by climate change, we must understand how, when, and why constituent species are affected.

The power of paleoecological deposits to address these questions hinges on several factors, including temporal resolution, spatial resolution, and bias of the depositional vector. Temporal resolution is a function of deposition and mixing through time, such that each layer or stratum is interpreted to represent a time-averaged sample of the environment across decades to millenia (Hadly 1999; Terry 2008). Both spatial resolution and bias are functions of the nature of the material being deposited and the depositional vector. One of the major types of paleoecological deposits in North America, woodrat (*Neotoma* spp.) middens, is actually a complex mix of materials representing different spatial scales and vectors, including pollen, raptor pellets, bones and teeth, seeds, plant clippings, and other debris. One of the most spatially resolved and least biased components of the midden also comprises much of its bulk: *Neotoma* spp. fecal pellets. The fecal pellets give us proof of occupancy at an extremely fine spatial and temporal scale because they are unlikely to be moved after deposition, and lack of depositional bias allows us to distinguish among the multiple ecologically distinct *Neotoma* spp. that build middens. Because middens are common across arid regions of western North America and can last for tens of thousands of years, *Neotoma* spp. have a virtually unparalleled paleoecological record through the Pleistocene-Holocene transition.

Neotoma spp. fecal pellets recovered from middens can provide tentative species identifications based on models of the relationship between pellet size and body size. However, these identifications are complicated by the fact that *Neotoma* spp. body sizes are inversely correlated to environmental temperature in accord with Bergmann's Rule (Brown & Lee 1969; Mayr 1956; Smith & Betancourt 2003, 2006; Smith *et al.* 1995; Smith *et al.* 1998; Smith *et al.* 2009; Smith *et al.* 2014). Hence, the best way to

determine species occupancy based on fecal pellets is through analysis of ancient DNA (aDNA). As with all aDNA sources, the quantity and quality of recoverable data depends not only on age but also preservation conditions. Fortunately, paleomiddens are often sheltered from the damaging effects of precipitation and temperature extremes, preserving *Neotoma* feces as reasonable targets for aDNA analysis. Although paleofeces carry relatively little DNA from the excreting individual and may contain a huge array of organic compounds that can inhibit molecular reactions, they have been a robust source of aDNA in comparison to other materials like bone and hair (Clack *et al.* 2012; Kuch *et al.* 2002; Poinar *et al.* 2001). Furthermore, advancements in library prep, indexing, enrichment, and high-throughput sequencing have dramatically enhanced our ability to detect and sequence aDNA from such degraded and complex samples (Carpenter *et al.* 2013; Enk *et al.* 2014; Kircher *et al.* 2012; Kuch & Poinar 2012; Meyer & Kircher 2010).

In this study, I use aDNA from *Neotoma* spp. paleomidden fecal pellets to determine the pattern and pace of species turnover along an elevational transect over 30,000 years. This transect follows Titus Canyon in the Amargosa Range of Death Valley National Park, CA/NV, USA (Fig. 2-1), which rises eastward nearly 1,300 m elevation and approximately 30 km from the floor of Death Valley. Two *Neotoma* species are found in Death Valley today: the large bodied and cold-adapted bushy-tailed woodrat (*N. cinerea*), which is found in the Panamint Range across the valley from Titus Canyon, and the small bodied and warm-adapted desert woodrat (*N. lepida*), which is found throughout Death Valley including Titus Canyon (Smith *et al.* 2009). Prior work based on *Neotoma* spp. fecal pellet size along this transect showed larger predicted body sizes in the Pleistocene (tentatively identified as *N. cinerea*), and smaller sizes in the

Holocene (tentatively identified as *N. lepida*; Smith *et al.* 2009). As the Pleistocene-Holocene transition brought a major global warming event (Alley 2004), the basic nature of this turnover from *N. cinerea* to *N. lepida* would be expected; in fact, it has been found in numerous paleoecological deposits across western North America (Grayson 2000a; Grayson 2000b; Hockett 2000; Mead *et al.* 1982).

For this study, I sequence paleofecal mitochondrial DNA (mtDNA), which is typically available at 100-1000x concentration compared to nuclear DNA, to definitively determine occupancy of these species along Titus Canyon. This unique opportunity of remarkable temporal and spatial sampling allows detailed questions about the pattern and pace of species turnover: (1) Was the turnover in Titus Canyon gradual or abrupt? Pace of turnover is relative (Williams *et al.* 2011), but here, I am interested in whether the turnover spanned the several thousand years of climatic oscillation during the Pleistocene-Holocene. (2) Did the pace of turnover mirror the pace of climate change during that period? I compare the timing and rate of the turnover to climate proxies to determine whether it appears to have been forced extrinsically by a sudden climate change. (3) If the turnover was gradual, did *N. cinerea* move upslope through that time? Theory (Brown 1971), models (Guralnick 2007; Waltari & Guralnick 2009), paleoecological evidence (Waltari & Guralnick 2009), and some modern resurveys (Moritz *et al.* 2008; Rowe *et al.* 2015) agree that montane mammals move upslope during periods of climate warming. Therefore, I would expect this pattern if gradual turnover was facilitated by the potential for *N. cinerea* to track its thermal niche upslope through the Pleistocene-Holocene.

METHODS

Ancient sampling and library prep

Samples of *Neotoma* fecal pellets were obtained from $n = 43$ paleomidden strata collected along an elevational gradient in Death Valley National Park, CA/NV, spanning ~1300 m elevation along 30 km (Fig. 2-1; Table 2-1). These strata were previously ^{14}C dated to 0–33,491 cal YBP (Smith *et al.* 2009). Because individual fecal pellets yielded very low amounts of amplifiable aDNA, pools of fecal pellets were sampled each totaling approximately 1 g and containing 9–34 pellets selected haphazardly from within each stratum. To evaluate repeatability, $n = 13$ strata were sampled in duplicate.

All subsampling, extraction, and library prep were carried out in a dedicated aDNA facility (McMaster Ancient DNA Centre, McMaster University, ON, CAN), which is physically separated from all modern DNA work and adheres to strict workflow regimes to minimize risk of sample contamination. To assess contamination, I introduced multiple negative controls at three major steps in the process (extraction $n = 11$; repair and adapter ligation, $n = 6$; and indexing, $n = 6$) and carried these controls through enrichment, sequencing, and data processing.

aDNA was extracted from each pool of *Neotoma* fecal pellets using a GuSCN buffer and silica column protocol, and I prepared full genomic libraries using a protocol (Kircher *et al.* 2012; Meyer & Kircher 2010) with the following amendments: for blunt-end repair, we reduced reaction volume to 50 μL including 25 μL of template DNA; I purified intermediate products with Qiagen MinElute columns (Qiagen, Hilden, GER) according to manufacturer's instructions but including two washes and eluting in 20 μL ;

and I performed indexing PCR in with 10 cycles using KAPA SYBR FAST qPCR mix (KAPA Biosystems Inc., Wilmington, MA).

Modern sampling and library prep

To provide a reference database for identifying fragments in the aDNA samples, I acquired $n = 125$ tissue samples from natural history museums and other collections from the Death Valley region, including southern California and Nevada (Fig. 2-1; Appendix 2-1). These specimens included *N. cinerea* ($n = 44$) and *N. lepida* ($n = 74$), as well as the closely related *N. bryanti* ($n = 7$), which is capable of hybridizing with *N. lepida* (Patton *et al.* 2008; Shurtliff *et al.* 2014) and is currently found approximately 100 km west of Death Valley. I chose samples to best represent the geographic distribution of the *Neotoma* species and major mtDNA clades found in this region (Hornsby & Matocq 2012; Patton *et al.* 2008).

I extracted DNA from modern tissue samples with DNeasy Blood and Tissue kits according to manufacturer's instructions. I quantified nucleic acid concentrations (NanoDrop, Wilmington, DE), diluted to average 10.5 ng/uL in 50 uL, and fragmented for 7 minutes in on/off 30s bursts in a focused-ultrasonicator (Covaris, Woburn, MA). Library preparation was as above, with the exception of 3-fold higher adapter concentration during ligation, and vacuum purification via Qiagen QiaQuick 96 plates with 60 uL elution volume. I used Agencourt AMPure XP beads (Beckman Coulter Inc., Brea, CA) to size-select for fragments with insert lengths ca. 300 bp prior to indexing, following manufacturer's instructions with the following volumes: to remove large fragments, I added 18 uL resuspended AMPure beads to 40 uL libraries and retained the

supernatant; to remove small fragments, I then added 7.5 uL beads to 50 uL of supernatant and retained the pellet; after two washes with 200 uL 80% EtOH, I eluted beads in 45 uL of 10 mM Tris and retained 40 uL of supernatant. Indexing was as above.

Enrichment and sequencing

To target *Neotoma* mtDNA for sequencing, I enriched the ancient and modern indexed libraries using custom biotinylated RNA baits. Because a complete *Neotoma* mitochondrial genome was not available at the time of bait design, I assembled a reference genome using available sequences from four *Neotoma* mtDNA loci covering ~18% of the mitochondrial genome (Appendix 2-1). The remainder of the mitochondrial genome was filled with sequences from the sister genus, *Peromyscus*, but as these were too divergent to enrich sufficiently, I do not present the results here. We constructed fifteen reference genomes for bait design in this manner, including up to five haplotypes per locus per species (*N. cinerea*, *N. lepida*, and *N. bryanti*), to represent known sequence variation and improve success in bait annealing. From these reference genomes, 80-mer baits were designed with 14 bp tiling and 5.7x coverage (MYbaits, MYcroarray, Ann Arbor, MI). I processed each indexed library separately using a protocol adapted from manufacturer's instructions, enriching the ancient libraries twice with 100 ng of baits per round, and the modern libraries once with 25 ng of baits. All enrichments were incubated at 55 C for 15-18 hours before bait capture on Dynabeads MyOne streptavidin C1 beads (Invitrogen, Carlsbad, CA), reamplification with primers IS5 and IS6 (Meyer & Kircher 2010), and purification with Qiagen MinElute columns.

To pool the ancient enriched libraries for sequencing, I first determined the concentration of mtDNA in 2 uL aliquots of the original extracts using a *Neotoma*-specific 80 bp qPCR assay of the 16S locus (primers 5'-CTTATTTCTAATCAGTGAAATTGACCTC-3' and 5'-TCCATAGGGTCTTCTCGTCTTAT-3'). As concentration of endogenous DNA in the extracts may be the best indicator of final number of reads in sequencing (Enk *et al.* 2013), I used these 16S estimates to normalize and pool the enriched libraries for sequencing. All negative controls were sequenced at the highest volume and concentration possible in the pooling scheme. Libraries were paired-end sequenced on an Illumina HiSeq 2500 (Illumina Inc., San Diego, CA) at the Farncombe Metagenomics Facility (McMaster University, ON, CAN) in rapid mode with 2 x 90 bp read lengths.

Analysis

Data processing: All ancient and modern data were demultiplexed (CASAVA v1.8, Illumina Inc.), after which we trimmed adapters and merged paired-end reads (leeHom; Renaud *et al.* 2014).

Reference database: To recover modern mtDNA haplotypes from modern samples and construct reference databases for aDNA read identification, we first mapped (bwa; Li & Durbin 2009) modern reads against the haplotypes used for bait design and combined these reads into a consensus mtDNA haplotype for each individual. I augmented the reference database with sequences from GenBank (Appendix 2-1) and separated alignments for each locus of interest to facilitate ancient DNA read identification. To account for the recent revision of *N. lepida* and *N. bryanti*, which are

largely distinguishable by mitochondrial phylogenies (Patton *et al.* 2008), I updated specimen taxonomy as needed based on the position of each sequence on neighbor-joining trees (not shown) built with package *ape* v3.5 (Paradis *et al.* 2004) in R (R Core Team 2016).

To create a custom reference database for species identification, I used a sliding window analysis in R package *spider* v1.3-0 (Brown *et al.* 2012) to identify genomic regions in each locus with discriminatory power between species. This approach creates a database of mini-barcodes that are appropriate for the minimum fragment size after aDNA read filtering. I defined discriminatory power as no heterospecific (non-conspecific) genetic distances equaling zero under the Kimura 2-parameter model, thus selecting windows in which sequences would never match a known heterospecific haplotype based on the available data. I included additional regional *Neotoma* species (*N. albigula* and *N. macrotis*) in early iterations of the reference database; however, as I recovered zero reads from these species in preliminary analyses of the aDNA samples, I omitted these species from consideration in final analyses in order to maximize the number of windows available to distinguish between *N. cinerea*, *N. lepida*, and *N. bryanti*. I set the sliding window size to match the minimum filtered aDNA fragment length (24 bp; see below), and concatenated all windows with discriminatory power into new reference haplotypes with Ns filling the intervening regions. I used the NCBI BLAST+ command line applications for Unix (Camacho *et al.* 2009; <https://blast.ncbi.nlm.nih.gov>) to convert the species and clade databases to nucleic acid format for query.

Ancient read identification: I mapped (bwa; Li & Durbin 2009) all fragments to a single *Neotoma* mtDNA haplotype to roughly estimate the endogenous (*Neotoma* mtDNA) content of the libraries and % exhaustion to determine whether most of the library complexity was sequenced. I did not retain these mappings for further analyses.

Because ancient *Neotoma* pellets were pooled for sampling, it is possible that DNA from multiple individuals and species were incorporated into each library. Thus, I chose to identify each read individually to species, rather than combine reads in consensus haplotypes which would have ignored any complexity within the libraries. I filtered reads to minimum length 24 bp (SAMtools; Li *et al.* 2009), and removed redundant sequences (FASTX-Toolkit; http://hannonlab.cshl.edu/fastx_toolkit) which presumably arose during PCR indexing. We queried the remaining unique reads against the reference database for species identification using BLASTN in the BLAST+ applications, keeping default parameters except aligning to a maximum of one target to identify each read to a single, best-fit reference. BLAST+ applications automatically adjust search parameters for short fragments, particularly the Expect value (E-value) threshold for alignment significance. For strata with more than one sample, we pooled all data after calculating statistics on read alignment between the samples.

aDNA extracts are highly degraded in a number of ways, including cytosine deamination causing C → U → T transitions particularly at fragment ends (Dabney *et al.* 2013). Because these transitions have the potential to cause species misidentification, we used a conservative threshold to determine whether a species contributing a minority of reads in a stratum could plausibly be considered present. This mixing threshold was calculated as the inverse number of fecal pellets in each stratum, representing the

expected proportion of reads from each pellet in the sample. If a species failed to meet this threshold within a stratum, it contributed fewer reads than expected by chance and we interpret its presence as unverified.

Paleoclimate, elevation, and species turnover: To understand the dynamics of *Neotoma* spp. in regard to paleoclimate, we compared patterns of occupancy to two climate proxies: the regional composite Leviathan chronology of 50-yr interpolated $\delta^{18}\text{O}$ values compiled from several sites in the southern Great Basin (Lachniet *et al.* 2014; <https://www.ncdc.noaa.gov/paleo/study/16517>, accessed Oct 2016), and the hemispheric GISP2 temperature (C) reconstruction from Greenland (Alley 2000; Alley 2004; <https://www.ncdc.noaa.gov/paleo/study/2475>, accessed Oct 2016). Though an even more proximal $\delta^{18}\text{O}$ record is available from Devil's Hole in Death Valley (Winograd *et al.* 1992), the Devil's Hole record shows some unusual trends that may be due to changes in groundwater infiltration rather than climate (Lachniet *et al.* 2014).

RESULTS

Reference database: The four loci differed greatly in discriminatory power between *Neotoma* species, but all yielded useful windows for ancient read identification between the three species (Table 2-2; Figure 2-2). There was little variation in the highly conserved 12S or 16S to differentiate species, while *cytb* and *COII* offered more regions with discriminatory power.

Ancient read identification: As is typical for aDNA libraries (Enk *et al.* 2013), endogenous content was extremely low (min = 0.00%, mean = 0.27%, max = 5.62%)

even after two rounds of enrichment. Most strata produced a sufficient number of reads to meet our threshold for analysis (min = 0, mean = 615, max = 4014). Concentration of 16S mtDNA in the original extracts, which is perhaps the best indicator of extract quality, was not correlated with age in cal YPB ($r^2 = 0.04$) or number of pellets in the sample ($r^2 = 0.01$).

Negative controls were sequenced at average 193-fold (min = 3, max = 7,320) higher effective volume than the libraries; thus, they represent a very sensitive test for background levels of contamination from extraction through sequencing. The controls with identifiable *Neotoma* reads included 8 of 11 extraction controls (min = 0, mean = 25.5, max = 102), 4 of 6 repair and ligation controls (min = 0, mean = 5, max = 15), and 0 of 6 indexing controls. As the maximum, outlier level of contamination was 31 reads at 1-fold effective volume, we chose a conservative threshold of 50 reads to choose strata for further analysis. N = 5 strata were discarded for failing to meet this threshold, leaving n = 38 strata for analysis of species composition (Table 2-1).

Paleoclimate, elevation, and species turnover: The most evident result from the aDNA read identification was the dramatic shift from predominance of *N. cinerea* to *N. lepida* between 13,092 and 13,225 cal YBP (Table 2-1, Figure 2-3). *Neotoma cinerea* was predominant in all strata prior to this turnover, although in several strata, *N. lepida* contributed a sufficient proportion of the reads to be considered present. After the turnover, *N. lepida* predominated in all strata. The occasional evidence of *N. cinerea* and *N. bryanti* after 13,000 cal YBP did not reach the threshold for plausible mixing. While the mixed strata in the late Pleistocene are from lower available elevations, there is no

strong evidence of protracted upslope expansion of *N. lepida* and contraction of *N. cinerea* along Titus Canyon (Figure 2-4B).

When aligned to regional and hemispheric temperature proxies, it is apparent that this abrupt species turnover occurred at the transition between the warm Bølling-Allerød interstadial and cold Younger Dryas stadial around 13,100 cal YBP (Figure 2-4). The Bølling-Allerød is not represented in the regional Leviathan chronology, but the hemispheric GISP2 reconstruction suggests a sudden warming nearly reaching late Holocene temperatures. These proxies vary notably in the severity of the Younger Dryas; the GISP2 data show a temperature drop nearly to the level at LGM, while the Leviathan data show a temperature plateau following the Bølling-Allerød sampling gap (Figure 2-4A). Due to this sampling gap, and differences between the two paleoclimate proxies, we cannot confidently extrapolate how extreme the Bølling-Allerød period was in the Death Valley region before the abrupt turnover from *N. cinerea* to *N. lepida*.

DISCUSSION

I found that the species turnover from *N. cinerea* to *N. lepida* in Titus Canyon occurred abruptly at the end of the Bølling-Allerød around 13,200 cal YBP. *Neotoma lepida* was present even at higher elevations throughout the late Pleistocene, though it contributed little to the paleomidden fecal record compared to *N. cinerea*. After the turnover, *N. lepida* was the only species present across all elevations. There was scant evidence of *N. cinerea* retracting upslope, which could be due to the speed of the turnover or lack of sufficient low-elevation Pleistocene strata in this transect.

Why was the replacement of *N. cinerea* by *N. lepida* abrupt? It was not because *N. lepida* was absent, as it was found at least intermittently in Titus Canyon through the late Pleistocene. Rather, I think this a basic illustration of the importance of ecology in understanding the timing, pattern, and pace of species turnover. *Neotoma cinerea* is highly reliant on caves and rocky outcrops for denning across most of its range (Smith 1997). While *N. lepida* will also readily den in rocks, it is capable of excavating underground burrows, and in fact inhabits the floor of Death Valley today in burrows at the base of mesquite trees (*Prosopis* spp.) (Smith *et al.* 2014). Because *N. cinerea* is behaviorally dominant, we suspect that it excluded *N. lepida* from the paleomidden sites in Titus Canyon until its thermal niche was exceeded suddenly in the Bølling-Allerød. Within less than 150 years, *N. cinerea* succumbed to this extrinsic force via direct mortality and/or insufficient recruitment, and *N. lepida* was able to disperse into and occupy all elevations of the canyon.

These results contrast with most regional paleoecological records showing Pleistocene-Holocene turnover between *N. cinerea* and *N. lepida* spanning several hundreds or thousands of years (e.g., Grayson 2006; Terry 2008). These differences could reflect variety in *N. cinerea* phenotype or adaptive potential, differences in the local microhabitat conditions, or simply data differences attributable to the depositional vectors. They could also reflect variety in the rate and severity of the Bølling-Allerød at each site. Indeed, the pace of species turnover was abrupt relative to the species dynamics before and after the turnover, and it tracked climate because the latter also changed abruptly; if climate change in Titus Canyon had been more gradual, and/or had not exceeded the thermal niche of *N. cinerea*, of course, a very different history of

turnover would be evident. The variety of responses found in the paleorecord may be simply a reflection of spatial variation in all of these factors. Further work on paleofecal aDNA across western North America, paired with appropriate local paleoclimate proxies, will provide a better understanding of how and why turnover of the same species pair through the same climatic event can differ so greatly.

Understanding how species react to environmental change is no less than a question of why there are limits to their distributions: dispersal limitation, ecological interactions (including competitive exclusion), abiotic tolerances, and limits on adaptive potential. Though simple in their basis, these questions have profound implications for our understanding of past biodiversity changes and our expectations as we watch future changes unfold.

REFERENCES

- Alley RB (2000) The Younger Dryas cold interval as viewed from central Greenland. *Quaternary Science Reviews* 19, 213–226.
- Alley RB (2004) GISP2 Ice Core Temperature and Accumulation Data. NOAA/NGDC Paleoclimatology Program, Boulder CO, USA, IGBP PAGES/World Data Center for Paleoclimatology.
- Blois JL, Gotelli NJ, Behrensmeyer AK, et al. (2014) A framework for evaluating the influence of climate, dispersal limitation, and biotic interactions using fossil pollen associations across the late Quaternary. *Ecography* 37, 1095-1108.
- Brown JH (1971) Mammals on mountaintops - nonequilibrium insular biogeography. *American Naturalist* 105, 467-478.
- Brown JH, Lee AK (1969) Bergmann's Rule and climatic adaptation in woodrats (*Neotoma*). *Evolution* 23, 329-&.
- Brown SD, Collins RA, Boyer S, et al. (2012) Spider: an R package for the analysis of species identity and evolution, with particular reference to DNA barcoding. *Molecular Ecology Resources* 12, 562-565.
- Camacho C, Coulouris G, Avagyan V, et al. (2009) BLAST+: architecture and applications. *BMC Bioinformatics* 10, 421.
- Carpenter ML, Buenrostro JD, Valdiosera C, et al. (2013) Pulling out the 1%: Whole-Genome Capture for the Targeted Enrichment of Ancient DNA Sequencing Libraries. *American Journal of Human Genetics* 93, 852-864.
- Clack AA, MacPhee RDE, Poinar HN (2012) Case Study: Ancient Sloth DNA Recovered from Hairs Preserved in Paleofeces. In: *Ancient DNA: Methods and Protocols* (eds. Shapiro B, Hofreiter M), pp. 51-56. Humana Press.
- Dabney J, Meyer M, Pääbo S (2013) Ancient DNA Damage. *Cold Spring Harbor Perspectives in Biology* 5, a012567.
- Enk J, Rouillard JM, Poinar H (2013) Quantitative PCR as a predictor of aligned ancient DNA read counts following targeted enrichment. *Biotechniques* 55, 300-309.
- Enk JM, Devault AM, Kuch M, et al. (2014) Ancient whole genome enrichment using baits built from modern DNA. *Molecular Biology and Evolution* 31, 1292-1294.
- Graham RW, Lundelius EL, Graham MA, et al. (1996) Spatial response of mammals to late quaternary environmental fluctuations. *Science* 272, 1601-1606.
- Grayson DK (2000a) Mammalian responses to Middle Holocene climatic change in the Great Basin of the western United States. *Journal of Biogeography* 27, 181-192.
- Grayson DK (2000b) The Homestead Cave mammals. In: *Late Quaternary Paleoecology in the Bonneville Basin* (ed. Madsen DB), pp. 67-89. Utah Geological Survey, Salt Lake City.
- Guralnick R (2007) Differential effects of past climate warming on mountain and flatland species distributions: a multispecies North American mammal assessment. *Global Ecology and Biogeography* 16, 14-23.
- Hadly EA (1999) Fidelity of terrestrial vertebrate fossils to a modern ecosystem. *Palaeogeography Palaeoclimatology Palaeoecology* 149, 389-409.

- Hockett BS (2000) Paleobiogeographic changes at the Pleistocene-Holocene boundary near Pintwater Cave, southern Nevada. *Quaternary Research* 53, 263-269.
- Hornsby AD, Matocq MD (2012) Differential regional response of the bushy-tailed woodrat (*Neotoma cinerea*) to late Quaternary climate change. *Journal of Biogeography* 39, 289-305.
- Jackson ST, Blois JL (2015) Community ecology in a changing environment: Perspectives from the Quaternary. *Proceedings of the National Academy of Sciences* 112, 4915-4921.
- Kidwell SM, Tomasovych A (2013) Implications of time-averaged death assemblages for ecology and conservation biology. *Annual Review of Ecology, Evolution, and Systematics* 44, 539-563.
- Kircher M, Sawyer S, Meyer M (2012) Double indexing overcomes inaccuracies in multiplex sequencing on the Illumina platform. *Nucleic Acids Research* 40, e3.
- Kuch M, Poinar H (2012) Extraction of DNA from paleofeces. *Methods in Molecular Biology* 840, 37-42.
- Kuch M, Rohland N, Betancourt JL, et al. (2002) Molecular analysis of a 11700-year-old rodent midden from the Atacama Desert, Chile. *Molecular Ecology* 11, 913-924.
- Lachniet MS, Denniston RF, Asmerom Y, Polyak VJ (2014) Orbital control of western North America atmospheric circulation and climate over two glacial cycles. *Nature Communications* 5, 3805.
- Li H, Durbin R (2009) Fast and accurate short read alignment with Burrows-Wheeler transform. *Bioinformatics* 25, 1754-1760.
- Li H, Handsaker B, Wysoker A, et al. (2009) The Sequence Alignment/Map format and SAMtools. *Bioinformatics* 25, 2078-2079.
- Mayr E (1956) Geographical character gradients and climatic adaptation. *Evolution* 10, 105-108.
- McGill BJ, Hadly EA, Maurer BA (2005) Community inertia of Quaternary small mammal assemblages in North America. *Proceedings of the National Academy of Sciences* 102, 16701-16706.
- Mead JI, Thompson RS, Van Devender TR (1982) Late Wisconsinan and Holocene fauna from Smith Creek Canyon, Snake Range, Nevada USA. *Transactions of the San Diego Society of Natural History* 20, 1-26.
- Meyer M, Kircher M (2010) Illumina sequencing library preparation for highly multiplexed target capture and sequencing. *Cold Spring Harbor Protocols* doi:10.1101/pdb.prot5448.
- Moritz C, Patton JL, Conroy CJ, et al. (2008) Impact of a century of climate change on small-mammal communities in Yosemite National Park, USA. *Science* 322, 261-264.
- Paradis E, Claude J, Strimmer K (2004) APE: Analyses of Phylogenetics and Evolution in R language. *Bioinformatics* 20, 289.
- Patton JL, Huckaby DG, Álvarez-Castañeda, Ticol S (2008) The evolutionary history and a systematic revision of woodrats of the *Neotoma lepida* group. *UC Publications in Zoology* 135, 1-411.

- Poinar HN, Kuch M, Sobolik KD, et al. (2001) A molecular analysis of dietary diversity for three archaic Native Americans. *Proceedings of the National Academy of Sciences* 98, 4317-4322.
- R Core Team (2016) R: A Language and Environment for Statistical Computing. R Foundation for Statistical Computing, Vienna, Austria.
- Renaud G, Stenzel U, Kelso J (2014) leeHom: adaptor trimming and merging for Illumina sequencing reads. *Nucleic Acids Research* 42, e141.
- Rowe KC, Rowe KM, Tingley MW, et al. (2015) Spatially heterogeneous impact of climate change on small mammals of montane California. *Proceedings of the Royal Society B* 282, 20141857.
- Shurtliff QR, Murphy PJ, Matocq MD (2014) Ecological segregation in a small mammal hybrid zone: habitat - specific mating opportunities and selection against hybrids restrict gene flow on a fine spatial scale. *Evolution* 68, 729-742.
- Smith FA (1997) *Neotoma cinerea*. *Mammalian Species* 564, 1-8.
- Smith FA, Betancourt JL (2003) The effect of Holocene temperature fluctuations on the evolution and ecology of *Neotoma* (woodrats) in Idaho and northwestern Utah. *Quaternary Research* 59, 160-171.
- Smith FA, Betancourt JL (2006) Predicting woodrat (*Neotoma*) responses to anthropogenic warming from studies of the palaeomidden record 33, 2061-2076.
- Smith FA, Betancourt JL, Brown JH (1995) Evolution of body-size in the woodrat over the past 25,000 years of climate-change. *Science* 270, 2012-2014.
- Smith FA, Browning H, Shepherd UL (1998) The influence of climate change on the body mass of woodrats *Neotoma* in an arid region of New Mexico, USA. *Ecography* 21, 140-148.
- Smith FA, Crawford DL, Harding LE, et al. (2009) A tale of two species: Extirpation and range expansion during the late Quaternary in an extreme environment. *Global and Planetary Change* 65, 122-133.
- Smith FA, Murray IW, Harding LE, Lease HM, Martin J (2014) Life in an extreme environment: a historical perspective on the influence of temperature on the ecology and evolution of woodrats. *Journal of Mammalogy* 95, 1128-1143.
- Stewart JR (2008) The progressive effect of the individualistic response of species to Quaternary climate change: an analysis of British mammalian faunas. *Quaternary Science Reviews* 27, 2499-2508.
- Terry RC (2008) Modeling the effects of predation, prey cycling, and time averaging on relative abundance in raptor-generated small mammal death assemblages. *Palaios* 23, 402-410.
- Waltari E, Guralnick RP (2009) Ecological niche modelling of montane mammals in the Great Basin, North America: examining past and present connectivity of species across basins and ranges. *Journal of Biogeography* 36, 148-161.
- Williams JW, Blois JL, Shuman BN (2011) Extrinsic and intrinsic forcing of abrupt ecological change: case studies from the late Quaternary. *Journal of Ecology* 99, 664-677.
- Williams JW, Jackson ST (2007) Novel climates, no - analog communities, and ecological surprises. *Frontiers in Ecology and the Environment* 5, 475-482.

Winograd IJ, Coplen TB, Landwehr JM, et al. (1992) Continuous 500,000-year climate record from Vein Calcite in Devils Hole, Nevada. *Science* 258, 255-260.

TABLES

Table 2-1. Characteristics of strata, aDNA extracts, and sequence data, including duplicated samples for a subset of strata. For strata reaching the minimum read threshold, the read proportion for predominant species in each stratum is shaded, and proportions reaching the mixing threshold indicating presence of multiple species are boxed.

Stratum	Calibrated YBP	Elevation (m)	Number of pellets	Extract 16S copies/2uL	Total unique reads
TiC1 modern	0	1200	17	49.4	304
TiC7 modern	0	1137	29 / 21	2.5 / 5.6	1982 / 195
UTic8 modern	0	1443	34	1.9	5
TiC9c-2	52	1156	22 / 25	0.5 / 67.9	1735 / 82
UTiC9	685	1447	24	127.9	956
Tic1	1265	1200	23	2.9	3691
UTiC3a (piece1)	1895	1583	23	265.9	303
TiC15b	2523	582	15	26.8	115
TiC14	2883	298	24	6.8	469
TiC8a Top2	3713	1220	15	146.1	107
TiC16	4150	1015	26 / 24	5.3 / 105.8	665 / 6
TiC8 Bottom B	4677	1220	24	31.6	433
UTiC12a	5187	1528	26	4.2	101
TiC11b	6246	1154	25	6.6	343
TiC9c-1	8084	1156	24	0.3	3
UTiC6	8447	1513	23	4.2	395
UTiC2b	8849	1576	17 / 16	1.8 / 2.4	177 / 909
TiC11a-1	8861	1154	16	0.0	255
UTiC2a	9522	1576	15	0.7	4014
UTiC11a	9628	1559	19	100.4	200
TiC13b	9655	1216	20	3.5	252
UTiC11b	9751	1559	31 / ~31	7.5 / 2.4	518 / 2882
UTiC10	11618	1400	25 / 20	4.7 / 14	401 / 190
TiC15a	12697	582	24	0.1	116
TiC11c-2	13092	1154	25	0.0	55
TiC2	13255	1190	14	123.8	77
TiC11c-3	15456	1154	25 / 22	14.8 / 33	610 / 134
TiC17-take 2	17261	1030	13	19.6	1764
TiC4a	18274	~1250	12 / 14	278.6 / 4754	65 / 82
TiC4c	18413	~1250	11	0.2	63
TiC4b	18544	~1250	18 / 17	25.1 / 619.7	132 / 168

Tic10c	19457	1200	12	0.0	0
TiC17ab	19991	1030	14 / 9	3.7 / 17.4	694 / 41
TiC6	20068	1200	9	3.5	6
TiC10a	21004	1200	11	113.2	4
UTiC1 back	23092	1345	10	186.4	102
TiC10c-1	23919	1200	13	227.2	207
TiC10d	24701	1200	16 / 12	9.9 / 105	626 / 85
UTiC1 front	26100	1345	10	2.6	0
TiC12 TopE	29116	1249	10	117.4	190
TiC12 TopD	31318	1249	10	87.0	606
TiC12 Bottom A	33439	1249	11 / 12	62.5 / 517.2	2954 / 69
TiC12 Bottom B	33491	1249	~10 / 10	655.2 / 15.8	496 / 3435

Table 2-1. Continued.

Stratum	% endogenous	Library % exhausted	Read proportions		
			N. cinerea	N. lepida	N. bryanti
TiC1 modern	0.71	95.50	0.00	1.00	0.00
TiC7 modern	0.07 / 0.13	96.4 / 95.2	0.002 / 0	0.998 / 1	0.001 / 0
UTic8 modern	0.01	96.60	0.00	1.00	0.00
TiC9c-2	0.01 / 0.1	96.5 / 95.4	0.003 / 0	0.994 / 1	0.003 / 0
UTiC9	2.57	89.60	0.00	1.00	0.00
Tic1	0.01	94.50	0.01	0.99	0.01
UTiC3a (piece1)	5.62	92.00	0.00	1.00	0.00
TiC15b	0.90	94.10	0.00	1.00	0.00
TiC14	0.21	96.00	0.00	1.00	0.00
TiC8a Top2	0.24	97.20	0.00	1.00	0.00
TiC16	0.05 / 0.10	98.2 / 85.1	0.003 / 0	0.967 / 1	0.03 / 0
TiC8 Bottom B	0.04	95.90	0.01	0.97	0.03
UTiC12a	0.08	93.00	0.01	0.99	0.00
TiC11b	0.02	96.60	0.00	1.00	0.00
TiC9c-1	0.47	64.30	0.00	1.00	0.00
UTiC6	0.04	98.70	0.01	0.98	0.01
UTiC2b	0 / 0.06	91.8 / 96.3	0.192 / 0.002	0.808 / 0.998	0 / 0
TiC11a-1	0.02	95.30	0.01	0.99	0.00
UTiC2a	0.02	95.50	0.00	0.99	0.00
UTiC11a	0.47	88.40	0.00	1.00	0.00
TiC13b	0.13	98.10	0.00	1.00	0.00
UTiC11b	0.01 / 0.05	91.4 / 94.9	0.012 / 0.005	0.981 / 0.974	0.008 / 0.021
UTiC10	0.01 / 0.02	95.4 / 93.5	0.012 / 0	0.985 / 1	0.002 / 0
TiC15a	0.00		0.00	1.00	0.00
TiC11c-2	0.00	95.60	0.04	0.96	0.00
TiC2	0.12		1.00	0.00	0.00
TiC11c-3	0.01 / 0.03	91.7 / 95.6	0.921 / 0.776	0.079 / 0.224	0 / 0
TiC17-take 2	0.22	95.50	0.91	0.09	0.00
TiC4a	0.09 / 0.07	77.9 / 37.1	1 / 0.976	0 / 0.024	0 / 0
TiC4c	0.04	99.20	1.00	0.00	0.00
TiC4b	0 / 0.03	92.5 / 76.9	0.97 / 0.988	0.03 / 0.012	0 / 0
Tic10c			0.00	0.00	0.00
TiC17ab	0 / 0.11	94.6 / 85.1	0.817 / 0.78	0.177 / 0.22	0.006 / 0
TiC6	0.03	90.30	1.00	0.00	0.00
TiC10a	0.02	71.50	0.75	0.25	0.00
UTiC1 back	0.11	87.70	1.00	0.00	0.00
TiC10c-1	0.06	77.30	1.00	0.00	0.00
TiC10d	0.03 / 0	96.4 / 81.9	0.949 / 0.988	0.051 / 0.012	0 / 0
UTiC1 front	0.08	94.60	0.00	0.00	0.00

TiC12 TopE	1.00	93.90	1.00	0.00	0.00
TiC12 TopD	0.13	95.30	0.96	0.04	0.00
TiC12 Bottom A	0.01 / 0.01	86.4 / 42.8	0.994 / 0.986	0.006 / 0.014	0 / 0
TiC12 Bottom B	0.34 / 0.06	88.2 / 95.8	0.992 / 1	0.008 / 0	0 / 0

Table 2-2. Loci and 24-bp windows used as mini barcodes for species identification.

Locus	Total bp	Discriminatory bp	Number of windows
12S	513	92	684
16S	563	47	281
COII	615	459	1906
cytb	1143	1103	2710

FIGURES

Figure 2-1. Location of paleomidden strata (A) in Death Valley National Park (black outline) and (B) along the Titus Canyon elevational transect. Strata are colored by age in calibrated years before present (cal YBP).

Figure 2-2. Positions of 24-bp windows across four mitochondrial loci with (red) and without (grey) discriminatory power between *Neotoma* spp. Discriminatory power was determined as no (zero proportion) heterospecific genetic distances equaling zero, based on known sequences in the reference database.

Figure 2-3. Proportion of aDNA reads from each species in strata with ≥ 50 total reads. Asterisks mark strata that reached the mixing threshold indicating presence of multiple species.

Figure 2-4. (A) Paleoclimate proxies from regional (Leviathan chronology) and hemispheric (GISP2 Greenland ice core) sources. Higher values in both proxies indicate warmer temperatures. (B) Strata with ≥ 50 aDNA reads plotted by age and elevation in Titus Canyon, and colored by species present. Strata that reached the mixing threshold are represented by pie charts showing proportion of reads from each species. The cold Younger Dryas (YD, light blue) and warm Bølling-Allerød (BA, light red) are shaded.

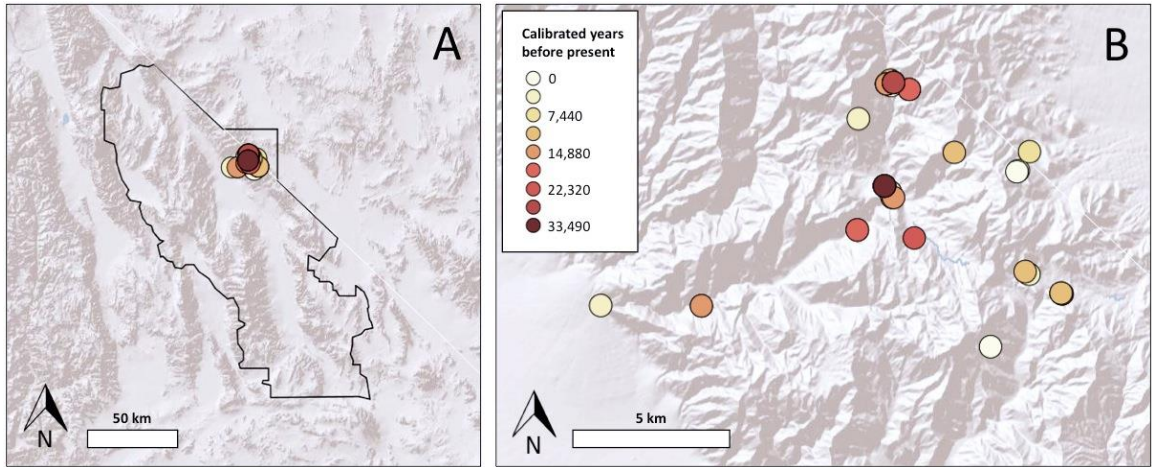


Figure 2-1.

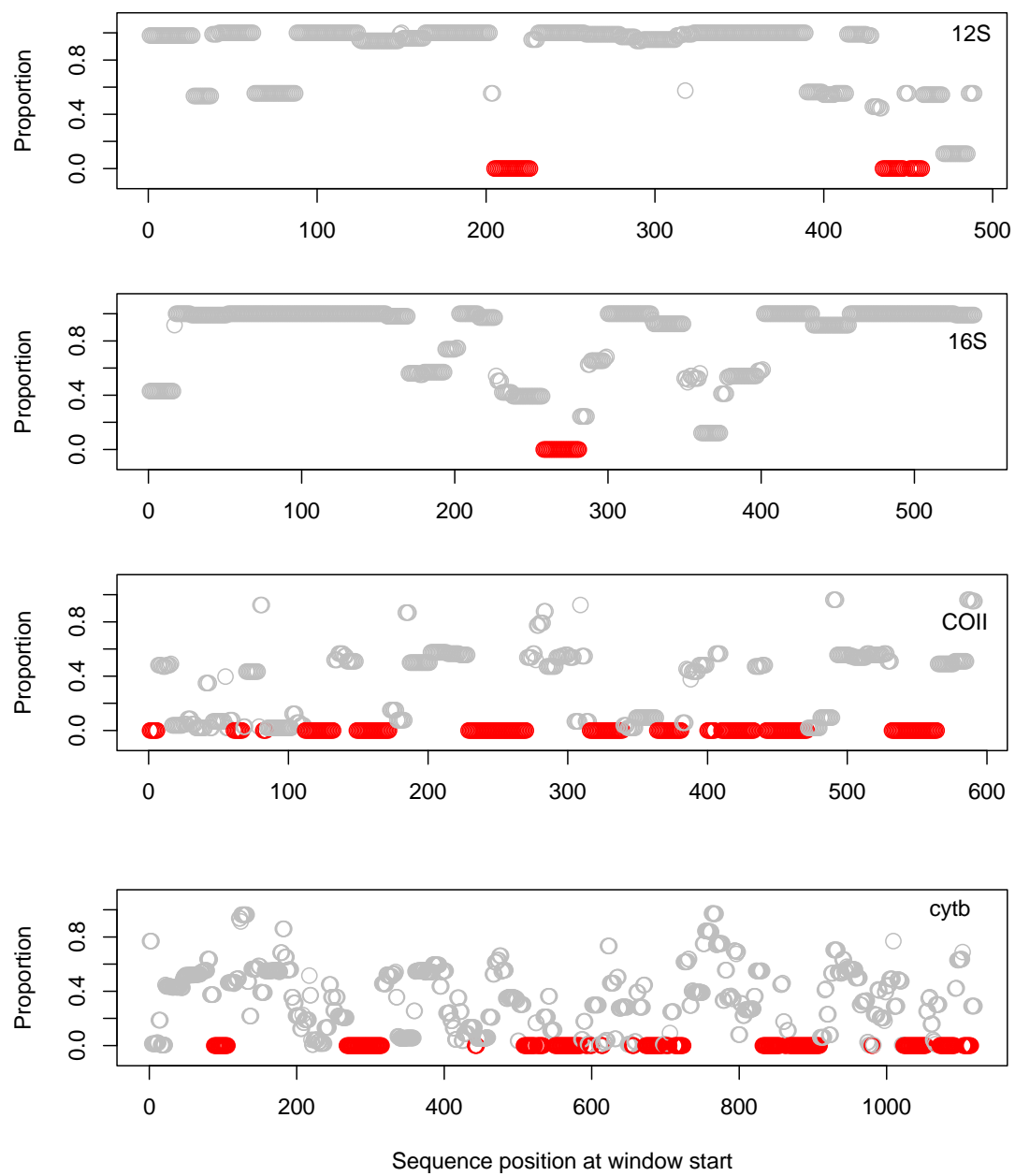


Figure 2-2.

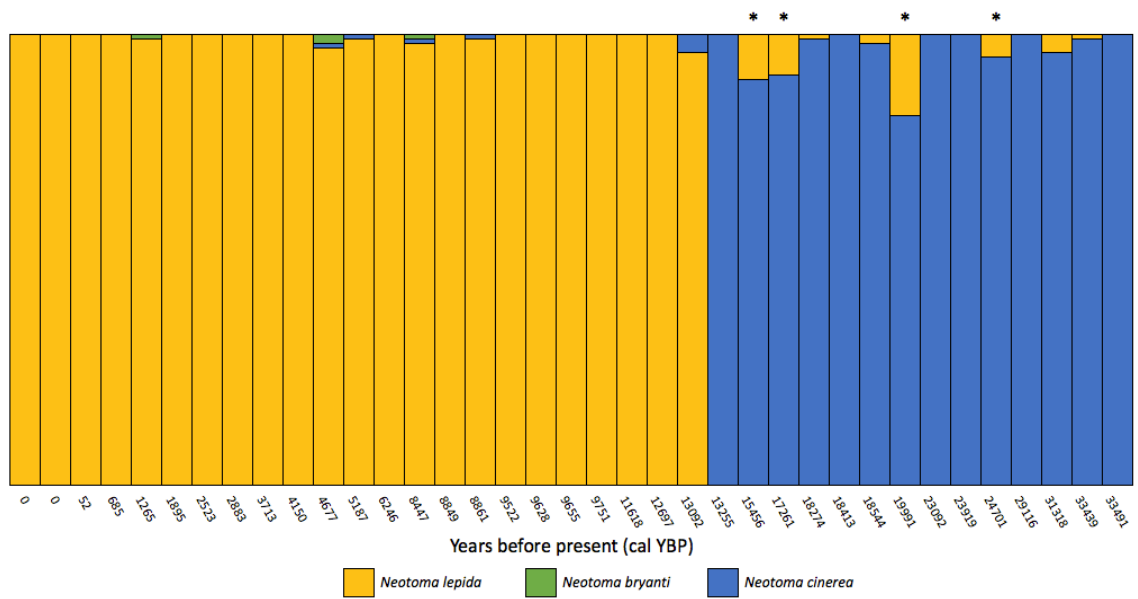


Figure 2-3.

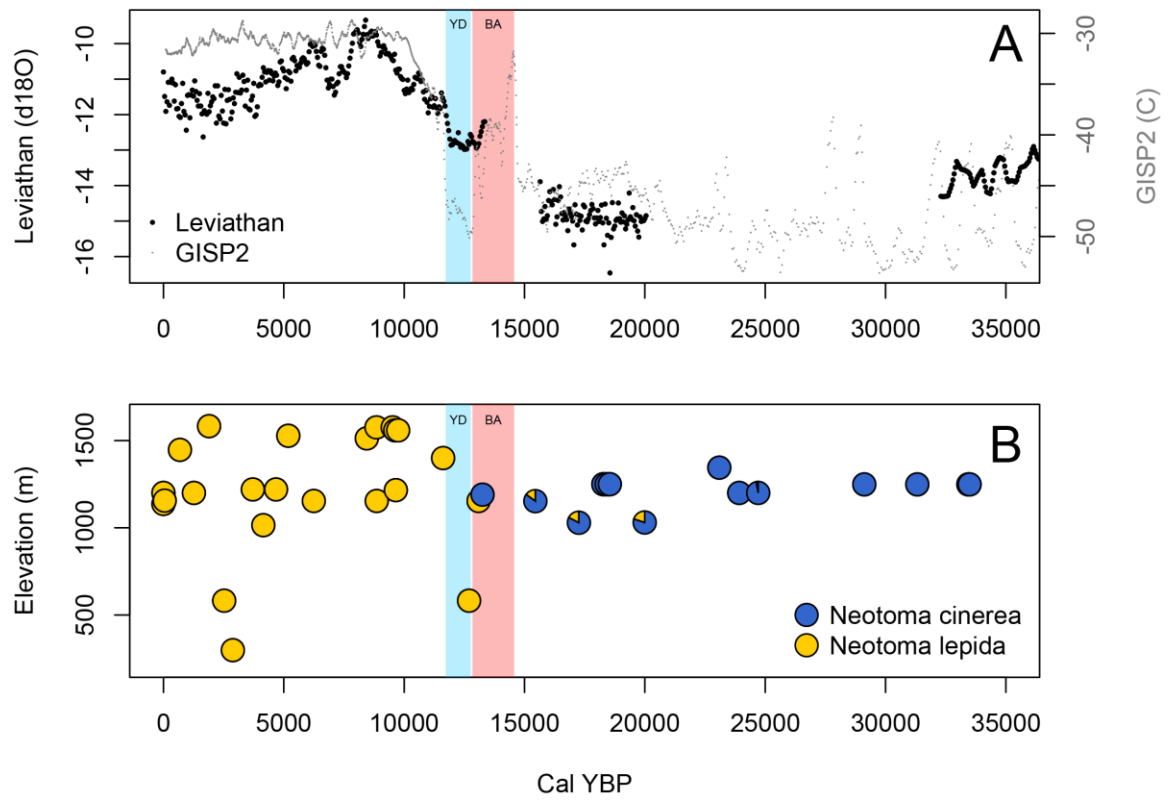


Figure 2-4.

APPENDIX 2-1

Table 2-S1. GUIDs/IDs, species, and locations for modern samples used in reference library construction.

ScientificName	GUID	Latitude	Longitude
<i>Neotoma bryanti</i>	MVZ:Mamm:195930	35.63685	-118.48968
<i>Neotoma bryanti</i>	MVZ:Mamm:195962	35.00687	-119.48707
<i>Neotoma bryanti</i>	MVZ:Mamm:196148	33.61085	-116.42115
<i>Neotoma bryanti</i>	MVZ:Mamm:198346	32.64228	-116.10304
<i>Neotoma bryanti</i>	MVZ:Mamm:198580	34.70951	-118.54447
<i>Neotoma bryanti</i>	MVZ:Mamm:198660	34.31499	-117.54019
<i>Neotoma bryanti</i>	MVZ:Mamm:202512	35.42600	-118.25107
<i>Neotoma cinerea</i>	MSB:Mamm:122449	37.38396	-113.03413
<i>Neotoma cinerea</i>	MSB:Mamm:152633	43.26126	-116.17776
<i>Neotoma cinerea</i>	MSB:Mamm:90783	38.33241	-119.55323
<i>Neotoma cinerea</i>	MVZ:Mamm:197087	40.10348	-120.08013
<i>Neotoma cinerea</i>	MVZ:Mamm:218379	40.96636	-120.13745
<i>Neotoma cinerea</i>	MVZ:Mamm:219950	37.53101	-118.16508
<i>Neotoma cinerea</i>	MVZ:Mamm:219951	37.53101	-118.16508
<i>Neotoma cinerea</i>	MVZ:Mamm:220623	40.44631	-121.40900
<i>Neotoma cinerea</i>	MVZ:Mamm:222570	36.09065	-118.22610
<i>Neotoma cinerea</i>	MVZ:Mamm:222571	35.94814	-118.32772
<i>Neotoma cinerea</i>	MVZ:Mamm:222573	35.94814	-118.32772
<i>Neotoma cinerea</i>	MVZ:Mamm:222723	36.17537	-118.20531
<i>Neotoma cinerea</i>	MVZ:Mamm:222724	36.17537	-118.20531
<i>Neotoma cinerea</i>	MVZ:Mamm:223394	39.21910	-117.13041
<i>Neotoma cinerea</i>	MVZ:Mamm:223395	39.22617	-117.14085
<i>Neotoma cinerea</i>	MVZ:Mamm:223396	39.11444	-114.30054
<i>Neotoma cinerea</i>	MVZ:Mamm:223397	39.11440	-114.29949
<i>Neotoma cinerea</i>	MVZ:Mamm:223401	42.68404	-112.97845
<i>Neotoma cinerea</i>	MVZ:Mamm:223404	41.62117	-117.54596
<i>Neotoma cinerea</i>	MVZ:Mamm:223434	36.25380	-115.64824
<i>Neotoma cinerea</i>	MVZ:Mamm:224329	36.47534	-118.12111
<i>Neotoma cinerea</i>	MVZ:Mamm:224330	36.47534	-118.12111
<i>Neotoma cinerea</i>	MVZ:Mamm:224331	36.47916	-118.12861
<i>Neotoma cinerea</i>	MVZ:Mamm:224332	36.43453	-118.28255
<i>Neotoma cinerea</i>	MVZ:Mamm:224333	36.43453	-118.28255
<i>Neotoma cinerea</i>	MVZ:Mamm:224334	36.43453	-118.28255

<i>Neotoma cinerea</i>	MVZ:Mamm:224455	36.55089	-118.35910
<i>Neotoma cinerea</i>	MVZ:Mamm:224456	36.55166	-118.35376
<i>Neotoma cinerea</i>	MVZ:Mamm:224536	36.17537	-118.20531
<i>Neotoma cinerea</i>	MVZ:Mamm:224537	36.25424	-118.13230
<i>Neotoma cinerea</i>	MVZ:Mamm:224538	36.25276	-118.13662
<i>Neotoma cinerea</i>	MVZ:Mamm:224539	36.25424	-118.13230
<i>Neotoma cinerea</i>	MVZ:Mamm:224540	36.25276	-118.13662
<i>Neotoma cinerea</i>	MVZ:Mamm:224541	36.76872	-118.40720
<i>Neotoma cinerea</i>	MVZ:Mamm:224542	36.76795	-118.40468
<i>Neotoma cinerea</i>	MVZ:Mamm:224543	36.77329	-118.40280
<i>Neotoma cinerea</i>	MVZ:Mamm:224594	36.79102	-118.59768
<i>Neotoma cinerea</i>	MVZ:Mamm:228371	40.09195	-120.08817
<i>Neotoma cinerea</i>	POOP SM 2446mA	36.25380	-115.64822
<i>Neotoma cinerea</i>	POOP SM 2446mB	36.25380	-115.64822
<i>Neotoma cinerea</i>	SAGE-NECI-A275	39.43179	-120.24073
<i>Neotoma cinerea</i>	UMNH:Mamm:31172	38.43659	-111.46604
<i>Neotoma cinerea</i>	UMNH:Mamm:31873	40.34539	-115.59535
<i>Neotoma cinerea</i>	UMNH:Mamm:32187	40.68811	-115.47072
<i>Neotoma cinerea</i>	UMNH:Mamm:32811	39.25398	-117.16357
<i>Neotoma cinerea</i>	UMNH:Mamm:33592	39.30549	-117.11863
<i>Neotoma cinerea</i>	UMNH:Mamm:35391	41.67466	-118.59863
<i>Neotoma lepida</i>	1263	36.46627	-116.87868
<i>Neotoma lepida</i>	1336	36.46666	-116.87859
<i>Neotoma lepida</i>	1410	36.46320	-116.87500
<i>Neotoma lepida</i>	1546	36.46568	-116.87683
<i>Neotoma lepida</i>	1550	36.46615	-116.87808
<i>Neotoma lepida</i>	1624	36.46482	-116.87664
<i>Neotoma lepida</i>	1188/1189	36.46525	-116.87548
<i>Neotoma lepida</i>	1362/1615	36.46500	-116.87714
<i>Neotoma lepida</i>	FMNH:Mamm:168474	38.99387	-114.17202
<i>Neotoma lepida</i>	FMNH:Mamm:179415	41.16143	-112.93515
<i>Neotoma lepida</i>	MSB:Mamm:157045	36.42538	-117.19470
<i>Neotoma lepida</i>	MSB:Mamm:76962	38.36028	-113.52472
<i>Neotoma lepida</i>	MSB:Mamm:86623	40.16556	-113.83972
<i>Neotoma lepida</i>	MSB:Mamm:86624	40.16556	-113.83972
<i>Neotoma lepida</i>	MSB:Mamm:86625	40.16556	-113.83972
<i>Neotoma lepida</i>	MVZ:Mamm:192239	35.97310	-116.27030
<i>Neotoma lepida</i>	MVZ:Mamm:192241	35.97310	-116.27030
<i>Neotoma lepida</i>	MVZ:Mamm:195245	35.47477	-114.85582
<i>Neotoma lepida</i>	MVZ:Mamm:195266	35.55540	-117.72568
<i>Neotoma lepida</i>	MVZ:Mamm:195286	37.17127	-118.21183

<i>Neotoma lepida</i>	MVZ:Mamm:195288	37.17127	-118.21183
<i>Neotoma lepida</i>	MVZ:Mamm:195289	37.17127	-118.21183
<i>Neotoma lepida</i>	MVZ:Mamm:195291	36.90922	-116.78607
<i>Neotoma lepida</i>	MVZ:Mamm:195307	36.90888	-116.78607
<i>Neotoma lepida</i>	MVZ:Mamm:195319	34.76470	-116.37733
<i>Neotoma lepida</i>	MVZ:Mamm:195932	35.63685	-118.48968
<i>Neotoma lepida</i>	MVZ:Mamm:197128	41.94693	-114.69157
<i>Neotoma lepida</i>	MVZ:Mamm:197131	37.59273	-114.75977
<i>Neotoma lepida</i>	MVZ:Mamm:197140	37.59273	-114.75977
<i>Neotoma lepida</i>	MVZ:Mamm:197159	41.58266	-120.03254
<i>Neotoma lepida</i>	MVZ:Mamm:197167	41.81567	-119.09500
<i>Neotoma lepida</i>	MVZ:Mamm:199360	36.98311	-113.82020
<i>Neotoma lepida</i>	MVZ:Mamm:199361	36.98311	-113.82020
<i>Neotoma lepida</i>	MVZ:Mamm:199363	36.98311	-113.82020
<i>Neotoma lepida</i>	MVZ:Mamm:199814	34.15139	-116.47908
<i>Neotoma lepida</i>	MVZ:Mamm:199816	33.63226	-115.49904
<i>Neotoma lepida</i>	MVZ:Mamm:202458	35.97663	-117.92000
<i>Neotoma lepida</i>	MVZ:Mamm:223464	35.96737	-115.54284
<i>Neotoma lepida</i>	MVZ:Mamm:223466	39.11665	-114.30403
<i>Neotoma lepida</i>	PL-NELE	39.88250	-119.61283
<i>Neotoma lepida</i>	UMNH:Mamm:31818	40.16402	-115.50397
<i>Neotoma lepida</i>	UMNH:Mamm:31937	39.79005	-112.36385
<i>Neotoma lepida</i>	UMNH:Mamm:31938	39.79005	-112.36385

CHAPTER THREE

Growth mechanisms and morphometric consequences of adherence to ecogeographic rules in a widespread rodent (*Neotoma cinerea*)

INTRODUCTION

Understanding the generation and maintenance of intraspecific variation is one of the central goals of evolutionary biology. In some cases, variation is structured across environments in consistent ways, prompting the use of ecogeographic rules to describe these presumably adaptive, convergent phenotypic responses to the same environmental forces. The ultimate causes of these rules are rightfully of great interest (Watt et al. 2009), as they point to the selective forces responsible for these patterns. However, it is the proximal causes—i.e., the developmental or physiological mechanisms facilitating adherence to these rules—that will allow us to understand how species converge on similar phenotypes across environments, including the potential rates, constraints, and secondary consequences of these processes.

Geographic variation in body size is one the most-studied ecogeographic traits, with much work dedicated to identifying patterns and testing ultimate causes of variation (e.g., Ashton et al. 2000; Meiri and Dayan 2003; Ashton 2004; Millien et al. 2006; Jetz et al. 2009; Clauss et al. 2013; Teplitsky and Millien 2014). The prevailing hypothesis of for body size patterns in endotherms is Bergmann's Rule (Mayr 1956; James 1970), which describes an inverse relationship between climatic temperature and intraspecific

body size. This is thought to be a function of the surface area to volume ratio, allowing better heat retention via low relative surface area in cool climates and heat dissipation via high relative surface area in warm climates (Mayr 1956). Bergmann's Rule has both a large number of examples (Blackburn and Hawkins 2004; Blois et al. 2007; Brommer et al. 2014) and exceptions (Taylor and Groves 2003; Medina et al. 2007; Ledevin et al. 2010), and alternative environmental causes of geographic body size variation have been proposed. One such hypothesis is that body size varies positively with resource availability (resource rule; McNab 2010), and variations on this rule are supported in a number of endothermic taxa (Huston and Wolverton 2011; Eastman et al. 2012; Gür and Kart Gür 2012; Terada et al. 2012; Correll et al. 2016). Regardless of its ultimate cause, body size variation within a species must stem proximally from global differences in the duration (either initiation or termination) or rate of growth, hence providing a testable set of alternative but not mutually exclusive hypotheses on the mechanism of adherence to these rules (Vrba 2005). Larger body sizes would result from a shift toward earlier growth initiation, higher growth rate, and/or later growth termination, either alone or in concert, while smaller body sizes would result from the converse.

Where we see body size variation, there is potential for shape to be affected secondarily by heterochrony, or changes in the rate of timing of growth and development. If size and shape are coupled in a consistent global allometric relationship, we would see the simplest consequence of body size variation: retention of juvenile shape, known as pedomorphism (Gould 1966; Alberch et al. 1979), because of truncated or slower growth in smaller-bodied individuals or groups. That smaller-bodied groups may be pedomorphic is not a foregone conclusion. In fact, we frequently see changes among

taxa in allometric relationships—dissociations between size, shape, and age—such that shape cannot be predicted from size (Gould 1977; Alberch et al. 1979; Mitteroecker et al. 2004; Galatius et al. 2011; Bhullar et al. 2012; Angielczyk and Feldman 2013). In these cases, heterochronic differences in the rate of shape change could cause isometry (proportional dwarfism) by compensating for smaller body size through higher rate of shape change per unit size.

Shape differences are classically assessed relative to the ancestral condition to understand the direction or polarity of change; however, we can also compare relative differences in shape with no explicit ancestral reference (Mitteroecker et al. 2004; Lieberman et al. 2007). In order to unambiguously test whether smaller-bodied groups are pedomorphic or isometric relative to larger-bodied groups, these groups must follow the same developmental (ontogenetic) trajectories in shape space (Mitteroecker et al. 2004; Mitteroecker et al. 2005; Gerber and Hopkins 2011). In this case, groups provide appropriate references to determine the rates of shape change and determine how heterochrony influences terminal adult shape.

To investigate the growth mechanisms and morphometric patterns involved in adherence to ecogeographic rules, I focus on North American woodrats (*Neotoma* spp.), which appear to broadly illustrate Bergmann's Rule intraspecifically in both space (Brown and Lee 1969) and time (Smith et al. 1995; Smith et al. 1998; Smith and Betancourt 2006; Smith et al. 2009). Consequently, body size differences are thought to be a major mode of climatic adaptation in this taxon. I use the bushy-tailed woodrat (*N. cinerea*) which inhabits the broadest geographic, elevational, and climatic range in the genus, and also shows substantial geographic morphological variation (Hooper 1940;

Cordero and Epps 2012; Hornsby and Matocq 2014), to investigate the proximal mechanisms underlying geographic body size variation and the shape consequences of that variation. This study focuses on three questions:

- 1) *Effect of climate on body size*: I test the prediction that body size varies inversely with climatic temperature (Bergmann's Rule) and/or positively with precipitation or ecosystem productivity (resource rule). Further, as organisms may not be ideally adapted to the current local environment due to constraints on adaptive potential, I determine the geographic scale at which these relationships exist.
- 2) *Effect of climate on growth rate*: Predicated on body size differences among climates, I identify the differences in timing or rate of growth leading to adult body size differences across climates. I predict that *N. cinerea* in colder or more productive climates grow larger via earlier growth initiation, higher growth rate, and/or later growth termination relative to *N. cinerea* in warmer or less productive climates. These differences may be present alone or in combination.
- 3) *Effect of climate on shape*: Predicated on body size differences among climates, I compare shape across climates and developmental stages to investigate three alternative hypotheses of adult shape in *N. cinerea*. The first two describe scenarios involving heterochrony, and the last does not.

H₀: Pedomorphism (i.e., ontogenetic scaling): Adults from warmer or less productive climates are pedomorphic relative to adults from colder or more productive climates, as a consequence of their smaller body size according to a consistent allometric relationship. In this case, *N. cinerea* across climates follow the same shape trajectories, with size and shape

coupled. This would indicate no developmental constraint or pressure on adult shape necessitating equal amounts of shape change.

H₁: Isometry (i.e., proportional dwarfism): Adults from warmer or less productive climates are isometric relative to adults from colder or more productive climates. In this case, *N. cinerea* across climates follow the same shape trajectories, but size and shape are decoupled such that all groups reach the same adult shape regardless of size. This would indicate presence of a developmental constraint or pressure causing equal amounts of shape change in *N. cinerea* regardless of amount of growth (body size).

H₂: Allometric repatterning: Adults from warmer or less productive climates are neither pedomorphic nor isometric compared to adults from colder or more productive climates, because these groups follow different shape trajectory directions either between climates or developmental stages. Because of these differences, there are no appropriate ways to compare shape among groups. This would indicate evolution of these trajectory directions by drift or selection.

METHODS

Data

All analyses were performed in R (R Core Team 2016). I quantified size and shape of *N. cinerea* skulls from natural history collections across the species range (Fig.

3-1; Table 3-S1) using 39 3-dimensional (x,y,z) landmarks (Fig. 3-2; Table 3-S2) digitized with a MicroScribe MX with precision to 0.0001 mm and internal accuracy to 0.0508 mm. Landmarks were visible from either the dorsal or ventral view, with four landmarks common to both views used to unify all data from each skull. To avoid bias from either mechanical or observer error through time, I assigned individuals to groups of up to 8 skulls and randomized the order in which I measured these groups. I measured each skull twice, averaged repeated coordinate measurements, and calculated the midline of each skull to average bilaterally symmetrical landmarks across sides (AMP and unifyVD functions by A. Haber, available at <http://life.bio.sunysb.edu/morph/soft-R.html>). To avoid artificially inflating the degrees of freedom (Klingenberg et al. 2002), I used only one half of the bilaterally averaged landmarks (hereafter, “shape”) for downstream shape analyses. I used Procrustes superimposition in package *geomorph* v3.0.2 (Adams and Otárola-Castillo 2013) to remove the primary effects of specimen size as well as location and rotation established during digitization (Rohlf 1999), and calculated centroid size as the square root of the summed squared distances of all landmarks from the average central point of each skull, which served as the metric of body size (hereafter, “size”). Finally, to assess the repeatability of landmark digitization, I re-measured a subset of $n = 38$ skulls and compared the pairwise Procrustes shape distances within and among specimens.

As the age from birth of each specimen was unknown, I estimated age (days after birth; hereafter “age”) using scores of suture closure (exoccipital-supraoccipital and basioccipital-basisphenoid) and degree of eruption and wear of the last upper molar (M3) compared to descriptions of known-age specimens in the literature (Appendix 3-1, Table

3-S3; Hamilton 1953; Finley 1958; Escherich 1981; Daly and Patton 1986). To assess the repeatability of aging, I re-scored a subset of $n = 36$ skulls and calculated the age differences within specimens.

I used the Bioclim variables (Hijmans et al. 2005; www.worldclim.org/bioclim) mean annual temperature (bio1), maximum temperature of the warmest month (bio5), and minimum temperature of the coldest month (bio6) to represent abiotic conditions thought to be important drivers of Bergmann's Rule in *N. cinerea* (Brown and Lee 1969; Smith et al. 1995; Smith et al. 1998; Smith and Betancourt 2006). I also used Bioclim mean annual precipitation (bio12) and net primary productivity (NPP; Imhoff et al. 2004; Imhoff and Bounoua 2006; <http://sedac.ciesin.columbia.edu>) as proxies of resource availability under the resource rule hypothesis. To assess the effects of climate at different geographic scales, I rescaled variables by averaging each layer across successively larger areas around each pixel, creating layers at five different scales with approximate radii at 45 degrees latitude of: original scales of Bioclim 0.04 degree (4 km) and NPP 0.25 degree (21 km); 0.5 degree (48 km); 1 degree (95 km); 3 degrees (285 km); and 5 degrees (475 km).

Effect of climate on body size

Because Bergmann's Rule is specific to adult body size, I restricted the response variable to centroid sizes of adult *N. cinerea* skulls aged > 240 days (after growth asymptote; Appendix 1), which is similar to the cut-off for distinguishing adult *Neotoma* based on M3 wear in other studies (Escherich 1981; Matocq 2002; Hornsby and Matocq 2014). To determine whether I could pool sexes and adults aged > 240 days for analyses,

I tested for sexual dimorphism in adult size using a linear model including the additive and interaction effects of sex and age [$lm(size \sim sex*age)$].

To determine whether and at what scale *N. cinerea* adheres to Bergmann's Rule and resource rule, I performed model selection using Akaike's information criterion (AIC) from candidate models using Bioclim and NPP variables at different scales. All variables were z-standardized prior to model development. I developed 51 candidate models (Table 3-S4) each including age and sex (see Results) and uncorrelated ($|r| < 0.5$) climate variables (data not shown), ranked these models by AIC, and used 95% confidence intervals (CI; ± 1.96 standard error) to determine parameter importance in the models ranked within $\Delta AIC < 2$ of the top model (Burnham and Anderson 1998). Based on the top model (see Results), I used mean annual temperature (hereafter "temperature") and NPP both at 95 km scale to represent climate in downstream analyses.

Effect of climate on growth rate

In many organisms, growth fits a sigmoidal curve (Ricklefs 1967) characterized by growth initiation (displacement), rate (slope), and termination (asymptote). However, early *N. cinerea* growth patterns are unusual in being linear from birth through the first 40–60 days (Egoscue 1962; Escherich 1981), and thus not showing early exponential growth typical of a sigmoidal function (such functions may still be fit, if not accurately; Martin 1973; Zullinger et al. 1984). Growth in congeners also shows a similar early linear phase (Knoch 1968; Cameron 1973; McClure and Randolph 1980). After 60 days, *N. cinerea* growth is again linear but at a different rate until at least 140 days (Escherich 1981), and timing of asymptote is unknown as no growth curves are available for *N.*

cinerea through adulthood. To accommodate the potential for poor fit to sigmoidal curves, I instead chose to fit local linear models to major phases of the growth curve.

I split the growth curves into four phases based on growth patterns and timing of sexual maturation (Fig. 3, Appendix 1): phase 1, first linear growth from post-weaning through immature age classes, 0–59 days; phase 2, second linear growth phase through subadult age class, 60–139 days; phase 3, inflection through sexual maturation and early adulthood, 140–240 days; and phase 4, asymptote during adulthood, > 240 days. For each phase, I first tested reduced models including only the additive and interaction effects of age and sex [$lm(size \sim sex*age)$] to determine which parameters to carry through downstream models; as age and sex were important in all phases (see Results), I included them in all models. Additionally, as the interaction of age and sex was important in phase 4, I analyzed the sexes separately in that phase. I used P -values ($\alpha = 0.05$) and 95% CI of parameters to assess the affects of climate on initiation, rate, and termination, in relevant phases of the growth curve.

Initiation: Because the dataset begins at post-weaning *N. cinerea*, it's not possible to directly test for differences in growth initiation (displacement) beginning from birth. However, if there was a difference in growth initiation prior to weaning, we would see a difference in body size even at the earliest available age classes. In this test, an additive effect of temperature and NPP on body size in phase 1 would be consistent with a difference in growth initiation [$lm(size \sim sex + age + temperature + NPP)$].

Rate: Growth rate (slope) is usually calculated across linear (pre-asymptotic) growth, so I restricted these analyses to body size in phases 1 and 2. In these tests, an

effect of the interaction between age and temperature or NPP on body size would indicate different growth rates across climates [$lm(size \sim sex + age*temperature + age*NPP)$].

Termination: Difference in growth termination (asymptote) would be apparent in the final phases of the growth curve, and could be tested in two ways. First, a difference in the value at asymptote would indicate different final adult body size, and is equivalent to the above test for adherence to Bergmann's Rule and resource rule in adult *N. cinerea*. Second, a difference in the strength or slope of asymptote would indicate difference in the rate of growth termination—whether abrupt or gradual—which could influence adult body size at older ages. In this test, an effect of the interaction between age and temperature or NPP would indicate different timing or rate of growth termination across climates [$lm(size \sim sex + age*temperature + age*NPP)$].

Effect of climate on shape

To determine whether sex affects shape after accounting for body size, and hence whether the sexes could be pooled for shape analyses, I used a Procrustes ANOVA in *geomorph* function `procD.lm` to relate the superimposed shape data to the additive and interaction effects of size and sex across all ages [$procD.lm(shape \sim size*sex)$]. Finding no strong effect of sex after accounting for size (see Results), I pooled the sexes for all remaining shape analyses.

Before testing the effects of climate on shape, I determined whether the allometric relationship between size and shape in adults (static allometry) was the same as in juveniles (ontogenetic allometry). If the directions of these trajectories in multivariate size-shape space are the same, then static allometry may be a simple extension of

ontogenetic allometry, and interpretation of adult shape in relation to juvenile shape is straightforward. I divided the specimens into ontogenetic (< 240 days) and static (adult, > 240 days) stages. To account for the fact that a unit of size difference is proportionally smaller at larger body sizes, I used $\log(\text{size})$ to represent body size. I used `advanced.procD.lm` in *geomorph* to test for differences in allometric trajectory direction and length between the two stages [`advanced.procD.lm(shape ~ log(size) + stage, log(size)*stage, group = stage, slope = log(age))`], with a null hypothesis of no difference between stages. This test assumes that shape trajectories are approximately linear within each stage, as has been found in other post-weaning rodents (Zelditch et al. 2003).

Although the variables ultimately of interest in examining shape variation are continuous (temperature and NPP), it was necessary to partition specimens into discrete climate groups for pairwise shape analyses. I used *k*-means clustering (R Core Team 2016) with user-defined $k = 3$ to separate specimens into climate groups (factor *climgroup*) representing three different climates. I used ANOVA [`lm(size ~ sex + climgroup)`] and posthoc Tukey HSD tests to confirm that the climate groups differed in adult size in accord with analyses involving climate as continuous variables (see above).

The three hypotheses of *N. cinerea* adult shape in smaller-bodied populations from warmer climates, relative to larger-bodied populations from colder climates, are H_0 : pedomorphism, H_1 : isometry, and H_2 : allometric repatterning. These hypotheses can be distinguished based on whether climate groups differ in the direction and length of ontogenetic trajectories in shape space (multivariate space constructed by principal components analysis) and allometric trajectories in size-shape space (regression of principal components against size; Gerber and Hopkins 2011). I tested these differences

using `advanced.procD.lm` in *geomorph* to compare nested models with and without the effect of climate group; in each case, the null is that the trajectories among climate groups match (overlap) in both direction and length. To represent shape space, I constructed a new “age-shape” space by regressing the principle components against age in the same way that they are regressed against size in size-shape space; this circumvented the need to predict shapes from unobserved age classes (e.g., Zelditch et al. 2003). I measured direction as angle, and lengths as rates of shape change (in units of Procrustes distance) per unit size or age, respectively. To account for the fact that the latter units are proportionally smaller at larger body sizes and older age classes, I used $\log(\text{size})$ and $\log(\text{age})$ to represent these variables.

I constructed models for shape trajectories [*advanced.procD.lm* (*shape* ~ $\log(\text{age})$, ~ $\log(\text{age}) + \text{climgroup}$, *group* = ~*climgroup*, *slope* = ~ $\log(\text{age})$)] and allometric trajectories [*advanced.procD.lm* (*shape* ~ $\log(\text{size})$, ~ $\log(\text{size}) + \text{climgroup}$, *group* = ~*climgroup*, *slope* = ~ $\log(\text{size})$)], followed by pairwise comparisons to determine the nature of any significant effects between climates. To support these results, I also used Procrustes ANOVA in `procD.lm` to compare shape among climates in juveniles (age < 60) and adults (age > 240) regardless of size or age [*procD.lm*(*shape* ~ *climgroup*)], with a null of no effect of climate on shape. I evaluated evidence for each hypothesis as follows. *H₀: Pedomorphism*: For smaller-bodied groups to be pedomorphic, the trajectories across climates must overlap both in direction in shape space, and direction and length in size-shape space. This would indicate that, among climates, shape changes in the same direction through ages, and in the same direction and amount per unit size. Under these conditions, it follows that smaller-bodied groups are

pedomorphic, and the Procrustes ANOVA null of no effect of climate on shape should be rejected. H_1 : *Isometry*: For smaller-bodied groups to be isometric, the trajectories across climates must overlap in direction in shape space, and in direction but not length in size-shape space. This would indicate that the rate of shape change per unit size is different among climates. Isometry would be confirmed by failing to reject the Procrustes ANOVA null, showing that climate does not affect terminal adult shape. H_2 : *Allometric repatterning*: In this scenario, the groups do not overlap in either shape space or size-shape space, and tests of heterochrony cannot be applied.

RESULTS

Data

I digitized a total of $n = 300$ *N. cinerea* skulls (female $n = 166$, male $n = 134$; pre-adult $n = 163$, adult $n = 137$). Landmark digitization was highly repeatable, with Procrustes distances of measurements from the same skull much smaller than distances among skulls (Fig. S1). Aging was similarly repeatable (Appendix 1, Fig. S2).

Effect of climate on body size

Adult size was predicted by the additive effects of age ($t_{(133)} = 3.19$, $P < 0.001$) and sex ($t_{(133)} = 7.08$, $P < 0.0001$), and the interaction of age:sex was marginal ($t_{(133)} = 1.93$, $P = 0.0563$). Because of these effects, I chose to include the additive and interaction effects of age and sex in all candidate models predicting adult size.

Two models relating adult size and climate ranked within 2 Δ AIC from the top model (Table 3-1, Table 3-S5). Aside from the additive and interaction effects of sex and age, the top two models included the additive effects of temperature and NPP. The second model also included the interaction of temperature:NPP; however, as this effect was insignificant and 95% CI overlapped zero (Table 3-1), I chose to omit the interaction from the final model. Thus, I selected the final model based on top-ranked AIC alone. This model (Table 3-1) predicts adult body size variation with the additive and interaction effects of age and sex, plus additive inverse effect of temperature and positive effect of NPP at 95 km scale (Fig. 3-4). Temperature and NPP were not strongly correlated (all $|r| < 0.3$) at any scale, with the strongest correlation ($r = 0.299$) at 95 km scale. The overall model was highly significant and explained a substantial portion of the variation in adult body size ($F_{(5,131)} = 21.69$, $P < 0.0001$, adjusted $r^2 = 0.432$).

Effect of climate on growth rate

The interaction of age and sex on body size was insignificant except in growth phase 4 (data not shown); therefore, I included the additive effects of sex and age in all models for phases 1–3, and split the analyses by sex for phase 4.

Initiation: In phase 1, the effects of both temperature and NPP on body size were significant and had 95% CIs not overlapping zero (Table 3-2). Consistent with the climate effects on adult body size, temperature had an inverse effect and NPP a positive effect, showing a difference in body size across climates from the earliest available age class.

Rate: The interactions between age and climate were not significant in either growth phase 1 or 2 (Table 3-2), which indicated no difference in growth rate in relation to climate. The additive effects of temperature and NPP were significant in these models, again consistent with the climatic effects on adult body size.

Termination: The interactions between age and climate were not significant in either growth phase 3 of either sex or phase 4 females (Table 3-2), indicating that climate did not affect the speed or timing of growth asymptote in these cases. However, body size in phase 4 males was explained by both the interactions of age:temperature and age:NPP, which suggests that climate influenced shape of male growth asymptote through adulthood. In phase 4 males, growth rate is higher (i.e., does not asymptote as strongly) at high temperatures and low NPP (Fig. 3-S3). As in the other growth phases, the additive effects of temperature and NPP were significant (Table 3-2).

Effect of climate shape

After accounting for size, shape was significantly affected by sex ($F_{(1,296)} = 3.826$, $P < 0.001$); however, as sex accounted for very little of the variation in shape ($r^2 = 0.009$), I chose to pool males and females by omitting sex from downstream analyses of shape.

In the test of static and ontogenetic allometries, the nested models supported separate trajectory slopes (Table 3-3). Though this effect was significant, very little variation was explained by splitting the stages ($r^2 = 0.008$); therefore, I pooled the stages for remaining analyses.

K-means clustering separated specimens into three climate groups: low temperature, low NPP ($\downarrow T\downarrow P$); high temperature, low NPP ($\uparrow T\downarrow P$); and high temperature, high NPP ($\uparrow T\uparrow P$) (Fig. 1A, Fig. 3-5A). Though these groups are spatially clustered, each represents a pool of several major mitochondrial DNA clades in *N. cinerea* (Hornsby and Matocq 2012), allowing some confidence that size and shape differences among the groups are affected by climate and not just phylogeny. After accounting for sex, climate group had a significant effect on size ($F_{(2,133)} = 13.283$, $P < 0.001$; Fig 3-5B). Consistent with the models of body size above, posthoc pairwise comparisons showed that the group $\uparrow T\downarrow P$ had significantly smaller adult body size after accounting for sex than either $\uparrow T\uparrow P$ (adjusted $P < 0.0001$) or $\downarrow T\downarrow P$ (adjusted $P = 0.0130$). The larger-bodied groups $\uparrow T\uparrow P$ and $\downarrow T\downarrow P$ did not differ significantly (adjusted $P = 0.0859$).

I rejected the null of no effect of climate on ontogenetic trajectory in age-shape space (Table 3-4); however, pairwise comparisons showed that only the lengths of these vectors, not the directions, differed nearing significance (Table 3-5, Fig. 3-6A-C). Assuming the effect of climate on ontogenetic trajectories was due to differences in trajectory lengths, I rejected H_2 : allometric repatterning, leaving H_0 : pedomorphism and H_1 : isometry. I likewise rejected the null of no effect of climate on allometric trajectories in size-shape space (Table 3-6), again with significant pairwise differences arising in length but not direction (Table 3-7, Fig. 3-6D-F). This test shows that while the direction of the size-shape relationships are consistent between climate groups, the trajectories do not overlap completely because of a dissociation between size and shape. Pairwise comparisons showed that the smaller-bodied $\uparrow T\downarrow P$ group had the highest rate of shape change per unit size, and differed marginally or significantly from the other two groups

(Table 3-7). These results support H_1 : isometry over H_0 : pedomorphism. The Procrustes ANOVA confirmed this result, as climate group alone had no effect on adult shape ($r^2 < 0.001$, $F_{(2,59)} = 0.043$, $Z = 0.031$, $P = 0.953$) despite the fact that it did affect juvenile shape ($r^2 = 0.129$, $F_{(2,134)} = 4.360$, $Z = 2.815$, $P = 0.019$).

DISCUSSION

In this study, I found that temperature and net primary productivity (NPP) influenced *N. cinerea* body size even from the earliest observed ages, and this size difference carried into adulthood with no consistent evidence of climatic differences in post-weaning rate or termination of growth. However, these differences in size did not affect final adult shape. Although adults from the high temperature, low productivity ($\uparrow T \downarrow P$) climates were smaller than adults from the high temperature, high productivity ($\uparrow T \uparrow P$) and low temperature, low productivity ($\downarrow T \downarrow P$) climates, the $\uparrow T \downarrow P$ group exhibited a higher rate of shape change per unit growth. Thus, higher rate of shape change in the $\uparrow T \downarrow P$ group compensated for the smaller body size, resulting in isometry rather than pedomorphism.

In regard to question 1 of this study, I found that adult body size in *N. cinerea* is related inversely to regional (95 km) mean annual temperature in accordance with Bergmann's Rule, and also related positively to net primary productivity (NPP) in accordance with the resource rule. As the standardized effect sizes of temperature and NPP were very close, they appear to exert equal amounts of influence on geographic variation in adult body size. Theoretically, the largest body sizes would be found in cold

climates with high NPP; however, this type of environment was not represented by the *N. cinerea* sampled here, and may not occur in real landscapes if NPP is limited by temperature. The fact that the best predictors of adult body size were climate variables at 95 km, as opposed to more local scales, could be due to a number of constraints including adaptation to past climates, lack of adaptive variation, or outbreeding depression from gene flow across different climates. The scale at which we observe ecogeographic rules, and the potential factors constraining them, will be important to consider as we continue to pursue both the proximal and ultimate causes of these patterns.

In regard to question 2, I found that the differences in *N. cinerea* body size are driven initially, and perhaps ultimately, by the effect of climate starting at least by weaning. At this stage, specimens from colder or more productive climates are already larger than specimens from warmer or less productive climates. These size differences appear to carry monotonically into adulthood, with no evidence for inverse effect of temperature or positive effect of NPP on growth rates at any age. Because very few pre-weaning specimens are available from natural history museums, extensive field collections of specimens starting at birth, and even in utero, would be necessary to determine how body size comes to differ among climates by weaning. Possible mechanisms that would produce larger body sizes include longer gestation length, increased growth rate during gestation, or increased growth rate during nursing.

In regard to question 3, I found that climate groups shared the same trajectories in shape (age-shape) space and size-shape space, which allowed me to make direct comparisons of evidence for heterochrony (rejection of H_3 : allometric rescaling). As the rate of shape change per unit size differed between climates, I rejected H_1 : pedomorphism

in favor of H₂: isometry. In corroboration, I found that, although shape in the youngest age classes was affected by climate, this effect was gone by adulthood. Because of this, I conclude that *N. cinerea* in ↑T↓P climates are not pedomorphic as a result of their smaller body size, and that they in fact appear to compensate for this size difference by developing at a faster rate per unit size than *N. cinerea* in either ↑T↑P or ↓T↓P climates. Similar patterns of compensation for smaller body size with faster developmental rates per unit size have been found in other taxa (Galatius et al. 2011; Angielczyk and Feldman 2013), though the interpretations of this phenomenon are varied. Although this pattern could reflect biomechanical pressures or other selective forces necessitating “adult” shape, in the case of *N. cinerea*, it is simpler to interpret this as an equivalent amount of morphological change in response to hormones during sexual maturation, regardless of size.

Body size is a complicated trait, likely under the control of many loci and influenced by myriad selective pressures which may be in conflict over time and space. In this study, temperature and NPP explained nearly half of the variation in adult body size, leaving much variation yet to be explained. Other forces that may affect size in *Neotoma* and related Cricetid rodents include weather (as opposed to climate; Eifler and Slade 1999), digestive efficiency (Smith 1995), and fasting endurance (Millar and Hickling 1990), any of which could have an effect on skeletal and cranial size through selection on body mass. Litter size also has an effect on mass and development: in *N. lepida*, pups from smaller litters are born heavier and grow faster than pups from larger litters (Cameron 1973). We do not know how *Neotoma* litter size varies, if at all, with temperature, climate, or geography; however, in the sister genus *Peromyscus*, there is a

positive relationship between latitude and litter size (Spencer and Steinhoff 1968). For taxa like *Neotoma*, which can be seasonally polyestrous under favorable conditions (Smith 1997, and references therein), larger litters at higher latitudes are thought to be a compensatory adaptation for the reduced number of litters possible in those climates (Spencer and Steinhoff 1968). The effect of litter size on mass, and latitude on litter size, would lead us to hypothesize smaller juvenile body masses at high latitudes (presumably colder and less productive climates), which is the opposite of what was found in this study. Further research into the natural history of this species would help clarify the relationships between size, climate, and reproductive strategy.

Ecogeographic rules lie at the intersection of two deep-rooted topics in evolutionary biology: intraspecific diversification and convergent evolution. Fully understanding these processes will include delving into the mechanisms, consequences, and potential constraints underlying observed patterns. The approach presented here provides initial hypotheses and a framework for testing how ecogeographic rules are met developmentally across a species range, and whether there are any secondary phenotypic consequences from meeting these adaptive demands. As we continue developing tools to assess the effects of genotype and environment on phenotype of non-model organisms, we will move closer to a complete view of how taxa respond to environmental pressures across space and time.

REFERENCES

- Adams, D. C. and E. Otarola-Castillo. 2013. geomorph: an r package for the collection and analysis of geometric morphometric shape data. *Methods in Ecology and Evolution* 4:393-399.
- Alberch, P., S. J. Gould, G. F. Oster, and D. B. Wake. 1979. Size and shape in ontogeny and phylogeny. *Paleobiology* 5:296-317.
- Angielczyk, K. D. and C. R. Feldman. 2013. Are diminutive turtles miniaturized? The ontogeny of plastron shape in emydine turtles. *Biological Journal of the Linnean Society* 108:727-755.
- Ashton, K. G. 2004. Comparing phylogenetic signal in intraspecific and interspecific body size datasets. *Journal of Evolutionary Biology* 17:1157-1161.
- Ashton, K. G., M. C. Tracy, and A. de Queiroz. 2000. Is Bergmann's rule valid for mammals? *American Naturalist* 156:390-415.
- Bhullar, B. A., J. Marugan-Lobon, F. Racimo, G. S. Bever, T. B. Rowe, M. A. Norell, and A. Abzhanov. 2012. Birds have paedomorphic dinosaur skulls. *Nature* 487:223-226.
- Blackburn, T. M. and B. A. Hawkins. 2004. Bergmann's rule and the mammal fauna of northern North America. *Ecography* 27:715-724.
- Blois, J. L., R. S. Feranec, and E. A. Hadly. 2007. Environmental influences on spatial and temporal patterns of body - size variation in California ground squirrels (*Spermophilus beecheyi*). *Journal of Biogeography* 35:602-613.
- Brommer, J. E., I. K. Hanski, and R. A. Väisänen. 2014. Size differentiation in Finnish house sparrows follows Bergmann's rule with evidence of local adaptation. *Journal of Evolutionary Biology* 27:737-747.
- Brown, J. H. and A. K. Lee. 1969. Bergmann's Rule and climatic adaptation in woodrats (*Neotoma*). *Evolution* 23:329-&.
- Burnham, K. P. and D. R. Anderson. 1998. *Model Selection and Inference: A Practical Information-Theoretical Approach*. Springer Science+Business Media, New York.
- Cameron, G. N. 1973. Effect of litter size on postnatal growth and survival in the desert woodrat. *Journal of Mammalogy* 54:489-493.
- Clauss, M., M. T. Dittmann, D. W. H. Mueller, C. Meloro, and D. Codron. 2013. Bergmann's rule in mammals: a cross-species interspecific pattern. *Oikos* 122:1465-1472.
- Cordero, G. A. and C. W. Epps. 2012. From desert to rainforest: phenotypic variation in functionally important traits of bushy-tailed woodrats (*Neotoma cinerea*) across two climatic extremes. *Journal of Mammalian Evolution* 19:135-153.
- Correll, R. A., Prowse, T. A. A., and Prideaux, G. J. 2016. Lean-season primary productivity and heat dissipation as key drivers of geographic body-size variation in a widespread marsupial. *Ecography* 39:77-86.
- Daly, J. C. and J. L. Patton. 1986. Growth, reproduction, and sexual dimorphism in *Thomomys bottae* pocket gophers. *Journal of Mammalogy* 67:256-265.

- Eastman, L. M., T. L. Morelli, C. J. Conroy, and C. Moritz. 2012. Size increase in high elevation ground squirrels over the last century. *Global Change Biology* 18:1499-1508.
- Egoscue, H. J. 1962. The bushy-tailed wood rat: a laboratory colony. *Journal of Mammalogy* 43:328-337.
- Eifler, M. A. and N. A. Slade. 1999. Effect of weather on individual growth rates in cotton rats, *Sigmodon hispidus*. *Journal of Mammalogy* 80:1277-1287.
- Escherich, P. C. 1981. *Social Biology of the Bushy-Tailed Woodrat*. University of California Publications in Zoology 110:1-132.
- Finley, R. B. J. 1958. *The wood rats of Colorado*. University of Kansas Publications, Museum of Natural History 10:213-552.
- Galatius, A., A. Berta, M. S. Frandsen, and R. N. Goodall. 2011. Interspecific variation of ontogeny and skull shape among porpoises (Phocoenidae). *Journal of Morphology* 272:136-148.
- Gerber, S. and M. J. Hopkins. 2011. Mosaic heterochrony and evolutionary modularity: the trilobite genus *Zacanthopsis* as a case study. *Evolution* 65:3241-3252.
- Gould, S. J. 1966. Allometry and size in ontogeny and phylogeny. *Biological Reviews* 41:587-638.
- Gould, S. J. 1977. *Ontogeny and Phylogeny*. Harvard University Press, Harvard, MA.
- Gür, H. and M. Kart Gür. 2012. Is spatial variation in food availability an explanation for a Bergmannian size pattern in a North American hibernating, burrowing mammal? An information-theoretic approach. *Journal of Zoology* 287:104-114.
- Hamilton, W. J. 1953. Reproduction and young of the Florida wood rat, *Neotoma f. floridana* (Ord). *Journal of Mammalogy* 34:180-189.
- Hijmans, R. J., S. E. Cameron, J. L. Parra, P. G. Jones, and A. Jarvis. 2005. Very high resolution interpolated climate surfaces for global land areas. *International Journal of Climatology* 25:1965-1978.
- Hooper, E. T. 1940. *Geographic variation in bushy-tailed wood woodrats*. University of California Publications in Zoology 42:407-424.
- Hornsby, A. D. and M. D. Matocq. 2012. Differential regional response of the bushy-tailed woodrat (*Neotoma cinerea*) to late Quaternary climate change. *Journal of Biogeography* 39:289-305.
- Hornsby, A. D. and M. D. Matocq. 2014. Patterns of evolutionary divergence and convergence in the bushy-tailed woodrat (*Neotoma cinerea*). *Journal of Mammalian Evolution* 21:243-256.
- Huston, M. A. and S. Wolverton. 2011. Regulation of animal size by eNPP, Bergmann's rule and related phenomena. *Ecological Monographs* 81:349-405.
- Imhoff, M. L. and L. Bounoua. 2006. Exploring global patterns of net primary production carbon supply and demand using satellite observations and statistical data. *Journal of Geophysical Research* 111.
- Imhoff, M. L., L. Bounoua, T. Ricketts, C. Loucks, R. Harriss, and W. T. Lawrence. 2004. HANPP Collection: Global Patterns in Net Primary Productivity (NPP). NASA Socioeconomic Data and Applications Center (SEDAC), Palisades, NY.
- James, F. C. 1970. Geographic size variation in birds and its relationship to climate. *Ecology* 51:365-390.

- Jetz, W., K. G. Ashton, and F. A. La Sorte. 2009. Phenotypic population divergence in terrestrial vertebrates at macro scales. *Ecology Letters* 12:1137-1146.
- Klingenberg, C. P., M. Barluenga, and A. Meyer. 2002. Shape analysis of symmetric structures: quantifying variation among individuals and asymmetry. *Evolution* 56:1909-1920.
- Knoch, H. W. 1968. The Eastern wood rat, *Neotoma floridana osagensis*: a laboratory colony. *Transactions of the Kansas Academy of Sciences* 71:361-372.
- Ledevin, R., J. R. Michaux, V. Deffontaine, H. Henttonen, and S. Renaud. 2010. Evolutionary history of the bank vole *Myodes glareolus*: a morphometric perspective. *Biological Journal of the Linnean Society* 100:681-694.
- Lieberman, D. E., J. Carlo, M. Ponce de Leon, and C. P. Zollikofer. 2007. A geometric morphometric analysis of heterochrony in the cranium of chimpanzees and bonobos. *Journal of Human Evolution* 52:647-662.
- Martin, R. J. 1973. Growth curves for bushy-tailed woodrats based upon animals raised in wild. *Journal of Mammalogy* 54:517-518.
- Matocq, M. D. 2002. Morphological and molecular analysis of a contact zone in the *Neotoma fuscipes* species complex. *Journal of Mammalogy* 83:866-883.
- Mayr, E. 1956. Geographical character gradients and climatic adaptation. *Evolution* 10:105-108.
- McClure, P. A. and J. C. Randolph. 1980. Relative allocation of energy to growth and development of homeothermy in the Eastern wood rat (*Neotoma floridana*) and hispid cotton rat (*Sigmodon hispidus*). *Ecological Monographs* 50:199-219.
- McNab, B. K. 2010. Geographic and temporal correlations of mammalian size reconsidered: a. *Oecologia* 164:13-23.
- Medina, A., D. A. Marti, and C. J. Bidau. 2007. Subterranean rodents of the genus *Ctenomys* (Caviomorpha, Ctenomyidae) follow the converse to Bergmann's rule. *Journal of Biogeography* 34:1439-1454.
- Meiri, S. and T. Dayan. 2003. On the validity of Bergmann's rule. *Journal of Biogeography* 30:331-351.
- Millar, J. S. and G. J. Hickling. 1990. Fasting endurance and the evolution of mammalian body size. *Functional Ecology* 4:5-12.
- Millien, V., S. Kathleen Lyons, L. Olson, F. A. Smith, A. B. Wilson, and Y. Yom-Tov. 2006. Ecotypic variation in the context of global climate change: revisiting the rules. *Ecology Letters* 9:853-869.
- Mitteroecker, P., P. Gunz, M. Bernhard, K. Schaefer, and F. L. Bookstein. 2004. Comparison of cranial ontogenetic trajectories among great apes and humans. *Journal of Human Evolution* 46:679-698.
- Mitteroecker, P., P. Gunz, and F. L. Bookstein. 2005. Heterochrony and geometric morphometrics: a comparison of cranial growth in *Pan paniscus* versus *Pan troglodytes*. *Evolution and Development* 7:244-258.
- R Core Team. 2016. R: A Language and Environment for Statistical Computing. R Foundation for Statistical Computing, Vienna, Austria.
- Ricklefs, R. E. 1967. A Graphical Method of Fitting Equations to Growth Curves. *Ecology* 48:978-983.

- Rohlf, F. J. 1999. Shape statistics: Procrustes superimpositions and tangent spaces. *Journal of Classification* 16:197-223.
- Smith, F. A. 1995. Scaling of digestive efficiency with body-mass in *Neotoma*. *Functional Ecology* 9:299-305.
- Smith, F. A. 1997. *Neotoma cinerea*. *Mammalian Species* 564:1-8.
- Smith, F. A. and J. L. Betancourt. 2006. Predicting woodrat (*Neotoma*) responses to anthropogenic warming from studies of the palaeomidden record. Pp. 2061-2076.
- Smith, F. A., J. L. Betancourt, and J. H. Brown. 1995. Evolution of body-size in the woodrat over the past 25,000 years of climate-change. *Science* 270:2012-2014.
- Smith, F. A., H. Browning, and U. L. Shepherd. 1998. The influence of climate change on the body mass of woodrats *Neotoma* in an arid region of New Mexico, USA. *Ecography* 21:140-148.
- Smith, F. A., D. L. Crawford, L. E. Harding, H. M. Lease, I. W. Murray, A. Raniszewski, and K. M. Youberg. 2009. A tale of two species: Extirpation and range expansion during the late Quaternary in an extreme environment. *Global and Planetary Change* 65:122-133.
- Spencer, A. W. and H. W. Steinhoff. 1968. An explanation of geographic variation in litter size. *Journal of Mammalogy* 49:281-286.
- Taylor, A. B. and C. P. Groves. 2003. Patterns of mandibular variation in *Pan* and *Gorilla* and implications for African ape taxonomy. *Journal of Human Evolution* 44:529-561.
- Teplitsky, C. and V. Millien. 2014. Climate warming and Bergmann's rule through time: is there any evidence? *Evolutionary Applications* 7:156-168.
- Terada, C., S. Tatsuzawa, and T. Saitoh. 2012. Ecological correlates and determinants in the geographical variation of deer morphology. *Oecologia* 169:981-994.
- Vrba, E. S. 2005. Mass turnover and heterochrony events in response to physical change. *Paleobiology* 31:157-174.
- Watt, C., S. Mitchell, and V. Salewski. 2009. Bergmann's Rule: a concept cluster? *Oikos* 119:89-100.
- Zelditch, M. L., B. L. Lundrigan, H. David Sheets, and T. Garland. 2003. Do precocial mammals develop at a faster rate? A comparison of rates of skull development in *Sigmodon fulviventer* and *Mus musculus domesticus*. *Journal of Evolutionary Biology* 16:708-720.
- Zullinger, E. M., R. E. Ricklefs, K. H. Redford, and G. M. Mace. 1984. Fitting sigmoidal equations to mammalian growth curves. *Journal of Mammalogy* 65:607-636.

TABLES

Table 3-1. Top model relating adult body size to climate, including estimates, standard errors, *t*-values (df), and *P*-values. All parameters have been standardized.

Model	Scale (km)	Parameter	Estimate	SE	$t_{(133)}$	<i>P</i>
age + sex + temp + NPP	95	(Intercept)	-0.018	0.065	-0.281	0.7793
		sex(M)	0.154	0.069	2.223	0.0279
		age	0.496	0.066	7.524	< 0.0001
		temperature	-0.249	0.068	-3.651	0.0004
		NPP	0.271	0.071	3.815	0.0002
		age:sex	0.130	0.065	1.996	0.0480

Table 3-2. Models testing the effects of climate on growth initiation, rate, and termination in respective growth phases, including estimates, standard errors (SE), *t*-values, and *P*-values. All parameters have been standardized.

Phase (Age)	Test	Parameter	Estimate	SE	<i>t</i>	<i>P</i>
1 (0-59)	Initiation	(Intercept)	0.000	0.077	0.00	1.0000
		sex	0.177	0.078	2.25	0.0281
		age	0.797	0.078	10.21	< 0.0001
		temperature	-0.162	0.081	-2.00	0.0500
		NPP	0.193	0.081	2.39	0.0202
1 (0-59)	Rate	(Intercept)	0.002	0.077	0.03	0.9756
		sex	0.194	0.079	2.44	0.0178
		age	0.782	0.079	9.95	< 0.0001
		temperature	-0.174	0.081	-2.15	0.0363
		NPP	0.195	0.081	2.42	0.0190
		age:temp	-0.088	0.073	-1.21	0.2330
		age:NPP	-0.048	0.081	-0.60	0.5546
2 (60-139)	Rate	(Intercept)	-0.022	0.122	-0.18	0.8572
		sex	0.133	0.129	1.03	0.3081
		age	0.416	0.124	3.35	0.0017
		temperature	-0.196	0.126	-1.56	0.1267
		NPP	0.292	0.129	2.26	0.0286
		age:temp	-0.136	0.124	-1.10	0.2788
		age:NPP	0.160	0.134	1.20	0.2371
3 (140-240)	Termination	(Intercept)	0.012	0.118	0.10	0.9191
		sex	0.453	0.126	3.58	0.0009
		age	0.381	0.124	3.07	0.0037
		temperature	-0.350	0.130	-2.70	0.0099
		NPP	0.211	0.123	1.72	0.0928
		age:temp	0.050	0.136	0.37	0.7131
		age:NPP	0.015	0.125	0.12	0.9038
4 (>240) female	Termination	(Intercept)	-0.476	0.080	-5.99	< 0.0001
		age	0.070	0.087	0.81	0.4209
		temperature	-0.168	0.079	-2.13	0.0364
		NPP	0.184	0.086	2.15	0.0351
		age:temp	0.022	0.084	0.27	0.7902
		age:NPP	0.110	0.086	1.28	0.2040
4 (>240) male	Termination	(Intercept)	0.630	0.116	5.44	< 0.0001
		age	0.363	0.107	3.38	0.0013
		temperature	-0.271	0.115	-2.36	0.0222
		NPP	0.195	0.110	1.77	0.0830
		age:bio1	0.279	0.119	2.36	0.0221
		age:NPP	-0.223	0.110	-2.02	0.0481

Table 3-3. Comparison of nested models with static and ontogenetic allometries pooled (common allometry) or separated (separate allometries) [*advanced.prodD.lm(shape ~ log(size), log(size) + stage, group = stage, slope = log(size))*].

	df	SSE	SS	r^2	F	Z	P
Common allometry	297	0.324					
Separate allometries	296	0.321	0.004	0.008	3.66	3.41	0.010

Table 3-4. Comparison of nested models with and without the effect of climate group on ontogenetic trajectories in age-shape space [*advanced.prodD.lm(shape ~ log(age), log(age) + climgroup, group = climgroup, slope = log(age))*].

Parameters	df	SSE	SS	r^2	F	Z	P
Log(age)	298	0.348					
Log(age) + climgroup	296	0.336	0.012	0.025	5.50	5.11	0.001

Table 3-5. Pairwise comparisons of ontogenetic trajectories in age-shape space, including direction and length of shape change. Absolute difference in length or angle direction (with *Z* scores in parentheses) are above the diagonal, and *P* values are below the diagonal.

		Value	Climate group		
			High temp, high NPP	Low temp, low NPP	High temp, low NPP
Direction	High temp, high NPP		-	12.81 (0.97)	12.94 (1.01)
	Low temp, low NPP		0.429	-	10.29 (0.83)
	High temp, low NPP		0.365	0.622	-
Length	High temp, high NPP	0.019	-	0.0028 (1.58)	0.0034 (1.93)
	Low temp, low NPP	0.022	0.118	-	0.0006 (0.37)
	High temp, low NPP	0.023	0.057	0.694	-

Table 3-6. Comparison of nested models with and without the effect of climate group on allometric trajectories in size-shape space [*advanced.prodD.lm(shape ~ log(size), log(size) + climgroup, group = climgroup, slope = log(size))*].

Parameters	df	SSE	SS	r^2	F	Z	P
Log(size)	298	0.331					
Log(size) + climgroup	296	0.320	0.011	0.022	5.01	4.69	< 0.001

Table 3-7. Pairwise comparisons of allometric trajectories in size-shape space, including direction and length of shape change. Absolute difference in length or angle direction (with *Z* scores in parentheses) are above the diagonal, and *P* values are below the diagonal.

	Climate group	Value	Climate group		
			High temp, high NPP	Low temp, low NPP	High temp, low NPP
Length	High temp, high NPP	0.2479	-	0.0001 (0.01)	0.0285 (1.81)
	Low temp, low NPP	0.2480	0.994	-	0.0284 (2.16)
	High temp, low NPP	0.2765	0.065	0.037	-
Direction	High temp, high NPP		-	11.88 (0.88)	13.29 (1.06)
	Low temp, low NPP		0.540	-	11.59 (1.17)
	High temp, low NPP		0.308	0.198	-

FIGURES

Figure 3-1. Locations of *Neotoma cinerea* skulls against species range map (dark grey), colored according to climate cluster (see text).

Figure 3-2. Cranial landmarks for geometric morphometric analysis. Landmarks with filled circles were taken from either the ventral or dorsal view of the skull, and landmarks with open circles were taken from both views and used to unify the data for each specimen into a single 3D shape. Landmarks off the midline were taken from both sides of the skull. See Table 3-S2 for anatomical descriptions of landmark placement. Engraving from Baird 1857.

Figure 3-3. Predicted ages and centroid sizes of *N. cinerea* skulls, split by sex: (A) black = female, (B) grey = male. Dotted lines show divisions between growth phases at 60, 140, and 240 days after birth.

Figure 3-4. Relationship between adult *Neotoma cinerea* size and (A) mean annual temperature (bio1) and (B) net primary productivity (NPP), both at 95 km scale. The linear model for each sex (black = female, grey = male) is shown with 95% confidence interval shaded.

Figure 3-5. (A) Climate (temperature and NPP at 95 km resolution) at specimen collection localities, colored according to climate groups at $k = 3$: ‘high temperature, high NPP’ (green); ‘low temperature, low NPP’ (blue); ‘high temperature, low NPP’ (red). (B) Boxplots of adult size split by sex and climate group and coded by significance in each sex separately.

Figure 3-6. Plots of common age or allometric component (CAC), first residual shape component (RSC1) against CAC, and predicted shape from trajectory analyses. (A-C) Ontogenetic trajectories in age-shape space, split by climate group. (D-F) Allometric trajectories in size-shape space, split by climate group.

Figure 3-7. Mean cranial shapes of juveniles and adults in each climate group, from the dorsal-ventral (left) and side views (right).

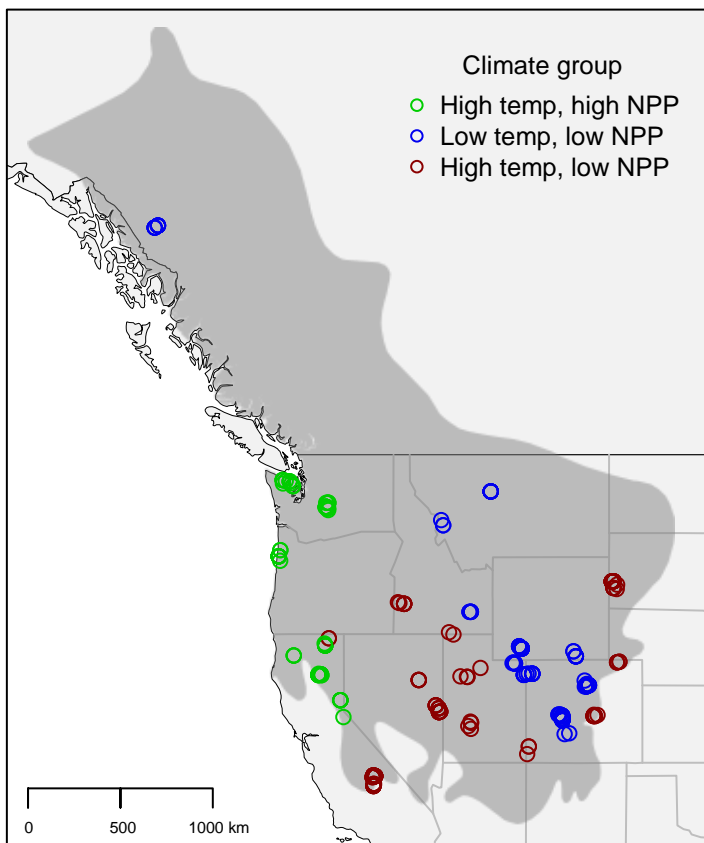


Figure 3-1.

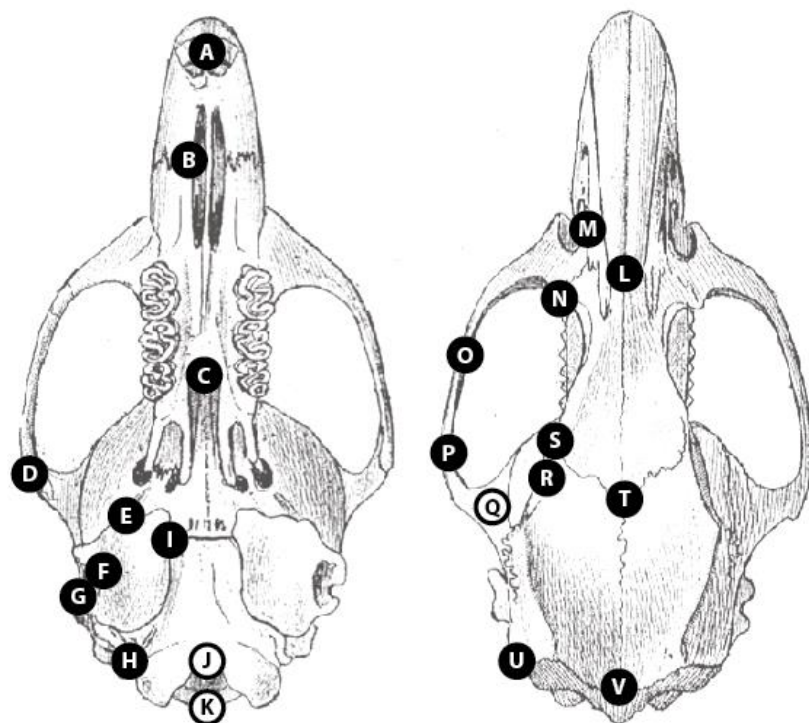


Figure 3-2.

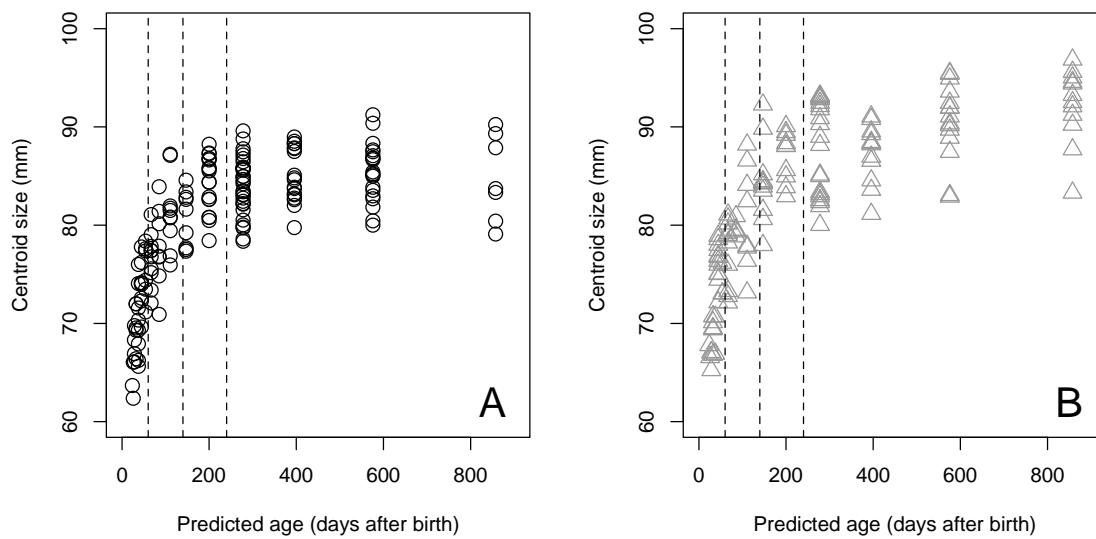


Figure 3-3.

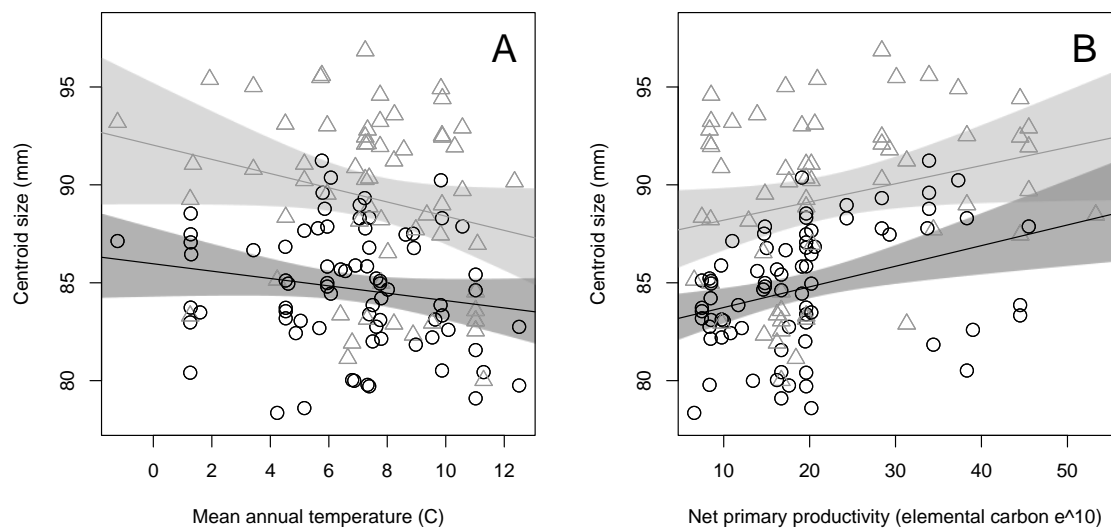


Figure 3-4.

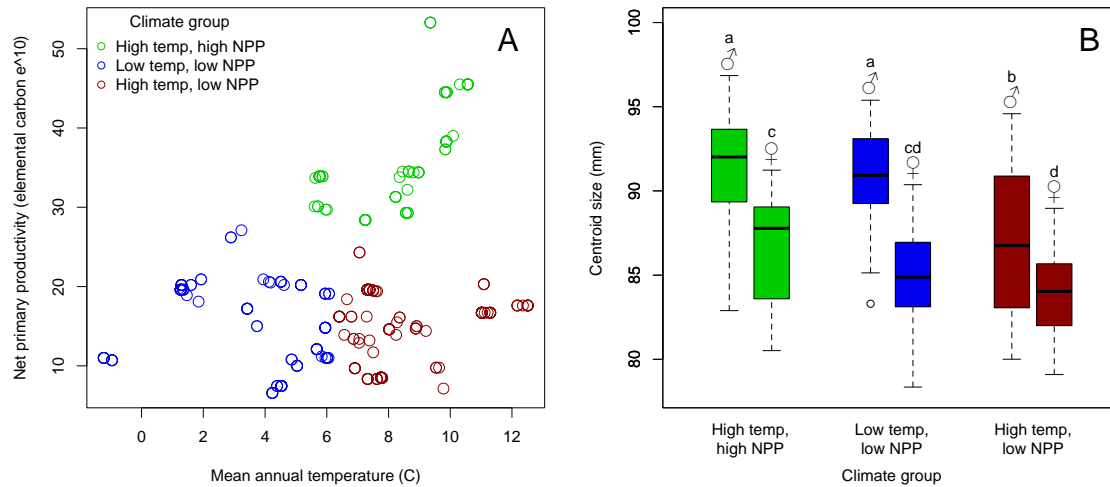


Figure 3-5.

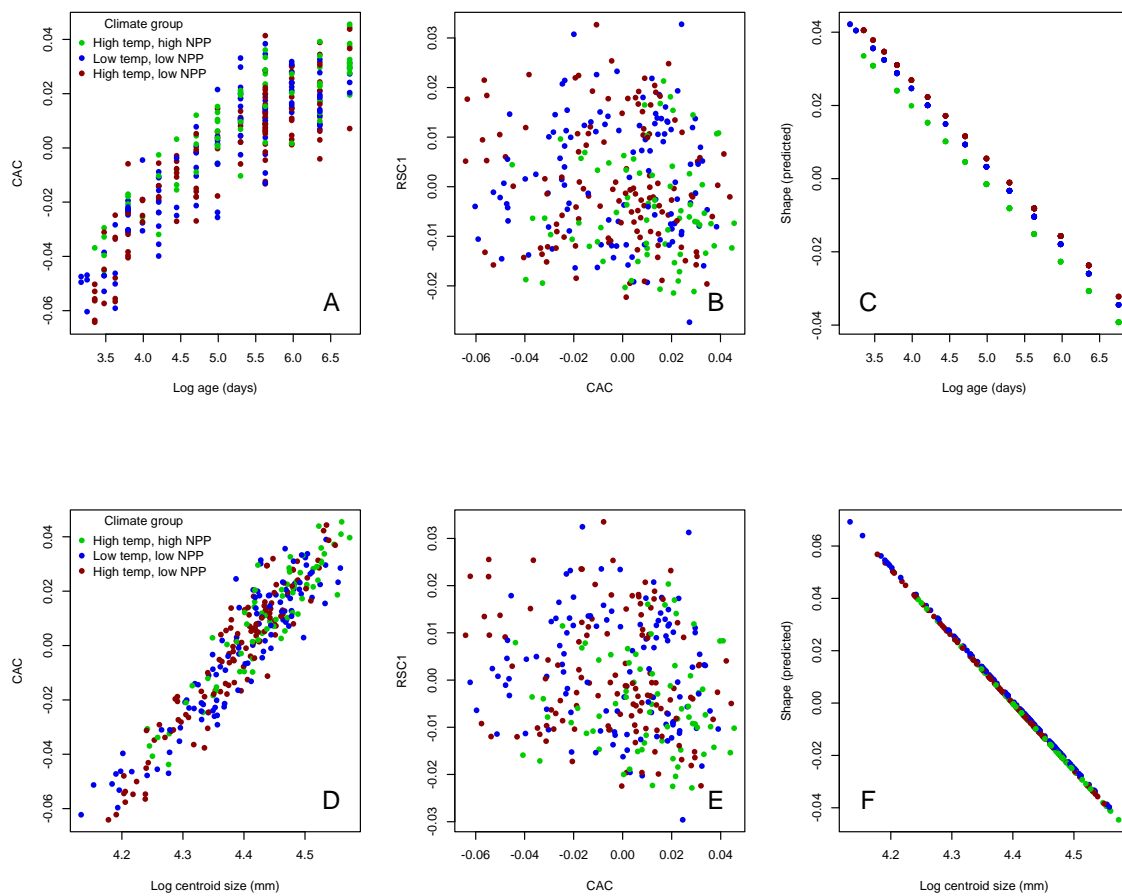


Figure 3-6.

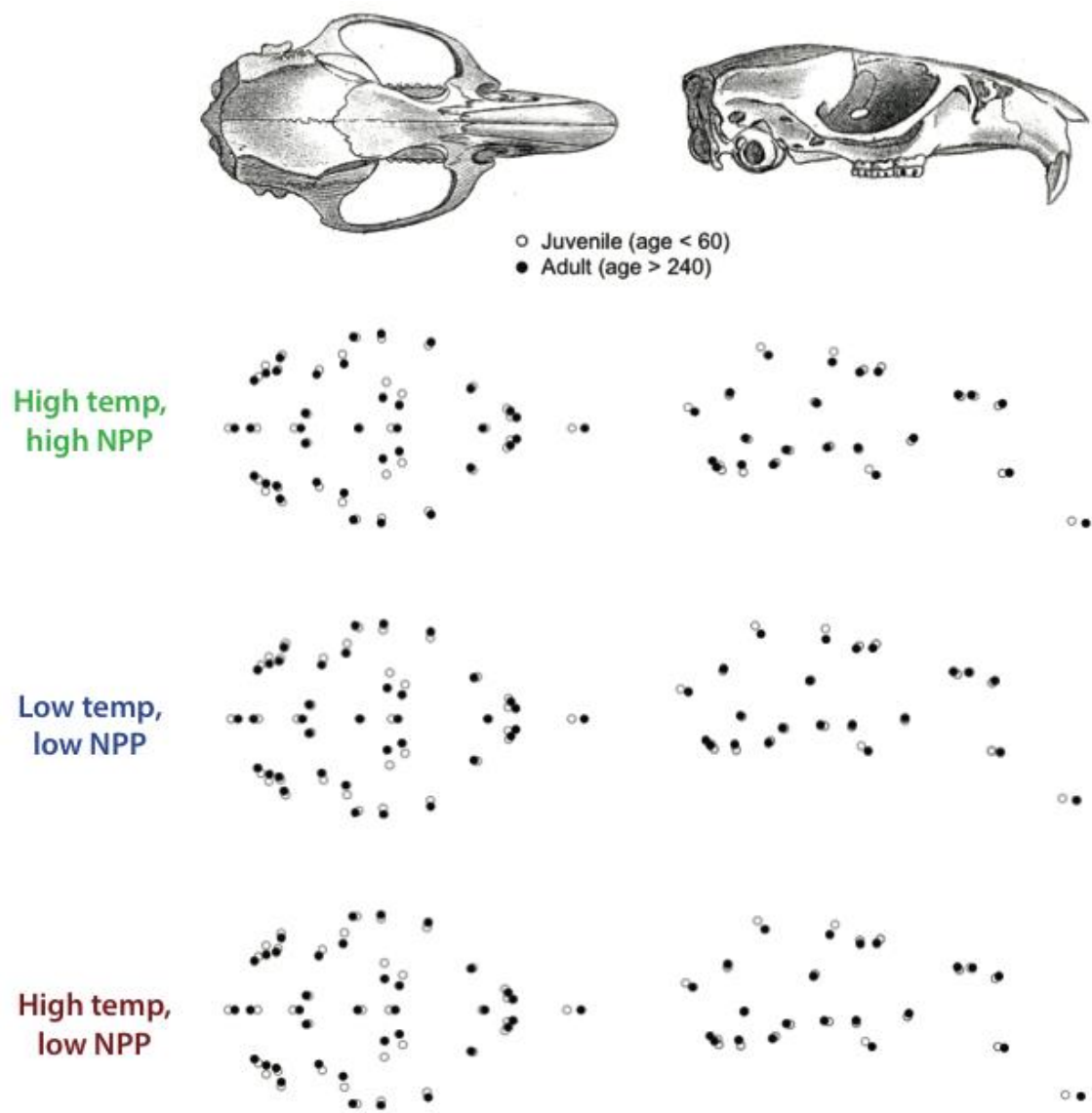


Figure 3-7.

APPENDIX 3-1

Age scoring and transformation.

Neotoma cinerea gestate for 27-32 days and wean 26-30 days after birth (Egoscue 1962). Juveniles are not likely to be caught in the field prior to weaning, and as such extremely few are present in museum collections (Escherich 1981), limiting this study to begin at the post-weaning stage. Neonates have curved incisors to facilitate nursing, and in congeners these incisors straighten through wear around 16 days (Hamilton 1953); curved incisors as well as markedly under-developed sutures (Finley 1958) suffice to distinguish pre-weaning from post-weaning juveniles, and allowed me to exclude the few available pre-weaning specimens from this study. Sexual maturation occurs as early as 120 days (Finley 1958), and though they may copulate in the year of their birth, *N. cinerea* are not known to breed successfully until the following year (Escherich 1981).

I used closure of two cranial sutures (exoccipital-supraoccipital and basioccipital-basisphenoid) and eruption and wear of the third upper molar (M3) to determine specimen age at collection (Table 3-S3, Figure 3-S4). This aging scheme assumes there are no broad geographic or climatic differences in the timing of suture closure or molar eruption and wear in *N. cinerea*. I scored each character separately from 1 (least developed) to 6 (most developed) and summed these scores to produce an age index from 3–18 (Table 3-S1). I then used known-age events in *Neotoma* cranial development (Hamilton 1953; Finley 1958; Escherich 1981; Daly and Patton 1986) to approximate the timing of the indices (Table 3-S3), and calculated the following reference points

expressed as (index,age): (3,21), (6,36), (9,56), (12,120), (15,240), (18,900). I fit the quadratic log-linear model $\log(\text{age}) = \text{index}^2$ through the aforementioned points (adjusted $r^2 = 0.9922$, $F = 25.23$, $P < 0.0001$; Figure 3-S5), and used it to predict the age of each specimen at collection in days after birth as $\text{age} = \exp(3.067 + 0.011I^2)$.

SUPPLEMENTAL TABLES

Table 3-S1. GUID, latitude, longitude, sex, and age scores (exoccipital-supraoccipital [occsut], basioccipital-basisphenoid suture [bassut], and M3 molar eruption and wear [molerup]) of specimens analyzed.

GUID	Latitude	Longitude	Sex	Occsut	Bassut	Molerup
FMNH:Mamm:11634	40.014982	-105.2700037	M	6	5	6
FMNH:Mamm:11635	40.014982	-105.2700037	M	6	6	6
FMNH:Mamm:11636	40.014982	-105.2700037	F	6	5	6
FMNH:Mamm:11637	40.014982	-105.2700037	F	6	4	5
FMNH:Mamm:11638	40.014982	-105.2700037	M	6	3	4
FMNH:Mamm:11639	39.9613749	-105.5102905	F	6	4	4
FMNH:Mamm:2125	38.77725	-120.02788	M	6	3	4
FMNH:Mamm:4911	43.9325	-103.5747	M	3	3	4
FMNH:Mamm:4912	43.7667	-103.5983	M	2	2	3
FMNH:Mamm:6286	47.8722	-123.6667	M	6	4	4
FMNH:Mamm:6294	48.0089	-123.685	M	6	6	6
FMNH:Mamm:6295	48.0089	-123.685	M	5	2	4
FMNH:Mamm:6296	48.0089	-123.685	M	6	6	5
FMNH:Mamm:6302	48.0089	-123.685	F	2	1	3
KU:Mamm:101416	44.05574115	-103.893601	F	1	2	2
KU:Mamm:101418	44.05574115	-103.893601	F	2	2	3
KU:Mamm:101420	44.05574115	-103.893601	F	6	4	5
KU:Mamm:101421	44.05574115	-103.893601	F	1	2	2
KU:Mamm:101422	44.05574115	-103.893601	F	1	3	3
KU:Mamm:101425	44.05574115	-103.893601	F	2	2	2
KU:Mamm:101426	44.06726333	-103.7846035	F	5	6	6
KU:Mamm:101428	44.06726333	-103.7846035	F	6	4	5
KU:Mamm:101429	44.06726333	-103.7846035	F	6	4	5
KU:Mamm:101430	44.06726333	-103.7846035	M	6	5	6
KU:Mamm:101431	44.06726333	-103.7846035	M	6	5	6
KU:Mamm:101434	44.06726333	-103.7846035	F	6	5	6
KU:Mamm:116917	39.99215	-105.47054	F	5	3	4
KU:Mamm:116919	39.97063	-105.40982	F	6	5	6
KU:Mamm:116920	39.97063	-105.40982	F	6	4	4
KU:Mamm:116921	39.97063	-105.40982	M	5	5	4
KU:Mamm:116922	39.97063	-105.40982	M	6	4	5
KU:Mamm:17237	41.528611	-109.465556	F	3	3	4
KU:Mamm:17238	41.528611	-109.465556	M	6	4	5

KU:Mamm:17239	41.528611	-109.465556	M	6	3	4
KU:Mamm:17240	41.528611	-109.465556	F	6	4	5
KU:Mamm:20576	46.2469	-114.03519	F	4	4	4
KU:Mamm:20577	46.2469	-114.03519	M	6	4	4
KU:Mamm:21043	40.1960105	-105.5197284	F	2	3	4
KU:Mamm:29204	37.3344	-108.9855	M	5	3	5
KU:Mamm:29205	38.82621	-106.86726	M	5	3	4
KU:Mamm:29206	38.82621	-106.86726	F	1	2	3
KU:Mamm:29207	38.82621	-106.86726	M	4	5	4
KU:Mamm:29208	38.82621	-106.86726	F	2	2	4
KU:Mamm:29209	38.82621	-106.86726	F	5	4	6
KU:Mamm:29210	38.82621	-106.86726	F	3	3	4
KU:Mamm:29213	38.70819	-106.8462	F	1	2	4
KU:Mamm:29214	38.70819	-106.8462	M	2	2	4
KU:Mamm:29217	38.70819	-106.8462	F	6	4	6
KU:Mamm:29220	38.70819	-106.8462	F	6	5	6
KU:Mamm:29221	38.70819	-106.8462	F	6	5	6
KU:Mamm:29222	38.1163	-106.72823	M	2	2	4
KU:Mamm:34794	37.6299	-108.88085	M	5	3	4
KU:Mamm:34822	38.70819	-106.8462	F	6	5	5
KU:Mamm:34828	38.1453	-106.45306	F	2	2	4
KU:Mamm:34841	37.6299	-108.88085	F	4	3	4
KU:Mamm:37145	40.90984	-103.57152	F	5	5	6
KU:Mamm:37146	40.90984	-103.57152	M	6	4	5
KU:Mamm:37147	40.90984	-103.57152	M	5	4	5
KU:Mamm:47224	40.2219	-115.4965	M	6	4	5
KU:Mamm:47229	40.2219	-115.4965	F	6	4	5
KU:Mamm:47230	40.2219	-115.4965	M	3	3	4
KU:Mamm:47233	40.2219	-115.4965	F	2	3	4
KU:Mamm:47235	40.2219	-115.4965	F	6	4	4
KU:Mamm:47255	42.8714	-112.445	F	6	5	6
KU:Mamm:53820	45.276944	-123.825278	M	6	5	6
KU:Mamm:53821	45.276944	-123.825278	F	6	6	6
KU:Mamm:6749	42.8714	-112.36622	M	6	4	5
KU:Mamm:6750	42.8714	-112.445	F	5	5	5
KU:Mamm:6752	42.8714	-112.36622	F	5	5	5
KU:Mamm:6753	42.8714	-112.36622	M	4	4	5
KU:Mamm:6754	42.8714	-112.36622	F	5	3	4
KU:Mamm:69607	40.93382	-103.43739	F	6	3	5
KU:Mamm:69609	40.93382	-103.43739	F	5	4	6
KU:Mamm:91220	41.33591439	-106.1996405	M	6	3	4
KU:Mamm:91221	41.33591439	-106.1996405	M	6	3	4

LACM:Mamm:6511	41.1693674	-123.0207793	M	6	4	6
LACM:Mamm:6512	41.1693674	-123.0207793	F	3	1	4
LACM:Mamm:6514	41.1693674	-123.0207793	M	2	3	4
LACM:Mamm:70414	46.90806	-121.02361	F	5	3	4
LACM:Mamm:70415	46.90806	-121.02361	F	6	5	4
LACM:Mamm:70416	46.83957	-120.94596	F	4	3	4
LACM:Mamm:8126	38.8647053	-104.9633353	F	6	4	5
MHP:Mamm:31404	46.44562531	-114.1491699	F	4	4	4
MSB:Mamm:108430	43.1848869	-116.3792763	F	5	5	5
MSB:Mamm:108432	43.1848869	-116.3792763	M	2	2	4
MSB:Mamm:108433	43.1848869	-116.3792763	F	2	1	2
MSB:Mamm:108434	43.1848869	-116.3792763	M	4	3	4
MSB:Mamm:108435	43.1848869	-116.3792763	M	2	2	4
MSB:Mamm:108436	43.1848869	-116.3792763	M	6	4	6
MSB:Mamm:112093	40.4641	-108.6691	F	2	2	3
MSB:Mamm:112095	40.4641	-108.6691	F	6	5	6
MSB:Mamm:112154	40.465	-108.6751	M	3	3	4
MSB:Mamm:112155	40.465	-108.6751	F	3	3	4
MSB:Mamm:112157	40.465	-108.6751	F	1	1	2
MSB:Mamm:113539	40.4641	-108.6691	M	2	1	3
MSB:Mamm:113605	40.41515	-109.18821	F	3	3	4
MSB:Mamm:115094	40.4247	-109.171	M	4	2	4
MSB:Mamm:115096	40.4247	-109.171	F	2	3	4
MSB:Mamm:115097	40.4247	-109.171	F	4	3	4
MSB:Mamm:115098	40.4247	-109.171	M	4	3	4
MSB:Mamm:115099	40.4247	-109.171	M	2	2	3
MSB:Mamm:115410	40.4547	-109.0162	F	6	3	4
MSB:Mamm:18486	39.43159	-120.22386	F	6	4	5
MSB:Mamm:18488	39.43159	-120.22386	F	5	4	4
MVZ:Mamm:109319	41.559333	-121.121	M	6	6	6
MVZ:Mamm:109321	41.559333	-121.121	M	6	6	6
MVZ:Mamm:109322	41.559333	-121.121	M	5	5	5
MVZ:Mamm:109323	41.559333	-121.121	F	5	4	5
MVZ:Mamm:109324	41.559333	-121.121	F	5	5	5
MVZ:Mamm:109326	41.559333	-121.121	F	1	2	3
MVZ:Mamm:125882	38.6898058	-106.8789134	F	2	2	4
MVZ:Mamm:132508	41.8413207	-120.9044757	F	5	5	6
MVZ:Mamm:132509	41.8413207	-120.9044757	F	6	4	6
MVZ:Mamm:15533	36.092861	-118.2262	M	2	2	4
MVZ:Mamm:15535	36.092861	-118.2262	M	2	1	2
MVZ:Mamm:15537	36.092861	-118.2262	F	5	4	5
MVZ:Mamm:15539	36.092861	-118.2262	F	4	5	6

MVZ:Mamm:15540	36.092861	-118.2262	M	4	4	4
MVZ:Mamm:15543	36.16332	-118.18188	M	6	5	6
MVZ:Mamm:15546	36.498353	-118.219906	M	6	5	6
MVZ:Mamm:15547	36.498353	-118.219906	M	5	3	4
MVZ:Mamm:15549	36.498353	-118.219906	M	6	4	6
MVZ:Mamm:15550	36.498353	-118.219906	F	6	5	6
MVZ:Mamm:15551	36.498353	-118.219906	M	5	4	6
MVZ:Mamm:15552	36.498353	-118.219906	F	6	4	5
MVZ:Mamm:15553	36.498353	-118.219906	F	2	2	3
MVZ:Mamm:15554	36.498353	-118.219906	F	6	5	5
MVZ:Mamm:15555	36.498353	-118.219906	M	6	4	6
MVZ:Mamm:15556	36.498353	-118.219906	F	6	6	6
MVZ:Mamm:15557	36.498353	-118.219906	M	2	2	2
MVZ:Mamm:15558	36.498353	-118.219906	F	2	2	3
MVZ:Mamm:15559	36.498353	-118.219906	M	3	3	4
MVZ:Mamm:15563	36.473421	-118.119206	F	5	6	6
MVZ:Mamm:15564	36.473421	-118.119206	M	1	2	2
MVZ:Mamm:15565	36.473421	-118.119206	M	6	3	4
MVZ:Mamm:183912	41.56081	-121.12136	M	6	5	6
MVZ:Mamm:220746	40.44631	-121.409	M	6	6	6
MVZ:Mamm:220747	40.40637	-121.36086	F	5	6	6
MVZ:Mamm:220748	40.40637	-121.36086	M	6	6	5
MVZ:Mamm:222570	36.090649	-118.226099	F	5	6	5
MVZ:Mamm:222723	36.175368	-118.205312	F	2	2	4
MVZ:Mamm:222724	36.175368	-118.205312	M	4	3	4
MVZ:Mamm:223397	39.1144	-114.29949	F	5	3	4
MVZ:Mamm:223398	39.11702	-114.30418	F	5	3	4
MVZ:Mamm:223399	39.1174	-114.30383	F	6	5	6
MVZ:Mamm:223400	39.1174	-114.30383	F	6	5	5
MVZ:Mamm:223425	41.43783	-109.3164	F	5	3	4
MVZ:Mamm:223426	41.43783	-109.3164	F	6	6	5
MVZ:Mamm:223427	41.43783	-109.3164	F	6	6	6
MVZ:Mamm:223428	41.43783	-109.3164	M	3	3	4
MVZ:Mamm:223429	41.45303	-109.30716	F	6	4	4
MVZ:Mamm:223430	41.45303	-109.30716	F	6	5	6
MVZ:Mamm:223431	41.45303	-109.30716	M	6	5	5
MVZ:Mamm:223432	41.45118	-109.30972	F	6	5	5
MVZ:Mamm:223433	41.43596	-109.31689	M	5	3	4
MVZ:Mamm:223435	38.65583	-106.85651	M	6	5	5
MVZ:Mamm:223436	38.65583	-106.85651	F	6	6	5
MVZ:Mamm:223437	38.65583	-106.85651	F	6	6	6
MVZ:Mamm:223438	38.65583	-106.85651	M	6	6	6

MVZ:Mamm:223439	38.65583	-106.85651	F	5	5	4
MVZ:Mamm:223444	44.04304	-103.88467	M	6	4	5
MVZ:Mamm:223445	41.14354	-106.05341	M	6	6	6
MVZ:Mamm:223446	41.14354	-106.05341	M	2	2	2
MVZ:Mamm:223447	41.14354	-106.05341	F	2	2	2
MVZ:Mamm:223448	41.14354	-106.05341	F	6	6	5
MVZ:Mamm:223449	41.14354	-106.05341	M	6	5	5
MVZ:Mamm:223450	41.14354	-106.05341	F	5	4	4
MVZ:Mamm:224101	36.49873	-118.20772	F	2	2	4
MVZ:Mamm:224328	36.47543	-118.11964	M	2	3	4
MVZ:Mamm:224329	36.47533557	-118.1211093	M	5	4	4
MVZ:Mamm:224330	36.47533557	-118.1211093	M	6	4	5
MVZ:Mamm:224331	36.47915687	-118.1286138	M	3	3	4
MVZ:Mamm:224332	36.43453	-118.2825533	M	2	3	4
MVZ:Mamm:224333	36.43453	-118.2825533	F	4	3	4
MVZ:Mamm:224334	36.43453	-118.2825533	M	6	5	5
MVZ:Mamm:224536	36.175368	-118.205312	F	5	2	4
MVZ:Mamm:30706	57.9167	-131.1833	M	6	4	5
MVZ:Mamm:30708	57.9167	-131.1833	F	5	4	5
MVZ:Mamm:30709	57.9167	-131.1833	M	6	3	5
MVZ:Mamm:30710	57.9167	-131.1833	F	5	4	5
MVZ:Mamm:30711	57.9167	-131.1833	F	6	3	6
MVZ:Mamm:30713	57.9167	-131.1833	M	6	3	5
MVZ:Mamm:30714	57.8333	-131.3833	M	2	1	1
MVZ:Mamm:30715	57.8333	-131.3833	F	3	2	4
MVZ:Mamm:30717	57.8333	-131.3833	M	1	1	1
MVZ:Mamm:30718	57.8333	-131.3833	F	2	1	1
MVZ:Mamm:33712	40.44423	-121.3938	F	6	6	6
MVZ:Mamm:33713	40.44423	-121.3938	F	3	3	4
MVZ:Mamm:34862	40.4147	-121.5319	F	6	6	6
MVZ:Mamm:34863	40.4147	-121.5319	F	2	3	3
MVZ:Mamm:34864	40.4147	-121.5319	F	5	4	5
MVZ:Mamm:34865	40.4147	-121.5319	M	6	5	6
MVZ:Mamm:34866	40.4147	-121.5319	M	2	2	4
MVZ:Mamm:34867	40.4147	-121.5319	M	2	1	3
MVZ:Mamm:34868	40.4147	-121.5319	M	6	4	5
MVZ:Mamm:34869	40.46392	-121.51845	M	6	5	6
MVZ:Mamm:34871	40.44334	-121.39613	M	6	4	5
MVZ:Mamm:41987	38.9889	-114.215	M	5	5	6
MVZ:Mamm:41988	38.9889	-114.215	F	6	4	5
MVZ:Mamm:41989	38.9889	-114.215	M	6	4	5
MVZ:Mamm:41991	38.9889	-114.215	F	6	4	5

MVZ:Mamm:41993	38.96917	-114.28	M	6	6	6
MVZ:Mamm:41994	38.96917	-114.28	F	5	4	5
MVZ:Mamm:41996	38.96917	-114.28	M	6	6	6
MVZ:Mamm:42002	38.96917	-114.28	F	6	4	5
MVZ:Mamm:42008	38.96917	-114.28	F	6	4	6
MVZ:Mamm:42009	38.96917	-114.28	M	1	2	2
MVZ:Mamm:42011	38.96917	-114.28	F	6	5	5
MVZ:Mamm:42014	38.96917	-114.28	M	6	5	6
MVZ:Mamm:46260	39.23333	-114.47222	F	6	4	5
MVZ:Mamm:46261	39.23333	-114.47222	F	2	3	4
MVZ:Mamm:46262	39.23333	-114.47222	M	5	5	5
MVZ:Mamm:46263	39.23333	-114.47222	M	6	4	5
MVZ:Mamm:46264	39.23333	-114.47222	M	2	2	4
MVZ:Mamm:64950	41.6380028	-121.1610146	F	6	6	6
MVZ:Mamm:67682	43.2183	-116.6702	M	6	5	6
PSM:Mamm:10825	39.4366092	-120.2061031	M	5	4	4
PSM:Mamm:10826	39.4366092	-120.2061031	F	6	3	4
PSM:Mamm:10828	39.4366092	-120.2061031	M	6	4	5
PSM:Mamm:13806	45.03337972	-123.922106	F	2	1	2
PSM:Mamm:13807	45.03337972	-123.922106	M	2	2	2
PSM:Mamm:13903	45.03337972	-123.922106	M	6	4	5
PSM:Mamm:13904	45.037	-123.917	M	6	6	6
PSM:Mamm:13905	45.037	-123.917	F	6	3	5
PSM:Mamm:13906	45.037	-123.917	F	6	4	5
PSM:Mamm:13907	45.0334	-123.9323	F	3	3	4
PSM:Mamm:13908	45.0334	-123.9323	F	6	4	6
PSM:Mamm:24746	43.2509	-116.7495	F	4	3	4
PSM:Mamm:2703	46.96194	-121.08278	F	3	3	4
PSM:Mamm:2704	46.96194	-121.08278	M	6	6	6
PSM:Mamm:5765	47.94889	-123.25806	M	6	4	4
PSM:Mamm:5766	47.96944	-123.49722	M	5	3	4
UAM:Mamm:24566	47.11388889	-120.9333333	F	6	3	4
UAM:Mamm:35061	47.13333333	-120.9666667	F	4	3	4
UAM:Mamm:49980	47.11388889	-120.9333333	M	6	5	6
UCM:Mamm:10003	38.86970858	-106.9878231	F	6	4	5
UCM:Mamm:10004	38.86970858	-106.9878231	M	2	2	4
UCM:Mamm:10008	38.80980684	-104.9035309	M	6	5	4
UCM:Mamm:10009	38.81804511	-104.8944317	F	6	5	4
UCM:Mamm:10013	38.8543388	-104.7516569	F	6	4	4
UCM:Mamm:10014	38.8155397	-104.9927565	F	3	3	4
UCM:Mamm:10023	38.87360192	-107.0969943	M	6	5	6
UCM:Mamm:10024	38.87360192	-107.0969943	M	6	4	4

UCM:Mamm:10029	38.8155397	-104.9927565	M	6	5	4
UCM:Mamm:10030	38.8155397	-104.9927565	M	6	3	4
UCM:Mamm:4728	40.47245837	-108.8945702	F	5	3	6
UCM:Mamm:5206	40.06323729	-105.4056824	F	6	4	5
UMMZ:Mamm:104408	43.8038689	-103.7838096	F	6	5	5
UMMZ:Mamm:104409	43.8038689	-103.7838096	F	2	2	3
UMMZ:Mamm:104412	43.8038689	-103.7838096	F	2	3	3
UMMZ:Mamm:104415	43.8038689	-103.7838096	M	2	2	2
UMMZ:Mamm:56190	38.8494289	-104.9588949	F	5	3	4
UMMZ:Mamm:56192	38.8494289	-104.9588949	M	5	3	4
UMMZ:Mamm:59164	40.8745	-109.85973	F	6	4	5
UMMZ:Mamm:59165	40.86122	-109.71822	F	3	3	4
UMMZ:Mamm:59166	40.86122	-109.71822	M	6	3	5
UMMZ:Mamm:59167	40.86122	-109.71822	F	6	4	5
UMMZ:Mamm:87622	47.562	-111.1684	M	6	4	6
UMMZ:Mamm:87623	47.562	-111.1684	M	6	4	4
UMMZ:Mamm:87624	47.562	-111.1684	M	2	2	4
UMMZ:Mamm:87626	47.562	-111.1684	M	4	3	4
UMMZ:Mamm:87627	47.562	-111.1684	F	1	1	1
UMMZ:Mamm:87628	47.562	-111.1684	F	3	3	4
UMMZ:Mamm:87629	47.562	-111.1684	F	6	6	5
UMMZ:Mamm:87631	47.562	-111.1684	F	6	5	5
UMMZ:Mamm:87632	47.562	-111.1684	F	6	5	5
UMMZ:Mamm:99519	38.7369603	-106.8878335	M	3	3	4
UMMZ:Mamm:99520	38.7369603	-106.8878335	M	5	5	6
UMMZ:Mamm:99815	46.9464	-121.1100771	F	6	4	5
UMNH:Mamm:15021	41.46668	-109.38349	F	2	2	3
UMNH:Mamm:15022	41.46668	-109.38349	M	2	2	4
UMNH:Mamm:17080	38.3167	-112.36116	F	6	4	5
UMNH:Mamm:17082	38.5625	-112.35694	F	6	6	5
UMNH:Mamm:17083	38.5625	-112.35694	F	6	3	4
UMNH:Mamm:17085	38.42417	-112.51722	M	6	4	5
UMNH:Mamm:17087	38.60104	-112.39592	F	2	3	4
UMNH:Mamm:19437	40.90924	-109.79908	M	2	2	4
UMNH:Mamm:2300	40.68895	-111.78595	M	6	5	5
UMNH:Mamm:27288	40.34722	-112.60333	F	6	4	5
UMNH:Mamm:27289	40.3375	-112.56667	M	6	4	5
UMNH:Mamm:27293	40.34133	-112.5778	F	6	4	5
UMNH:Mamm:27295	40.35922	-112.99904	M	4	2	4
UMNH:Mamm:2916	40.85713	-109.73069	M	3	3	4
UMNH:Mamm:5045	41.99389	-113.41833	F	6	5	5
UWBM:Mamm:51172	46.905123	-120.9513899	F	6	4	4

UWBM:Mamm:59945	47.7716	-123.067	F	4	3	4
UWBM:Mamm:59946	47.7716	-123.067	M	6	6	6
UWBM:Mamm:59947	47.7716	-123.067	M	5	4	4
UWBM:Mamm:61470	46.9619	-121.0828	F	5	4	4
UWBM:Mamm:61472	46.9619	-121.0828	F	6	5	6
UWBM:Mamm:61474	46.9619	-121.0828	M	5	3	4
UWBM:Mamm:61480	46.9619	-121.0828	F	6	4	4
UWBM:Mamm:70131	47.7716	-123.067	F	6	5	6
UWBM:Mamm:73257	46.9619	-121.0828	F	6	3	5
UWBM:Mamm:73810	47.1166667	-121.0666667	F	6	4	6
UWBM:Mamm:78604	47.95133333	-123.2556667	F	5	4	4
UWBM:Mamm:78606	47.94966667	-123.2645	F	5	3	4
UWBM:Mamm:78852	47.88216667	-123.1451667	F	5	4	4
UWBM:Mamm:79495	44.86016667	-123.8371667	F	6	5	5
UWBM:Mamm:79658	42.08116667	-113.6816667	M	2	2	4

Table 3-S2. Measurement view, type, abbreviation, and description of landmarks used in geometric morphometric analyses. Marker code refers to landmark placement on Figure 1.

Marker	View	Type	Abbreviation	Description
A	ventral	midline	IS	dorsal point of incisive suture
B	ventral	bilateral	PM	edge of premaxillary-maxillary suture where it recedes into incisive foramen; often reaches posteriorly
C	ventral	midline	PNS	posterior point of postnasal suture
D	ventral	bilateral	ZYGO	posterior point of zygomatic bone; often reaches dorsally
E	ventral	bilateral	TS	end of temporal-sphenoid suture at bulla or foramen, often reaches laterally
F	ventral	bilateral	SEAM	superior auditory meatus, measured at suture on lateral margin
G	ventral	bilateral	IEAM	inferior auditory meatus, measured at nadir of lateral scoop on inferior margin
H	ventral	bilateral	POP	inferior end of paraoccipital process; often reaches anteriorly
I	ventral	bilateral	APET	end of sphenoid-basioccipital suture at auditory bulla
J	both	midline	BA	basion, inferior margin of foramen magnum at midline
K	both	midline	OPI	opisthion, superior margin of foramen magnum at midline
L	dorsal	midline	NAS	nasion, anterior-most junction of nasals at midline suture
M	dorsal	bilateral	PMF	anterior point of frontal bone visible dorsally at premaxillary-maxillary junction
N	dorsal	bilateral	LAC	posterior end of nasal-frontal suture at lacrimal bone
O	dorsal	bilateral	ZS	anterior-lateral point of zygomatic bone
P	dorsal	bilateral	ZI	anterior-dorsal point of temporal bone on zygomatic arch
Q	both	bilateral	TP	temporal pit, measured perpendicular to skull
R	dorsal	bilateral	PT	pterion, posterior-dorsal end of sphenoparietal suture
S	dorsal	bilateral	FSP	anterior end of sphenoparietal suture at frontal, sphenoid, and parietal bones
T	dorsal	midline	BR	bregma, intersection of coronal and sagittal sutures; often off-center and measured so
U	dorsal	bilateral	AS	posterior end of the parietomastoid (squamous) suture at occipital; measured at occipital even it fuses with the lambdoid suture
V	dorsal	midline	LD	lambda, junction of sagittal and lambdoid sutures

Table 3-S3. Age scores (1–6) for cranium developmental characters, with known ages (literature) and estimated ages (this study).

Feature	Score	Description (this study)	Known age (days)	Estimated age (days)	Reference
Exoccipital-supraoccipital suture (occsut)					
	1	open and smooth		21	
	2	ridging		36	
	3	ridged but not fused	< 120	56	Finley 1958
	4	fused but not remodeled		120	
	5	remodeled, readily visible	120-900	240	Finley 1958
	6	remodeled, faintly visible	120-900	900	Finley 1958
Basioccipital-basisphenoid suture (bassut)					
	1	open and straight	*	21	
	2	ridging	*	36	
	3	ridged but not fused	*	56	
	4	fused but not remodeled	*	120	
	5	partially remodeled	*	240	
	6	remodeled	*	900	
M3 eruption and wear (molerup)					
	1	M3 not erupted from maxilla	< 36	21	Hamilton 1953, Finley 1958
	2	M3 < half height of posterior margin of M2	21-56	36	Hamilton 1953, Finley 1958
	3	M3 > half height of posterior margin of M2 but not yet flush with M2		56	
	4	M3 showing wear, but root beyond buccal folds not visible	60-120	120	Finley 1958, Hamilton 1953
	5	root visible, buccal folds spanning > half height of molar row	180-240, 120-900	240	Escherich 1981, Finley 1958
	6	root visible, buccal folds spanning > half height of molar row	> 900	900	Finley 1958

*Similar in developmental timing to the exoccipital-supraoccipital suture (sensu Daly and Patton 1986)

Table 3-S4. Ranked candidate models and AICs from model selection relating adult body size to climate.

Model	Scale (km)	AIC	Delta AIC
age + sex + age:sex + bio1 + NPP	95	319.15	0
age + sex + age:sex + bio1 + NPP + bio1*NPP	95	320.49	1.33
age + sex + age:sex + bio1 + NPP	475	322.33	3.17
age + sex + age:sex + bio1 + NPP + bio1*NPP	475	323.35	4.20
age + sex + age:sex + bio1 + NPP	285	323.45	4.29
age + sex + age:sex + bio1 + NPP + bio1*NPP	285	324.69	5.54
age + sex + age:sex + bio1 + bio12	475	325.89	6.73
age + sex + age:sex + bio1 + bio12 + bio1*bio12	475	326.42	7.27
age + sex + age:sex + bio5	475	326.67	7.51
age + sex + age:sex + bio1 + bio12	95	328.43	9.28
age + sex + age:sex + bio5 + bio6	475	328.51	9.36
age + sex + age:sex + bio1 + NPP	48	329.09	9.93
age + sex + age:sex + bio1 + bio12 + bio1*bio12	95	329.17	10.01
age + sex + age:sex + bio1	475	329.28	10.13
age + sex + age:sex + bio12	475	329.40	10.24
age + sex + age:sex + bio1 + bio12	285	330.16	11.01
age + sex + age:sex + NPP	475	330.35	11.20
age + sex + age:sex + NPP	95	330.43	11.28
age + sex + age:sex + bio1 + NPP + bio1*NPP	48	330.58	11.43
age + sex + age:sex + NPP	285	330.92	11.76
age + sex + age:sex + bio5	285	330.92	11.77
age + sex + age:sex + bio1 + bio12 + bio1*bio12	285	330.95	11.79
age + sex + age:sex + bio1	95	331.58	12.43
age + sex + age:sex + NPP	48	332.11	12.96
age + sex + age:sex + bio1	285	332.16	13.00
age + sex + age:sex + bio5	95	332.65	13.50
age + sex + age:sex + bio5 + bio6	285	332.85	13.70
age + sex + age:sex + NPP	21	333.26	14.10
age + sex + age:sex + bio12	285	333.70	14.55
age + sex + age:sex + bio1 + NPP	4, 21	333.77	14.61
age + sex + age:sex + bio1 + bio12	48	334.22	15.06
age + sex + age:sex + bio5 + bio6	95	334.62	15.47
age + sex + age:sex + bio1	48	335.05	15.90
age + sex + age:sex + bio1 + bio12 + bio1*bio12	48	335.31	16.15
age + sex + age:sex + bio12	95	335.33	16.17
age + sex + age:sex + bio1 + NPP + bio1*NPP	4, 21	335.39	16.24
age + sex + age:sex + bio5	4	335.58	16.42
age + sex + age:sex + bio1	4	335.61	16.46

age + sex + age:sex +	n/a	336.04	16.89
age + sex + age:sex + bio1 + bio12 + bio1*bio12	4	336.46	17.30
age + sex + age:sex + bio12	48	336.49	17.33
age + sex + age:sex + bio5	48	336.66	17.51
age + sex + age:sex + bio5 + bio6	4	336.99	17.84
age + sex + age:sex + bio1 + bio12	4	337.49	18.33
age + sex + age:sex + bio6	95	337.59	18.44
age + sex + age:sex + bio6	4	337.60	18.45
age + sex + age:sex + bio6	475	337.66	18.51
age + sex + age:sex + bio6	48	337.86	18.70
age + sex + age:sex + bio6	285	337.95	18.80
age + sex + age:sex + bio12	4	338.00	18.85
age + sex + age:sex + bio5 + bio6	48	338.54	19.39

Table 3-S5. Top models ($\Delta AIC < 2$) from model selection relating adult body size to climate, including estimates, standard errors (SE), t -values, and P -values. All parameters have been standardized. Scale for all parameters is 95 km.

Model	AIC	Parameter	Estimate	SE	t	P
age + sex + age:sex + bio1 + NPP	321.259	(Intercept)	-0.018	0.065	-0.281	0.7793
		age	0.154	0.069	2.223	0.0279
		sex	0.496	0.066	7.524	< 0.0001
		bio1	-0.249	0.068	-3.651	0.0004
		NPP	0.271	0.071	3.815	0.0002
		age:sex	0.130	0.065	1.996	0.0480
age + sex + age:sex + bio1 + NPP + bio1*NPP	321.925	(Intercept)	0.006	0.072	0.081	0.9353
		age	0.154	0.069	2.229	0.0275
		sex	0.498	0.066	7.541	< 0.0001
		bio1	-0.262	0.070	-3.730	0.0003
		NPP	0.314	0.089	3.518	0.0006
		age:sex	0.121	0.066	1.818	0.0714
		bio1:NPP	-0.078	0.098	-0.797	0.4266

Table 3-S6. Reduced models relating age and sex to body size in each growth phase.

Phase (Age)	Parameter	Estimate	SE	<i>t</i>	<i>P</i>
1 (0-59)	(Intercept)	0.000	0.081	-0.004	0.9965
	sex(M)	0.140	0.082	1.721	0.0906
	age	0.772	0.082	9.440	< 0.0001
	sex:age	0.046	0.083	0.551	0.5837
2 (60-139)	(Intercept)	-0.003	0.127	-0.024	0.9809
	sex(M)	0.066	0.129	0.514	0.6096
	age	0.467	0.129	3.622	0.0007
	sex:age	-0.072	0.130	-0.555	0.5814
3 (140-240)	(Intercept)	-0.014	0.124	-0.110	0.9129
	sex(M)	0.446	0.126	3.548	0.0009
	age	0.452	0.126	3.588	0.0008
	sex:age	-0.060	0.127	-0.474	0.6379
4 (>240)	(Intercept)	-0.019	0.070	-0.271	0.7870
	sex(M)	0.495	0.070	7.084	< 0.0001
	age	0.226	0.071	3.185	0.0018
	sex:age	0.134	0.070	1.926	0.0563

SUPPLEMENTAL FIGURES

Figure 3-S1. Pairwise Procrustes shape distances for multiple measurements within the same specimen and among specimens.

Figure 3-S2. Difference in age index (on a scale of 3–18) between specimens aged multiple times.

Figure 3-S3. Adult (age > 240 days) male centroid sizes across ages and at different levels of (A) temperature and (B) NPP.

Figure 3-S4. Guide to age scores for cranial developmental characters, including specimen GUID for reference.

Figure S5. Relationship between age indices (scored from cranial characters) and predicted log age, with 95% confidence interval shaded.

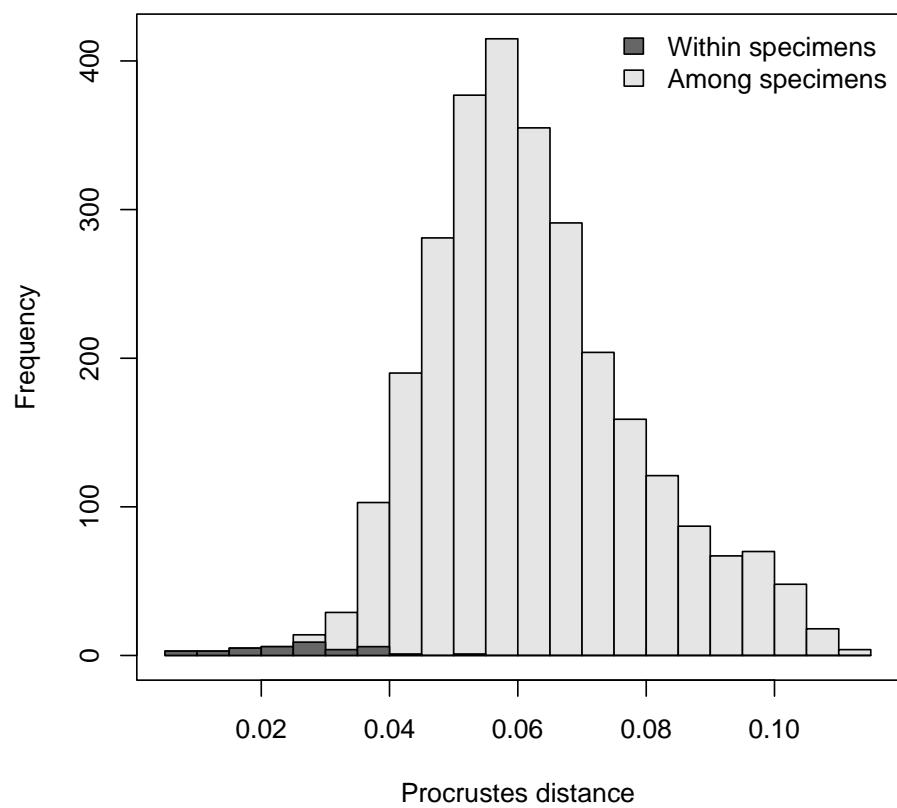


Figure 3-S1.

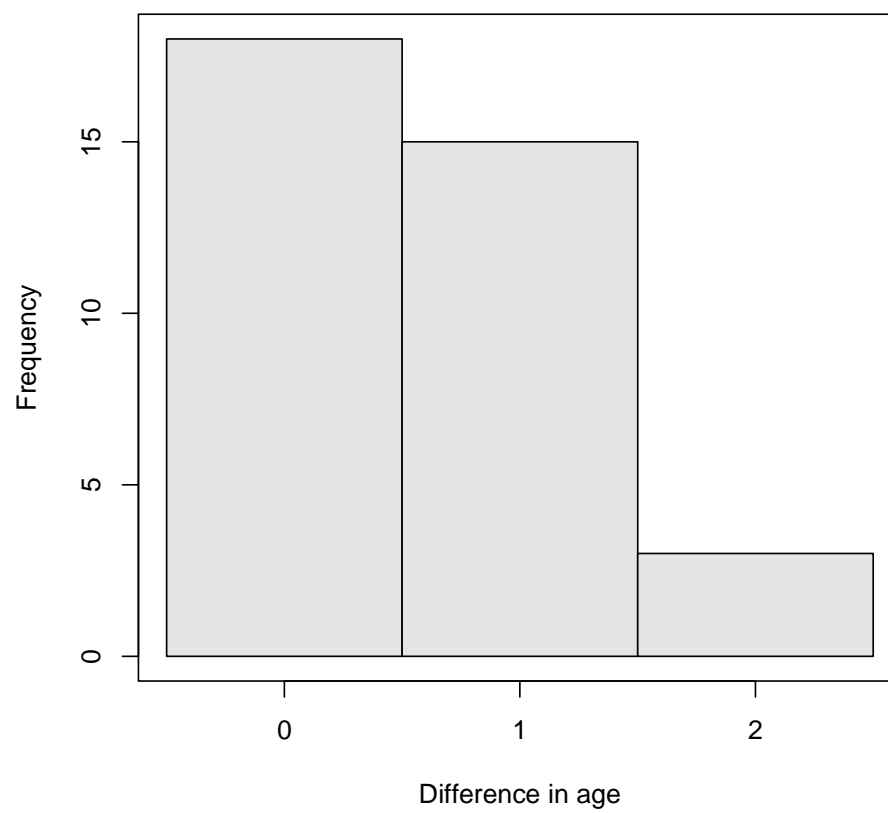


Figure 3-S2.

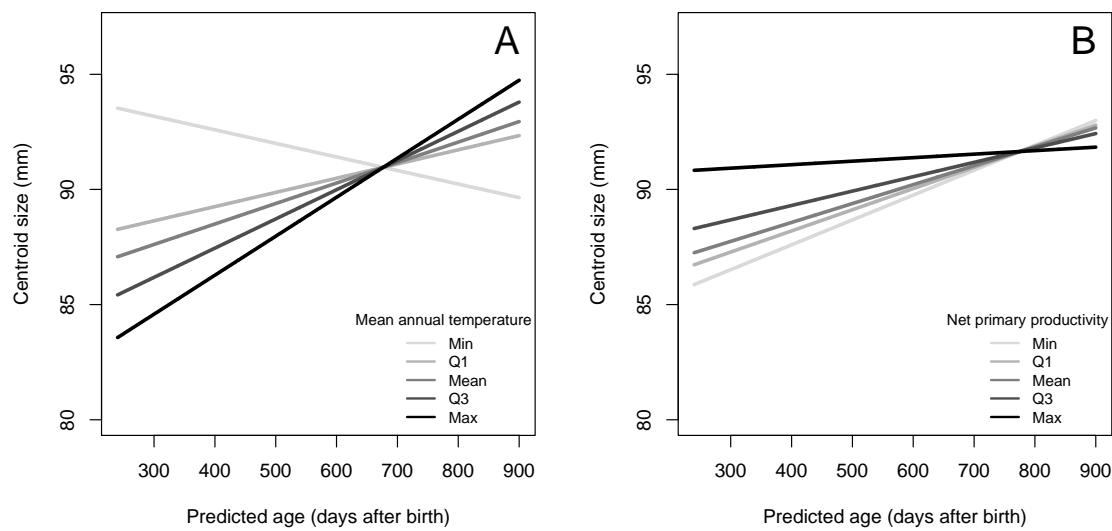


Figure 3-S3.

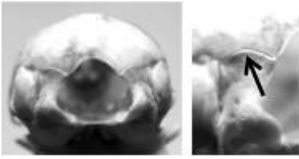

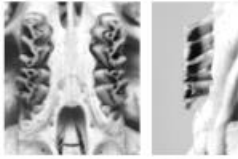
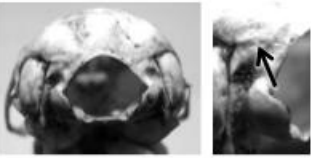

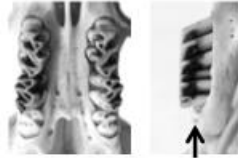
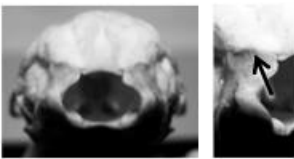

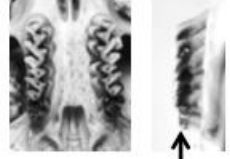
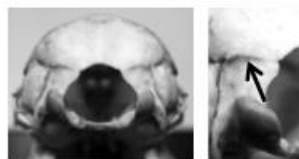


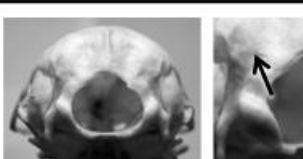

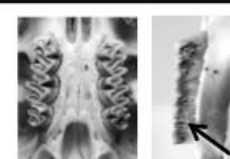
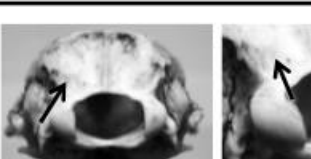
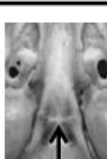

Score	Exoccipital-supraoccipital suture (occsut)	Basioccipital-basisphenoid suture (bassut)	M3 eruption and wear (molerup)
1	 MVZ:Mamm:53223	 MVZ:Mamm:30714	 MVZ:Mamm:30714
2	 MVZ:Mamm:15558	 MVZ:Mamm:15558	 MVZ:Mamm:64467
3	 MVZ:Mamm:24994	 MVZ:Mamm:24994	 MVZ:Mamm:15558
4	 MVZ:Mamm:222827	 MVZ:Mamm:49269	 MVZ:Mamm:49269
5	 MVZ:Mamm:49269	 MVZ:Mamm:67682	 MVZ:Mamm:41988
6	 MVZ:Mamm:41993	 MVZ:Mamm:41993	 MVZ:Mamm:223396

Figure 3-S4.

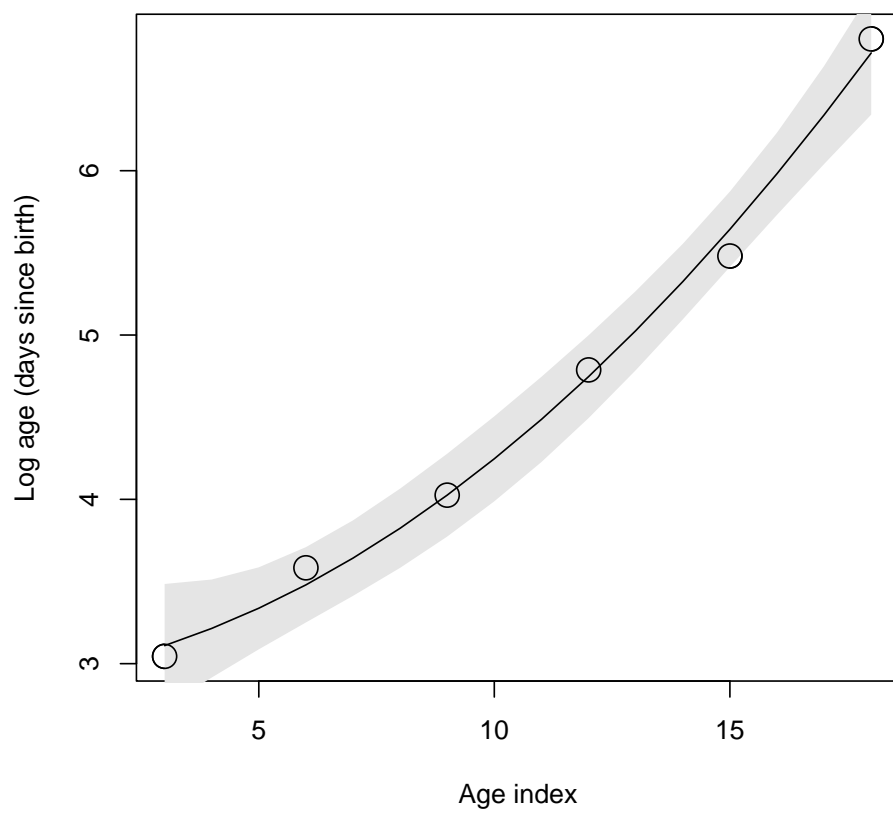


Figure 3-S5.